THE DISSOLUTION OF OLIVINE IN ACID

A COST EFFECTIVE PROCESS FOR THE ELIMINATION OF WASTE ACIDS

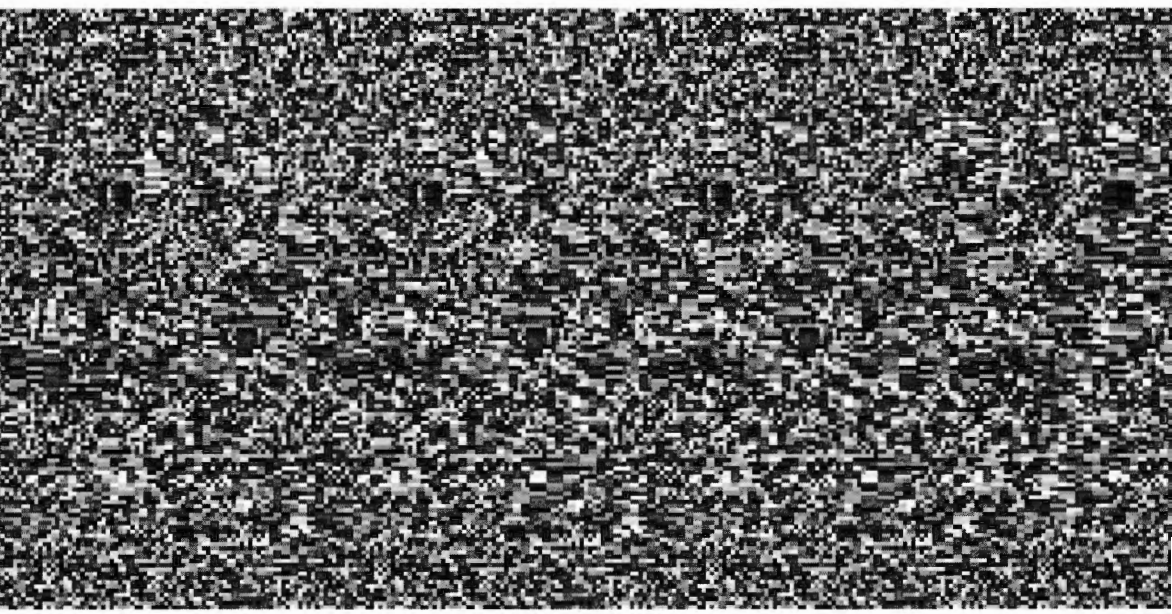

R.C.L. JONCKBLOEDT

THE DISSOLUTION OF OLIVINE IN ACID

A COST EFFECTIVE PROCESS FOR THE ELIMINATION OF WASTE ACIDS

HET OPLOSSEN VAN OLIVIJN IN ZUUR

EEN ECONOMISCH AANTREKKELIJKE MANIER OM AFVALZUREN ONSCHADELIJK TE MAKEN

(MET EEN SAMENVATTING IN HET NEDERLANDS)

PROEFSCHIFT

TER VERKRIJGING VAN DE GRAAD VAN DOCTOR
AAN DE UNIVERSITEIT UTRECHT OP GEZAG VAN DE RECTOR MAGNIFICUS, PROF. DR. H.O. VOORMA, INGEVOLGE HET BESLUIT VAN HET COLLEGE VAN DEKANEN IN HET OPENBAAR TE VERDEDIGEN OP MAANDAG 15 DECEMBER 1997 DES MORGENS OM 10.30

DOOR

RONALD CHRISTIAN LEONARD JONCKBLOEDT
GEBOREN OP 28 JULI 1969, TE WYMBRITSERADEEL

PROMOTORES: PROF.DR.IR. J.W. GEUS
Verbonden aan de faculteit Scheikunde
van de Universiteit Utrecht

PROF.DR. R.D. SCHUILING
Verbonden aan de faculteit Aardwetenchappen
van de Universiteit Utrecht

This research has been financed by Geochem Research B.V. through a grant of the
E.C. Brite Euram II program. E.C. Agreement Number: BRE2-CT92-0.344.
Title of Research Project: Olivine/Dunite for Industrial and Environmental Applications

ISBN 90-393-1643-0

Aan mijn ouders

En mijn broer

Cover:

In order to find anything

one must look for something

Table of Contents

Samenvatting

Introductie
Vergeleken met conventionele methoden voor de verwerking van afvalzuren, zoals neutralisatie met kalk of regeneratie processen, is neutralisatie met olivijn (olivijn proces) goedkoper en het produceert geen nieuwe afvalstromen. De productie van bruikbare bijproducten, zoals geprecipiteerde silica, de lage energie consumptie en het feit dat olivijn relatief goedkoop en in grote hoeveelheden in de natuur beschikbaar is, maken het olivijn proces een interessant alternatief voor conventionele behandelings methoden.
In dit proefschrift worden een aantal uiteenlopende aspecten van het olivijn proces, die essentieel zijn voor de opschaling van het proces tot industrieel niveau, nader uiteengezet. De verschillende onderwerpen worden ingedeeld in drie gedeelten. In het eerste gedeelte, "Het oplossen van olivijn ", worden het mechanisme en de snelheid van olivijn oplossing in zwavelzuur onderzocht, wordt het oplosgedrag van verschillende soorten olivijn vergeleken en wordt de reactie warmte die vrijkomt bij het oplossen van olivijn in zwavelzuur gemeten. In het tweede gedeelte, "Neutralisatie van afvalzuren", wordt het gebruik van het olivijn proces voor de neutralisatie van een aantal afvalzuren onderzocht. In het derde gedeelte, "Synthese van magnetische ferrieten", wordt een procedure ontwikkeld voor de verwijdering van metalen uit de geneutraliseerde oplossing, door middel van de vorming van magnetische ferrieten.

1) Het oplossen van olivijn

Het industriële ontwerp van een fabriek voor de neutralisatie van afvalzuren met olivijn vereist een grondige kennis van de factoren, die de oplossnelheid van olivijn in zuur bepalen. Helaas zijn in de literatuur alleen gegevens beschikbaar voor het oplossen van olivijn onder natuurlijke verwerings omstandigheden. Daarom worden de reactie mechanismen geïdentificeerd door het combineren van gegevens uit de literatuur met experimentele gegevens over het oplossen van olivijn in sterk zuur. Dit toont aan dat in geconcentreerd zuur dikke silica lagen worden afgezet op de oplossende olivijn korrels, wanneer de olivijn niet wordt geroerd. Deze silica lagen remmen verdere oplossing en leiden uiteindelijk tot volledige cementatie van het olivijn bed. Om de afzetting van silica op de olivijn korrels te vermijden moet het mengsel van olivijn en zuur continu geroerd worden. Onder stevige roering wordt de oplossnelheid van olivijn kinetisch gecontroleerd door oppervlakte reacties. Vervolgens wordt een model gemaakt dat de kinetiek van olivijn oplossing beschrijft. Het model wordt gemaakt voor één soort Noorse olivijn (FO_{93}) met korrelgroottes variërend van 63 tot 300 μm, in 3 M zwavelzuur en bij temperaturen van 60 tot 90 °C. Helaas zijn conventionele methoden voor het bestuderen van de reactiekinetiek niet toepasbaar voor het bestuderen van de olivijn oplossnelheid in zwavelzuur bij hoge temperaturen. Daarom is besloten de reactiesnelheid te bestuderen door een aantal experimenten uit te voeren, waarbij het zuur compleet wordt geneutraliseerd. De H^+ activiteit, die nodig is voor de interpretatie van de experimentele gegevens, wordt berekend met het Pitzer model, gebruik makende van het computer programma PHRQPITZ. Met behulp van het Pitzer model is het mogelijk berekeningen te doen aan chemische evenwichten in oplossingen met een zeer hoge ion sterkte. Vanwege de hoge zuursterkte en de hoge temperaturen is het niet mogelijk om nauwkeurig de H+ activiteit te bepalen door middel van pH metingen. Dit onderzoek toont

aan dat de het verloop van de neutralisatie goed kan worden gemodelleerd met behulp van het geometrische oppervlak van de oplossende olivijn korrels. Het geometrische oppervlak kan worden berekend als functie van het olivijn volume, uitgaande van de initiële korrelgrootte verdeling en een bolvormige korrelgeometrie. De resultaten worden samengevat in de volgende snelheidsvergelijking:

$$\frac{d\,[H^+]}{dt} = -\ e^{-\frac{E_{act}}{R \cdot T}} \cdot 10^8 \cdot (1.92 \pm 0.12) \cdot S_{geom} \cdot A_{H^+}^{0.33} \qquad [mol \cdot minuut^{-1}]$$

waarbij E_{act} de activerings energie is van 66.5±2 kJ·mol^{-1}, S_{geom} het geometrische oppervlak van de olivijn korrels en A_{H+} de H^+ activiteit berekend met het Pitzer model. Met deze vergelijking kan het verloop van de neutralisatie berekend worden.
Voor het bestuderen van de oplossnelheid is een maximum korrelgrootte van 300 μm gekozen, aangezien dit de grootte is van de grootste olivijn korrels (van de gebruikte Noorse olivijn) zonder interne breukjes. Onderzoek naar het oplosgedrag van olivijn fracties met grotere korrelgroottes, variërend van 300 tot 630 μm, toont aan dat de korrels preferent langs de breukjes oplossen, hetgeen leidt tot uiteenvallen van de korrels. De disintegratie resulteert in een groter olivijn oppervlak en daarmee in een hogere oplossnelheid.
De eigenschappen van de natuurlijke grondstof olivijn zijn variabel, en hangen af van de herkomst van de olivijn. De geschiktheid van een bepaald type olivijn hangt af van een aantal factoren, i) de mineralogische samenstelling van het olivijn gesteente, ii) de deformatie/alteratie geschiedenis van het olivijn gesteente en iii) de chemische samenstelling van de olivijn zelf. Het oplosgedrag van olivijn uit twee mogelijke productie gebieden in Griekenland wordt onderzocht en vergeleken met de Noorse olivijn, die gebruikt is bij het onderzoek naar de oplossnelheid. De samenstelling van de Griekse olivijn varieert van FO_{90} tot FO_{92}. Deze studie toont aan dat de Griekse olivijn sneller reageert, vergeleken met de Noorse olivijn. Het is belangrijk om op te merken dat de effecten van variërende olivijn eigenschappen op de neutralisatie snelheid klein zijn vergeleken met, bijvoorbeeld, het effect van temperatuur op de reactiesnelheid.
De lage energie consumptie van het olivijn proces is te wijten aan de exotherme reactie van olivijn en zuur. Helaas waren nauwkeurige metingen van de reactie warmte niet beschikbaar. Daarom wordt de reactie warmte gemeten voor de oplossing van drie verschillende olivijn types (twee Noorse olivijnen, allebei FO_{93} en één Griekse, FO_{92}) in 3 M zwavelzuur. De verschillen in gemeten reactie warmte van de drie olivijnen vallen binnen de meetnauwkeurigheid. De gemiddelde reactie warmte voor het oplossen van olivijn in 3 M zwavelzuur is (223±2.9) kJ·mol^{-1}

2) Neutralisatie van afvalzuren
Elk afvalzuur heeft een karakteristieke samenstelling. Voor een succesvolle behandeling van een afvalzuur met het olivijn proces is het noodzakelijk om te weten of specifieke aanpassingen gemaakt moeten worden, om het reactieverloop of de eigenschappen van de bijproducten te verbeteren. De verwerking van drie afvalzuren met het olivijn proces is getest. Het gaat om de volgende afvalzuren, i) zwavelzuur (2.9 M) met anorganische verontreinigingen van de titaanwitproductie ii) zwavelzuur (12.8 M) met organische verontreinigingen en iii) zoutzuur (9.7 M) eveneens met organische verontreinigingen. Het neutralisatie gedrag van de afvalzuren wordt vergeleken met zuiver zwavelzuur. De

geneutraliseerde oplossing van het titaanwit afvalzuur wordt verder verwerkt, om te onderzoeken of het mogelijk is een zuivere magnesiumsulfaat oplossing als bijproduct te maken. Het geconcentreerde zwavelzuur met organische verontreinigingen wordt verdund tot een concentratie van 3M, om het neerslaan van magnesiumsulfaat tijdens de neutralisatie te voorkomen. Deze verdunning veroorzaakt het neerslaan van meer dan 80 gewichts% van de organische verontreinigingen, die met behulp van filtratie verwijderd kan worden.
De neutralisatie snelheid van het titaanwit afvalzuur is iets lager vergeleken met zuiver zwavelzuur van dezelfde concentratie. De lagere neutralisatie snelheid wordt waarschijnlijk veroorzaakt door de hogere ion sterkte van het afvalzuur. De aanwezigheid van organische verontreinigingen verhoogt de neutralisatie snelheid.
De silica die wordt geproduceerd door neutralisatie van de afvalzuren is wit. De silica van het titaanwit afvalzuur bevat doorgaans ongeveer 2 gewichts% TiO_2. Het specifiek oppervlak van de silicas geproduceerd met beide afvalzwavelzuren is vergelijkbaar met dat van silica gemaakt met zuiver zwavelzuur. De silica van het afvalzoutzuur heeft een aanmerkelijk lager specifiek oppervlak.
Het grootste deel van de metalen in de geneutraliseerde oplossing van het titaanwit afvalzuur kan verwijderd worden met behulp van een twee-staps neerslag procedure. In de eerste stap wordt de pH verhoogd tot een waarde van 4 à 5, waardoor metalen zoals Ti, Al, V, Cr, and Fe^{III} neerslaan. Het neerslag kan vervolgens door filtratie worden verwijderd. In de tweede stap wordt een magnetische ferriet gevormd, door de pH te verhogen naar een waarde van 7 à 8, waarbij gelijktijdig de Fe^{II} in oplossing geoxideerd wordt. Een magnesiumoxide slurry kan gebruikt worden om de pH te verhogen, dit heeft als voordeel dat er geen nieuwe kationen in de oplossing geïntroduceerd worden.

3) Synthese van magnetische ferrieten

In de literatuur wordt een aantal procedures voor de vorming van magnetische ferrieten in Fe^{II} houdende oplossingen beschreven. De ferrieten kunnen worden gevormd door langzame oxidatie van Fe^{II} oplossingen, met bijvoorbeeld lucht of nitraat, bij pH $\geq$ 8 en bij temperaturen boven 50 °C. Helaas kunnen de in de literatuur beschreven procedures niet direct worden toegepast voor de geneutraliseerde oplossing van het olivijn proces. De benodigde reactietijd voor de vorming van magnetische ferrieten door middel van oxidatie met lucht is bijvoorbeeld voor de geneutraliseerde oplossing vijf maal langer dan de langste oxidatie tijd vermeldt in de literatuur.
Het gebruik van nitraat als oxidator heeft twee belangrijke voordelen, i) het kan in precies stoichiometrische hoeveelheden worden toegevoegd en ii) in vergelijking met het gebruik van lucht veroorzaakt het nauwelijks verdamping. Een procedure wordt ontwikkeld voor de synthese van magnetische ferrieten in geconcentreerde sulfaat oplossingen met behulp van een mengsel van magnesiumoxide en magnesiumnitraat. Drie verschillende sulfaat oplossingen worden gebruikt, i) Mg/Fe sulfaat oplossing bereid uit zuivere chemicaliën, ii) oplossing gemaakt door neutralisatie van zuiver zwavelzuur met olivijn en iii) oplossing gemaakt door titaanwit afvalzuur te neutraliseren met olivijn. De ferriet neerslagen worden onderzocht met behulp van ICP, XRD and TEM, verder worden een aantal magnetische eigenschappen gemeten. Experimenten worden uitgevoerd bij temperaturen variërend van 80 tot 150 °C, gedurende reactie tijden van 2 tot 10 uur. De effecten van het toevoegen van magnetiet kiemkristallen, en variërende hoeveelheid nitraat worden onderzocht.
De experimenten tonen aan dat de synthese van magnetische ferrieten gunstig wordt

beïnvloed door een hogere temperatuur, een langere reactietijd, een hogere initiële Fe^{II} concentratie en toevoeging van magnetiet kiemkristallen. Merkwaardig genoeg hebben deze reactieparameters hoofdzakelijk invloed op de kristalliniteit van de ferrieten, de korrelgrootte van de ferrieten (50 tot 750 nm) blijft bij benadering gelijk.
De berekening van een massabalans van de belangrijke elementen geeft aan dat, na afscheiding van de magnetische ferriet, ongeveer 1 gewichts% van de totale hoeveelheid Ni en ongeveer 3 gewichts% van de totale hoeveelheid Mn in oplossing achterblijven.

Introduction

The disadvantages of continuing industrialisation, such as environmental impacts and the decreasing resources of natural raw materials, have to be mitigated by the development of sustainable technologies. By studying geochemical processes and properties of natural materials, new sustainable processes can be designed. This field of study is known as Geochemical Engineering (Schuiling 1990, 1991).
A typical example of Geochemical Engineering is the use of olivine for the neutralisation of industrial waste acids (Schuiling et al. 1986). Olivine, the fastest weathering silicate mineral, is available in large quantities and provides an excellent buffer for naturally produced acids. The use of olivine for the neutralization of industrial waste acids is therefore appealing. Compared to conventional methods for the neutralisation of waste acids, the use of olivine has the advantage that it produces valuable by-products, like precipitated silica and magnetic ferrites, while it generates no new waste streams (Schuiling et al. 1986). Since the olivine dissolution rate under natural conditions is too low for industrial application, the rate must be increased by raising the temperature or by using higher concentrations of acid or higher olivine surface areas. The properties of the first by-product, precipitated silica, depend strongly on the reaction conditions (Lieftink 1997). A wide range of precipitated silica qualities can be produced by varying temperature, grain size and quantity of olivine and acid concentration. The Olivine Process may, therefore, also be considered as an interesting alternative for current production processes of precipitated silica.
The Olivine Proccess for the neutralization of waste acids was invented in 1985 at the University of Utrecht and patented (Duth Patent PCT NL 85/00026), the patent is currently owned by Geochem Research B.V. From 1986-1987 research on the improvement of the neutralization process and on applications of the neutralization products has been carried out, supported by a grant from the Dutch Ministry of Housing and Environment (VROM). In 1993 research continued under a project financed by the E.C. Brite Euram programme titled "Olivine/Dunite for Industrial and Environmental Applications" (GR-OLIV BRE2-CT92-0.344). Part of the research carried out for this project is presented in this thesis. The main purpose of the investigations was to collect sufficient data, necessary for the design of a pilot plant.
In the first chapter, "*Introduction to the Olivine Process*", a general description of the olivine process is presented. First, existing waste acid problems and conventional solutions are briefly described. Subsequently the potential use of olivine for the neutralization of waste acids is illustrated. This includes a general description of the methodology of the Olivine Process and a discussion of possible uses of the by-products. It is demonstrated that the Olivine Process provides an economically viable and interesting solution for waste acid problems.
One of the prerequisites for the industrial design of any reaction system is a thorough understanding of the reaction mechanisms and reaction kinetics. Chapter 2, "*Mechanism of Olivine Dissolution*", presents a description of the reaction mechanisms of olivine with concentrated acids. In literature several studies on olivine dissolution under natural weathering conditions have been published. These studies are reviewed and combined with data from olivine dissolution experiments in concentrated acid. Main issues that are addressed are the identification of the rate controlling process (diffusion processes ↔ surface reactions) as a function of reaction conditions and the occurrence of leached/precipitated surface layers

and their stability. The identification of the reaction meachansims facilitates the interpretation of the kinetic data, presented in chapter 3, "*Olivine Dissolution in Sulphuric Acid at Elevated Temperatures*". A kinetic rate law for the dissolution of one olivine type is derived by fitting mathematical functions to experimental dissolution data. The influence of temperature, olivine grain size and -amount are quantified. For this study olivine grain sizes smaller than 300 μm were used. This upper limit was used since it is the size of the largest crystals of this olivine type, without internal fractures.

The dissolution behaviour of larger olivine grain size fractions is presented in chapter 4, "*Dissolution Rates of Olivine Grain Size Fractions Larger than 300 μm*".

The chemical and physical properties of natural materials are in general subject to considerable variations. Chapter 5, "*Olivine Type, Implications for the Olivine Process*", describes the neutralization behaviour of olivine from four different sources. It is shown that the differences in olivine properties all influence, in varying degrees, the neutralization rate. The effects are, however, subordinate to the variation of other process parameters like temperature.

For an industrial design of the Olivine Process it is necessary to have accurate measurements of the (exothermic) reaction heat of the dissolution of olivine. In literature no reaction heat measurements of olivine dissolution in acid have been reported. In chapter 6, the results of the measurement of "*Heat of Reaction of the Dissolution of Olivine in Sulphuric Acid*" are presented. Furthermore the experimental reaction heat flux versus time curves are compared with curves calculated with the kinetic olivine dissolution model to provide additional evidence for the validity of the model.

Chapter 7, "*The Olivine Process for the Neutralization of Waste Acids*", describes the neutralization of several types of waste acid with olivine. As each waste acid has its own characteristic composition, specific adaptions have to be made to the Olivine Process for an optimal reaction progress and optimal properties of the reaction products. Three different types of waste acids have been successfully tested: a waste sulphuric acid with inorganic contaminants from the titanium-dioxide production, a waste sulphuric acid and a hydrochloric acid, both with organic contaminants.

The residual solution from the olivine process contains considerable amounts of contaminating metals, like iron and nickel. Since it is necessary to produce a clean rest solution, whether it is used as a raw material or is being dumped, the contaminating metals have to be removed from the solution. The best way to achieve this is by the synthesis of a magnetic ferrite, that can be separated easily from the solution by means of magnetic separation. Chapter 8, "*Theory on Synthesis and Magnetic Properties of Magnetic Ferrites*" presents an overview of literature data on magnetite syntheses and a brief description of the magnetic properties of magnetite and related ferrites. The most promising method for synthesizing magnetic ferrites in the residual solution of the Olivine Process is selected for the experiments described in the next chapter.

The final chapter, "*Synthesis of Magnetic Ferrites in Concentrated Magnesium Sulphate Solutions by Oxidation with Nitrate*", describes the development of the optimal procedure for the synthesis of magnetic ferrites in the residual solutions of the Olivine Process. The residual solutions from the neutralization of both technical grade sulphuric acid and waste sulphuric acid from the titanium-dioxide production have been succesfully tested.

Chapter 1

Introduction to the Olivine Process

Abstract
The use of olivine for the neutralization of waste acids (Olivine Process) has several advantages as compared to conventional techniques for the treatment of waste acids. The potential of the use of olivine is illustrated by reviewing the waste acid production in the European Community, and the conventional disposal procedures. At present, sulphuric waste acid from the production of titanium dioxide constitutes the largest waste acid stream in the EC. Conventional methods for the treatment of waste acids have several disadvantages; neutralization generally produces harmful neutralization cakes and recycling/regeneration processes are energy intensive and expensive.
In order to demonstrate the advantages of the use of olivine for the treatment of waste acids a concise description of the properties of olivine and the Olivine Process is presented. This is followed by a description of possible applications for the by-products of the process.
The main advantages of the use of olivine are the production of precipitated silica, the low energy consumption and the relative low price of olivine.
Studies on the economic viability of the new technique show that the production of precipitated silica makes the process an interesting alternative for current disposal methods.

Introduction

Before any effort is put into the design of a new environmental technology, it is imperative to know whether the new technology has profound advantages, such as a sustainable input of energy and raw materials, and the manufacturing of useful products.
This chapter indicates the potential of the use of olivine for the neutralization of waste acids. The production of waste acid in the European Community, and the conventional treatment techniques are briefly described. Subsequently, the properties of olivine and the methodology of the Olivine Process are discussed, followed by a description of possible applications of the products of the Olivine Process. The reported information provides a general framework for the research presented in this thesis.

Waste acid production in the E.C.

Industrial waste acids are produced by a wide range of industries. A recent investigation of waste acid production in the European Community (v. Enk, 1994) has revealed that more than 95 % of all waste acids is produced by the following branches of industry:
chemical industry, titanium dioxide industry, steel processing, base metal production, electrical engineering, glass industry, automobile industry, energy supply, cokes production and waste incineration.
The waste acids range in concentration from high, used as process solvents or catalysts, to intermediate, used for pickling of metal surfaces and galvanic solutions, and weak, resulting from flue gas treatment.
The total waste acid production in the European Community in 1987 was estimated at 5027 kilotons of 100 % H_2SO_4 - and 876 kilotons of 100 % HCl equivalents.
Due to stricter regulations regarding the dumping of acidic wastes (waste acids and neutralization sludges), the production of waste acids has decreased considerably. This was achieved either by the regeneration of spent acids or by adaptations of waste acid producing processes.
The decrease resulted in an estimated waste acid production in 1994 of 2000 kilotons of 100 % H_2SO_4- and 100 kilotons of 100 % HCl equivalents. About 70 % of the total amount of sulphuric waste acids is of high concentration (pH < -1) and results entirely from chemical processing; 61% from titanium dioxide production and 39 % from the organic chemical industry.
It is expected that increasing regeneration of concentrated waste acids, and process adaptions will further decrease the amount of concentrated spent acids. However, the amount of weak waste acids from flue gas treatment may increase in view of the tightening legislation on sulphur and chlorine emissions.

Conventional waste acid disposal

Conventional methods for waste acid disposal can be divided into three categories:
(i) Dumping (ii) Neutralization and (iii) Recycling/regeneration. Nowadays it is clear that dumping of waste acid directly in the environment is unacceptable. Under special conditions, however, dumping does occur; in the United States underground disposal of dilute waste acids is permitted (Brower et al., 1989; de Graaff, 1997), under the constraint that hazardous waste is geochemically transformed into non-hazardous waste. At present Dutch legislation prohibits the dumping of potentially harmful waste. Storage or disposal of wastes in the subsurface is arranged under the Mine-law and permitted under the constraint that the

environmental risk is acceptable. However, apart from some back-fill operations related to salt solution-mining, underground disposal of wastes is not applied in the Netherlands.
The second option for waste acid disposal, neutralization with bases, is frequently applied. Limestone is widely employed, since it is relative cheap (1.4-3.5 US$ per kmol H^+). Other bases such as sodium and magnesium hydroxide (7.3-17.5 US$ per kmol H^+) are also used in order to achieve a better process control. The reaction product of the neutralization is a sludge that, after de-watering, yields a neutralization cake. Under certain conditions it can be disposed of as ordinary waste; otherwise it has to be stockpiled on special disposal sites, chemically treated, or incinerated. The processing costs of waste sulphuric acid from a titanium dioxide plant using soda-ash was estimated by Hahn and Hendriks (1994) at 11.2 MUS$ per year (for 330 kilotons waste acid per year).
The last method, regeneration, is used for an increasing amount of waste acids. For sulphuric waste acids this is done by concentration of the acid, to about 70 % H_2SO_4, followed by incineration at 1000 °C. Subsequently the sulphur oxides are reconverted to sulphuric acid. A disadvantage of recycling processes is, however, their high energy consumption.
The conventional waste acid treatment techniques have several disadvantages. Dumping in geochemically safe environments is currently not applied for concentrated waste acids, neutralization produces generally harmful neutralization cakes, that require further treatment or storage in special deposits, and recycling processes are expensive.
In order to overcome the disadvantages of conventional neutralization and regeneration/recycling processes the Olivine Process was designed. This process uses olivine, a magnesium silicate, for the neutralization of waste acids. In the following section a brief description of olivine properties is presented, followed by a concise description of the neutralization process and the properties of the by-products.

Properties and current uses of olivine

The mineral olivine $(Mg,Fe)_2SiO_4$ is the main component in ultramafic rocks such as dunite (> 90 % olivine) and peridotites (40-90 % olivine). The chemical composition of these ultramafic rocks reflects the composition of the earth's mantle. At the earth surface ultramafic rocks are generally present as large intrusive bodies.
Other minerals present in ultramafic rocks are pyroxenes (usually enstatite $(Mg,Fe^{II})SiO_3$ and diopside $Ca(Mg,Fe^{II})Si_2O_6$), amphiboles, spinel $(Mg,Fe^{II})(Cr,Al)_2O_4$ and minor amounts of phlogopite, apatite and sulfides. Generally some minor amounts of the natural alteration products of olivine are also present in these ultramafic rocks, such as serpentine $(Mg_3Si_2O_5(OH)_4)$, brucite $(Mg(OH)_2)$, magnesite $(MgCO_3)$, talc $(Mg_6Si_8O_{20}(OH)_4)$, magnetite (Fe_3O_4) and chlorite $((Mg,Al,Fe)_{12}(Si,Al)_8O_{20}(OH)_{16})$.
The olivine crystals in ultramafic rocks are generally broken up, and the fractures form irregular networks, rather than regular cleavage patterns (Nockolds, 1979; Ehlers, 1982)
Chemically the mineral olivine forms a complete (isomorphous) solid solution series between the pure Mg end-member forsterite (< 10 % Fe) and the pure Fe end-member fayalite (< 10 % Mg). The composition is generally described as $FO_{\%}$ which represents the atomic percentage of forsterite in the forsterite-fayalite mixture. The magnesium-rich olivine is the most abundant type. Trace elements usually present in natural olivine are Ni (especially in Mg-rich olivines), Mn, Ca and Co.
The olivine crystal structure consists of individual $[SiO_4]$ tetrahedra, linked by Mg/Fe atoms, that are consequently octahedrally surrounded by O-atoms. It is important to note that in the

olivine structure no Si-O-Si bonds are present, that are generally very strong and resistant to weathering. Consequently, olivine is the fastest weathering silicate mineral (Goldich, 1938; Loughnan, 1969). According to van Herk and Pietersen (1987), the reactivity of olivine towards acid is at least ten times higher compared to the other magnesium silicates serpentine and enstatite, usually present in ultramafic rocks.

In table 1.1 some physical properties of olivine are presented. Important to note is the high hardness and the high melting temperature. Due to these properties magnesium-rich olivine has found important industrial applications. The annual global consumption of olivine amounts to 7000 kilotons (EC report, 1995). The main application is the use in steel industry as an additive in blast-furnaces, for adjustment of the viscosity of the slag (thereby replacing the combined use of dolomite ($CaMg(CO_3)_2$) and quartz, and increasing the thermal efficiency). The refractory properties enable one to use olivine as foundry sand for metal-casting (mainly high-manganese steels) and as oven-linings, (mainly for iron and steel processing installations). In this field of applications it competes with chromite and zircon as foundry sands and with high-alumina refractories. The application of olivine as blasting abrasive and in water jet cutting is gaining in popularity due to tightening legislation on the use of abrasives containing free silica.

Property	Forsterite	Fayalite
Hardness	6.5 - 7	
Density [$\cdot 10^3$ kgm^{-3}]	3.21	4.34
Melting temperature [°C]	1910	1503

Table 1.1 Physical properties of olivine

At present the largest producers of olivine are located in Norway (A.S. Olivine & North Cape Minerals) and Spain (Pase Espana), smaller amounts are produced in Austria (Magnolith Gmb), Italy (Nuova Cives Sp. A.) and Sweden. The price varies, depending on the quality, between US$ 25-100 per ton.

Concise description of the Olivine Process

The Olivine Process for the neutralization of waste acids will be described, using waste sulphuric acid from the titanium dioxide industry as an example. A schematic process flow diagram is presented in Figure 1.1. In the first section the waste acid is neutralized at elevated temperatures with ground forsteritic olivine rock. The reaction equation is :

$$(Mg,Fe)_2SiO_4 + 4\ H^+ \rightarrow Si(OH)_4 \downarrow + 2\ (Mg,Fe)^{2+}$$

The neutralization is preferably carried out under a nitrogen atmosphere, in order to prevent oxidation of the Fe^{II}. The reaction goes to completion (pH 9-10) even at room temperature. For an industrial application, however, the reaction rate has to be increased, e.g. by increasing the temperature or decreasing the grain size of the olivine (acceptable reaction times, < 10 hours, are obtained in the temperature range 70-100°C with olivine grain sizes < 200 μm). Although it is theoretically possible to neutralize the acid completely, the neutralization is stopped at pH 2, firstly in order to prevent contamination of the silica with metal precipitates, and secondly because the reaction rate falls progressively at decreasing H^+ concentration. The neutralization yields a mixture of a magnesium/iron-salt solution, precipitated silica, the contaminants originally present in the waste acid and unreacted olivine and inert minerals.

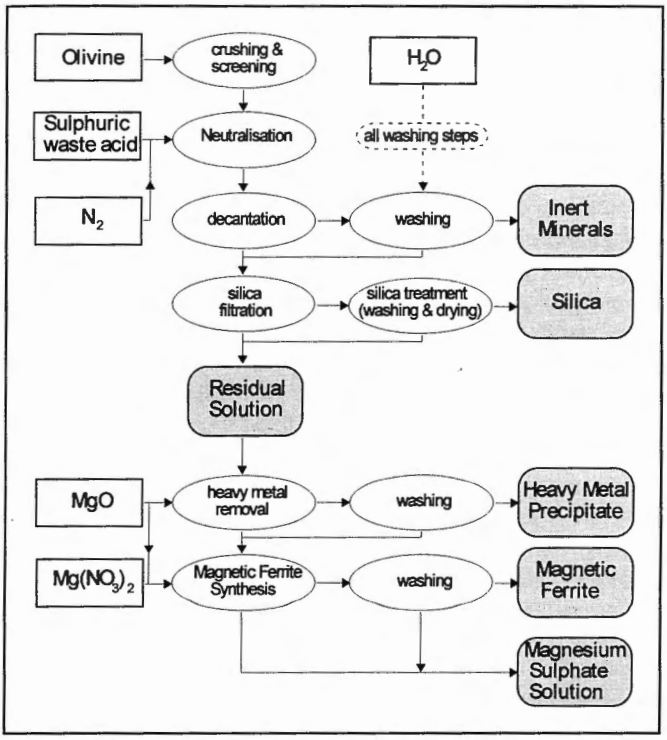

Figure 1.1 Schematic flow diagram of the Olivine Process for the neutralization of waste sulphuric acid from titanium dioxide production.

In the next process section the unreacted olivine and inert minerals are removed from the reaction suspension by gravitational separation, followed by decantation. Subsequently the precipitated silica is separated from the (mainly $MgSO_4$) solution by pressure filtration. The filtration is preferably carried out using nitrogen gas, in order to prevent the oxidation of Fe^{II} and subsequent precipitation on the silica. A detailed description of the pressure filtration is presented in Appendix 1.1. The filtration is followed by thorough washing of the silica cake in order to remove any soluble salts. The remaining $MgSO_4$ solution contains Fe, Ni, Co and Mn from the olivine, and the contaminants originally present in the waste acid.

Table 1.2 gives a model mass balance for the neutralization of 1 kg of waste sulphuric acid. It is clear that the magnesium salt solution constitutes the largest product stream. Therefore it is necessary that, regardless of the fate of this product (use as raw material or disposal) it is clean. Depending on the type of acid neutralized and the nature of

Input		Output	
Waste acid	1 kg	Residual olivine &	36 g
Ground olivine	190 g	inert minerals	
MgO	26 g	Silica	65 g
		Heavy metal precipitate (Ti, Al, V, Cr, Fe^{III})	13 g
		Magnetic ferrite	33 g
		$MgSO_4$ solution	1.1 kg

Table 1.2 Approximate mass balance for the processing of waste sulphuric acid from TiO_2 industry with the Olivine Process.

contaminants, different strategies have to be followed. The waste sulphuric acid from the titanium dioxide industry contains metals such as Fe^{III}, Mg, Ti, Al, V, Cr and Mn. These metals can be separated as metal hydroxides from the magnesium-sulphate solution by increasing the pH. The pH is raised by addition of a base, a MgO-slurry is most appropriate for this purpose, since it will not introduce 'new' metals in the solution (e.g. Guise and Castro, 1996). Since there is at present no application for a precipitate containing all metals, which therefore has to be dumped, the metals are preferably separated in two steps. In the first step Ti, Al, V, Cr and Fe^{III} are precipitated at a pH of 4, the remaining metals (Fe^{II}, Ni, Mn and Co) are separated at neutral pH. The metal separation efficiency of the second precipitation stage can be improved by simultaneous oxidation of the Fe^{II}. Depending on the rate of oxidation, this results in the precipitation of a magnetic ferrite or an amorphous Fe^{III}-hydroxide containing all other metals. The precipitation of a magnetic ferrite, using O_2 from air as oxidant (Schuiling et al., 1986) is illustrated by the following reaction equation:

$$3\ Fe^{2+} + \tfrac{1}{2}O_2 + 3\ H_2O \rightarrow Fe^{II}Fe^{III}_2O_4 + 6\ H^+$$

The Fe^{II} can be replaced by other divalent metals. The precipitation of magnetic ferrite has the advantage that it can be easily removed from solution by magnetic separation.
The neutralization of waste sulphuric acid with olivine thus generates four products: precipitated silica, magnesium sulphate solution, magnetic ferrite and a small amount of (Ti, Al, V, Cr)-hydroxide precipitate. The last precipitate has at present no application and therefore has to be dumped in a controlled disposal site, possible applications of the other products are discussed in the following section.

Possible applications for the products of the Olivine Process

1) Precipitated silica

At present a wide range of silica products is manufactured industrially for a diverse array of applications. Silicas are mainly used for reinforcing, thickening and flattening purposes. In 1990 the world precipitated silica production capacity was 800 kilotons (Ullmanns Encyclopedia, 1993). It is expected that in the future the silica market will continue to grow due to the development of new uses and the expansion of existing applications.
According to the production procedure two main silica-categories can be recognized: silicas produced in solution, under 100 °C (precipitated silica and silica-gel), and silicas produced at high temperatures from gaseous silica compounds (fumed and fused silica). Precipitated silicas constitute about 75 % of the silica market. The main applications of the different types of silica are displayed in table 1.3.
At present precipitated silica is made by mixing water glass (an alkali-silicate solution) with acid (usually sulphuric acid). As a result the pH of the silicate solution is lowered from about 12.5 to 2, which leads to the precipitation of silica. In this way either silica gel, or, under vigorous stirring and at elevated temperatures, precipitated silica is formed. Precipitated silica is subsequently filtered in filter presses, washed, and dried.
Important silica properties are a.o. specific surface area, particle size and the amounts of silanol-groups (Si–OH) and micropores. The properties of precipitated silica are determined by a large number of reaction parameters, which enables one to produce silicas 'tailor-made' for each application. The most important reaction parameters are the concentration of the reactants, the temperature, the precipitation rate, and the stirring rate. Also the filtration, washing and drying procedure are of influence. Since it is difficult to keep all the parameters constant, precipitated silicas are generally manufactured in batch processes. Silica gels are

produced in both batch and continuous processes.
The silica price varies greatly, depending on the properties; US$ 70 per ton for certain ground silicas to US$ 13000 per ton for surface-treated fumed silica. The price averages around US$ 500 per ton. Technologically the above described industrial synthesis of precipitated silica is complicated, and requires a considerable number of raw materials and process steps. The basis, water glass, is manufactured by melting a mixture of fine quartz sand and alkali carbonate in gas furnaces at 1300-1500 °C (about 5 hours), and subsequently dissolving the alkali silicate product (within several hours) in a slightly caustic solution at 150°C. The final precipitation of silica requires the addition of sulphuric acid. The alkali sulphate by-product is generally diluted and dumped.
It is obvious that silica production according to the olivine process requires less raw materials and process steps. The raw material costs are in addition to that low; the processing of waste acid will even yield revenues. The properties of the 'olivine silica' depend, similarly to those of industrial precipitated silica, on a large number of reaction parameters, such as temperature, reaction rate, stirring rate and the filtration, washing and drying procedure. 'Olivine silicas' have been produced with specific surface areas between 100 and 500 m^2/g with typical particle sizes of 10 nm to 50 nm. Lieftink (1997) has presented a detailed description of silicas produced by the Olivine Process.
There are numerous applications for precipitated silica, depending on its properties. The 'olivine silica' has, as compared to silica produced by conventional processes, the advantage that it can be produced at considerably lower costs due to cheaper raw materials and a reduced number of process steps. The economic opportunities of the silica produced as a by-product of the olivine neutralization process are therefore considerable. Since the possible applications and the prices of silica depend on its properties, it is necessary to establish the influence of all neutralization reaction parameters on the silica properties, in order to produce the desired types of silica. If it is not possible to produce the desired types of silica immediately during neutralization, it is possible to subsequently perform beneficiation processes, which will increase the value of the silica. As a lower end alternative there is the possibility to use the 'olivine silica' as a raw material (e.g. for the production of synthetic clays, zeolites etc.).

Precipitated Silica	Silica-gel	Fumed/Fused Silica
rubber reenforcement adsorbents free-flow carrier filler in paper, foils, paint, glue, tooth-paste & asphalt pesticide support beer clarifier	adsorbents of liquids & gases drying of gases & fluids filler in paint, glue & tooth-paste	viscosity adjuster high-voltage insulators filler in paper catalyst support concrete reenforcement

Table 1.3. Main applications of different silica types

2) Magnesium salt solutions
Depending on the type of waste acid to be neutralized different types and concentrations of magnesium salt solutions are produced as final by-product of the Olivine Process. Several applications exist for Mg-salt solutions. For most applications it is required that the solution is pure.

Since sulphuric and hydrochloric waste acids constitute the largest part of industrial waste acids, the production and application of both magnesium sulphate and magnesium chloride is briefly discussed.

Magnesium salts are mainly produced from natural salt deposits. They are either obtained as by-product from KCl production or directly mined from magnesium-rich salt deposits. Magnesium chloride is furthermore produced from sea-water. Natural magnesium salts are generally highly hydrated, and known to form double salts with mainly K and Ca. Natural compositions of magnesium-sulphate range between epsomite ($MgSO_4 \cdot 7H_2O$) and kieserite ($MgSO_4 \cdot H_2O$), with 6, 5, 4 and 5/4 hydration water molecules. Magnesium chloride occurs mainly as bischofite ($MgCl_2 \cdot 6H_2O$).

Magnesium sulphate is used as a fertilizer (kieserite), as a binder in Sorel cement, as raw material for MgO, Mg-silicates and Mg-stearates, and in the sugar and paper industry. The worldwide production of $MgSO_4$ is, according to Ullmans Encyclopedia (1982), 120 kiloton and that of kieserite 2300 kiloton.

Magnesium chloride is mostly used for electrolytic Mg production, and furthermore as raw material for Sorel cement, as fertilizer, drilling fluid, in the sugar industry, and for the production of MgO. The prices of the different magnesium salts depend on the application, the average price for epsomite is US$ 270 per ton, kieserite is about US$ 400 per ton.

The annual production of $MgCl_2$ as a raw material for the production of metallic Mg is estimated at 500 kiloton, and the production of solutions and hydrates at 171 kiloton (Ullmanns Encyclopedia, 1982).

Although several applications exist for pure magnesium salt solutions, as produced by the Olivine Process, the marketing possibilities also depend on the amounts produced. When, e.g., neutralization of the waste acid of one average titanium dioxide plant is considered, the annual production of magnesium sulphate would roughly amount to 118 kiloton (as $MgSO_4$), which is quite considerable if compared with the annual worldwide production.

3) Iron (hydr)oxide precipitates

A minor product of the olivine process is an iron precipitate, either a magnetic ferrite or amorphous Fe^{III} hydroxide, containing a wide range of other metals, depending on the composition of the waste acid neutralized. The iron precipitates always contain traces of Mg and the trace elements present in olivine, Ni, Mn and Co.

Pure magnetite (Fe_3O_4) has several industrial applications; it is used as electrode material, catalyst, pigment in glass and building materials, and as a filler in plastics and rubber. The magnetic properties are used in heavy media separation and to produce magnetic exchange-resin pellets for water treatment. Natural magnetite is a very good raw material for iron production.

Amorphous Fe^{III} hydroxide is used in gas-cleaning, for water treatment, and as a raw material for certain paints.

For most applications it is required that the ferrites are chemically pure and have well defined physical properties (grain size, crystal structure, magnetic properties). It is therefore unlikely that ferrites produced from the neutralized solution of the Olivine Process can be used directly for existing industrial applications.

However, the high nickel content of the precipitate, up to 3 wt%, makes it a very interesting raw material for nickel production; natural Ni ores contain typically 1-2.5 wt% Ni (Roorda and Queneau, 1973).

Economic considerations

The use of olivine has several advantages, first it produces precipitated silica, an economically interesting by-product. In addition olivine is relatively cheap, between 0.7 and 1.8 US$ per kilomol neutralized H^+. Finally, the energy consumption of the Olivine Process is low due to the exothermic reaction of olivine and acid. Hahn and Hendriks (1994) estimated the annual cost of processing sulphuric waste acid from a titanium dioxide plant (330 kiloton per year) with the Olivine Process at 16.4 MUS$. These processing costs are higher than those involved with the neutralization with soda-ash. However, the production of precipitated silica (about 37 kiloton per year) makes the use of olivine economically interesting. At an average price of 500 US$ per ton, the net annual cash flow will be +0.7 MUS$ (including depreciation).

Conclusions

- Sulphuric waste acid from the production of titanium dioxide, constitutes the largest waste acid stream in the European Community.
- Conventional methods for the treatment of waste acids have several disadvantages. Neutralization generally produces harmful neutralization cakes and recycling / regeneration processes are energy-intensive and expensive.
- Olivine, the fastest weathering silicate mineral can be used for the neutralization of waste acids.
- Compared to conventional methods, the use of olivine has several advantages:
  1) Production of precipitated silica, an economically interesting by-product
  2) Low energy consumption, due to the exothermic reaction of olivine and acid
  3) Relatively low price of olivine
- The production of precipitated silica makes the use of olivine, for the neutralization of waste acids, economically viable.

Appendix 1.1 Silica Filtration

Introduction

The product of the neutralization of 3 M sulphuric acid with olivine is a suspension of precipitated silica in a magnesium sulphate solution. The best way to separate the silica from solution is pressure-filtration, resulting in a silica filtercake. This appendix presents quantitative data on the filtration, and the washing of the silica, on both laboratory (1 liter) and pilot-scale (up to 20 liter reaction volume).

Laboratory scale

For filtration experiments on laboratory scale, a pressure filter with a maximum volume of 2.5 liter was used. In general nitrogen gas was used for filtration, in order to prevent oxidation of Fe^{II} and subsequent precipitation on the silica.
Indicative characteristic silica filtration data are presented in Table 1.4. It is important to note that a significant fraction of the residual solution remains in the filtercake, which calls for washing of the silica cake.

Suspension-pH (25°C)		ranging from 1-2
Volume % of residual suspension, after first filtration (pressure filter 4 bar), in :	Filtrate	60 %
	Filtercake	40 %
Percentage of magnesium sulphate solution in silica cake		35 %
Water content of washed and filtered silica (pressure filter 4 bar)		80 %
Silica yield (washed and dried (100°)) per liter 3 M H_2SO_4		75 g

Table 1.4 General silica filtration data.

According to Coulson et al. (1991) cake-filtration can be described by the following equation:

The relation between filtration time and filtrate volume is given by :

$$\frac{t-t_1}{V-V_1} = k_1 \cdot (V-V_1) + k_2 \quad \textbf{1.}$$

Where t is the filtration time, V the filtrate volume and t_1 and V_1 the time and filtrate-volume passed during the initial, pressure build-up stage respectively. The constants k_1 and k_2 depend on the properties of the cake and the filtration equipment.

The constant k_1 is given by :

$$k_1 = \frac{r \cdot \mu \cdot l}{2 \cdot A \cdot V_f \cdot (-\Delta P)} \quad \textbf{2.}$$

With r a constant depending only on cake properties, μ the solution viscosity, l the cake thickness, A the filtration surface area, V_f the total filtrate volume and ΔP the filtration pressure.

According to equation 1, plotting $(t-t_1)/(V-V_1)$ versus $(V-V_1)$ yields a straight line, the slope can be used to determine the specific cake resistance.

A typical filtration curve, of silica prepared at 70 °C, from Norwegian olivine (N2) with grain size fraction 355-630 μm and 3M H_2SO_4 (reaction time 19 hours) is represented in Figure 1.2. The cake resistance calculated from these data is $2.65 \cdot 10^{14}$ [m^{-2}]. This cake resistance can be considered to be representative for silicas produced by the neutralization of sulphuric acid

with olivine. Since the cake resistance depends on the silica properties, silicas produced under different reaction conditions may have varying cake resistances.

Washing of the silica on laboratory scale was carried out by re-slurrying the silica filtercake in demineralized water, followed by filtration. This procedure can approximately be described by a linear mixing model of the volume of residual solution in the filtercake and the volume of wash water used in each washing step. Chemical analyses (by ICP) of the residual solution and the washing waters, collected in Table 1.5 (data from Jonckbloedt, 1995) illustrate the validity of the linear mixing model. The table presents the Mg and Fe concentrations and the dilution factors of the filtrate and the wash waters produced during neutralization of 1 liter waste sulphuric acid from a titanium dioxide plant. The volume of filtrate remaining in the silica cake was determined at 300 ml (from 1 liter of waste acid). In each washing step the cake was resuspended in 1 liter demineralized water, resulting in a dilution factor of 4.3 for linear mixing behavior. The average dilution factor (for Mg and Fe) in Table 1.5 is 4.6, which is close to the factor predicted by the linear mixing model.

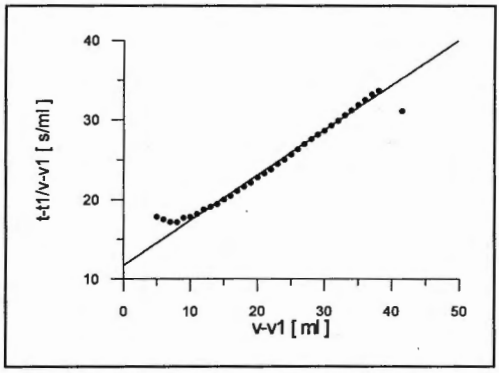

Figure 1.4 Filtration curve. Filtration data (symbols as in equation 2): $A=2\cdot10^{-3}$ m^2, $V_t=4.2\cdot10^{-5}$ m^3, ΔP = 3 bar, $l=1.35\cdot10^{-2}$ m, and $\mu \approx 8\cdot10^{-3}$ kg·s^{-1}·m^{-1}.

Sample	Mg [g/l]	Dilution factor	Fe [g/l]	Dilution factor
Filtrate	70.3	-	30.4	-
1st wash	15.2	4.6	6.48	4.7
2nd wash	3.54	4.3	1.40	4.6
3rd wash	0.78	4.5	0.32	4.4
4th wash	0.16	4.9	0.06	(5.3)

Table 1.5 Mg and Fe concentrations in filtrate and wash waters, produced by processing of waste sulphuric acid from a TiO_2-plant and dilution factors of the washing steps.

Filtration on pilot scale

Filtrations were performed with a recessed plate filter press. The press consists of a number of plates with recessed ribbed surfaces, by pressing the plates together filter chambers are formed between successive plates. Each plate is covered by filter cloth. During filtration the suspension is fed into the filter chambers through a central channel, the filtercake builds up in the chambers, and the filtrate is discharged through a system of channels in the filter plates. A main advantage of this type of filter is the fact that after filtration the filtercake can be washed immediately by pressing clean water through the filtercake. By monitoring the concentration

of solutes in the wash water, washing can be stopped at the desired degree of silica purity.

Table 1.6 shows some data on the filter press used for the filtration experiments. The filtration and washing performance will be illustrated for the filtration of silica, prepared by neutralizing 3 M H_2SO_4 with Norwegian olivine (AFS 50, 100-300 μm) at 90 °C (reaction time 3.5 hours). The data of a large number (20) of filtration runs was averaged. For the filtration of 9.5 liter of silica suspension 4 of the 22 filter chambers were used. At a temperature of 25 °C and a pressure of 4-5 bars, the filtration took an average period of time of 15 minutes (range:11to19 minutes). This yields a filtration capacity of 119 [liter·m^{-2}·hour^{-1}] (flow rate of silica suspension per unit surface area of the filtration equipment). Subsequent washing of the silica filtercake was carried out by pressing tap water, with a temperature of 10-15 °C, through the filtercake. At a pressure of 4-5 bars, the flow rate of water through the 4 filter chambers containing the filtercake was on an average 0.7 liter·minute^{-1}. This yields a wash water flow rate of 125 [liter·m^{-2}·hour^{-1}] per unit surface area. Figure 1.5 shows a typical wash curve (% of solute remaining in the filtercake versus the ratio of wash-water volume and filtercake volume). The amount of solute remaining in the filtercake was determined by monitoring the wash water volume and measuring the chemical composition (by ICP) at regular time intervals. The curve shows that the washing efficiency of silica cake in the filter press is not high; for a reduction of 50 % of the solutes in the cake about 6 times the cake volume of wash water is required. The low efficiency can be attributed to leakage of wash water, and probably also to boundary effects, in the relatively small press. The ratio of boundary length and filtration surface area is 10 m·m^{-2}, which is more than 6 times higher than with a large-scale filter press with plates of 1.5 x 1.5 m. It is therefore to be expected that the washing efficiency is better in larger filter presses.

Type	Tefsa HPL 300/16
Size of plates	30 x 30 cm
Number of chambers	maximum 22
Chamber thickness	2 cm
Surface area per chamber side	400 cm^2
Chamber volume	0.9 liter

Table 1.6 Technical data of the filter press used with filtration experiments on pilot scale.

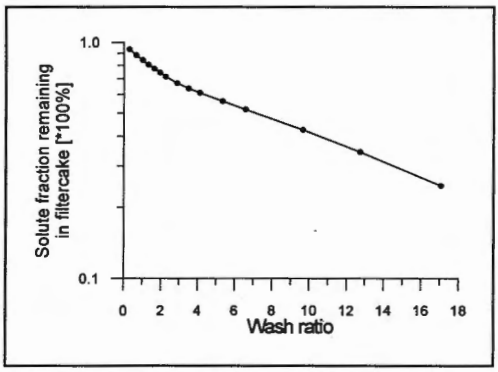

Figure 1.5 Typical wash-curve for the washing of olivine-silica in a HPL 300/16 filter press

Conclusions

The resistance of silica filter cake was determined by laboratory scale pressure filters at $1.32 \cdot 10^{14}$ [m^{-2}] for silica produced by the neutralization of 3M H_2SO_4 at 70 °C with Norwegian olivine (355-630 μm) and a reaction time of 19 hours.

The silica cake typically contains 35 volume % of the total amount of residual solution, it is therefore necessary to wash the silica.

In laboratory scale experiments the silica can be washed by resuspension of the silica cake in water. In this case, the decrease in solute content, in the filter cake due to dilution by wash-

water, can be described by a linear mixing model of wash-water volume and solution volume in the cake.

The use of a filter press for the separation of silica from the neutralized solution, has the advantage that the silica filter cake can be washed immediately, thus obviating resuspension of the cake. Filtration experiments in a pilot-scale filter press showed that the filtration capacity, of silica produced from 3M H_2SO_4 and Norwegian olivine (AFS 50, 100-300 μm) at 90 °C and 3.5 hours reaction time, is 119 [liter·m^{-2}·hour^{-1}] at a pressure of 4-5 bar.

The washing efficiency of silica in the filter press is low, it is expected that scaling-up of the press will improve the efficiency. The wash-water flow rate at 4-5 bars pressure was typically 125 [liter·m^{-2}·hour^{-1}].

Chapter 2

Mechanism of Olivine Dissolution

Abstract

Understanding of the factors that determine the rate of dissolution of olivine in acids at elevated temperatures is essential for the design of an industrial plant for the neutralization of waste acids with olivine. The reaction mechanism of olivine with concentrated acid is described, in order to facilitate the interpretation of kinetic data presented in chapter 3.

The reaction mechanisms are identified by combining literature data, which is only available for dissolution under natural weathering conditions, with experimental studies on olivine dissolution in concentrated acid.

Nowadays it is generally accepted that under natural weathering conditions, the dissolution of olivine is controlled by surface reactions and not by diffusion processes through a surface layer. In unstirred concentrated acid, the silica, released during the dissolution, polymerizes and precipitates close to the olivine surface, thus inhibiting further dissolution. Continued precipitation leads to complete solidification of the olivine bed. In order to prevent this the olivine bed has to be stirred continuously; under these conditions the rate of olivine dissolution is controlled by surface reactions.

Introduction

A prerequisite for the industrial application of any chemical process is a thorough understanding of the reaction mechanisms and reaction kinetics. Hence a profound knowledge of the factors that determine the rate of dissolution of olivine in acids at elevated temperatures is essential for the design of an industrial plant for the neutralization of waste acids with olivine. In this chapter a description of the reaction mechanisms of olivine with concentrated acids is given, in order to facilitate the interpretation of kinetic data to be presented in chapter 3.

In literature several studies on the mechanisms and kinetics of the dissolution of olivine under natural conditions have been published to assess the natural weathering rate. Kinetic data on olivine dissolution is available for the pH range from 1 to 12 at 25 ° C. Some experimental data is available for higher temperatures, up to 70 ° C, but no studies have been reported for lower pH ranges.

The reaction mechanisms for olivine dissolution in concentrated acid are identified by combining literature data with experimental studies on the dissolution of olivine in concentrated acid.

Mechanism and rates of olivine dissolution under natural conditions

Dissolution mechanism

The dissolution of olivine can be subdivided in a number of processes. During dissolution hydrogen atoms are transported from the bulk of the solution to the surface by convection or diffusion. Subsequently they form an activated complex (surface species) and finally the reaction products, Mg^{2+} and $Si(OH)_4$, are transported away from the surface by either convection or diffusion. The overall dissolution rate is determined by the slowest step in this sequence, and is, depending on the reaction conditions, controlled by either diffusion or surface reaction processes.

In early studies on the dissolution of olivine under natural conditions it was suggested that during dissolution leached or precipitated layers could be formed on the surface of the dissolving grains. The formation of a surface layer greatly affects the dissolution rate. If a surface layer is present, the rate is generally controlled by diffusion processes in the surface layer. The distinction between control by aqueous diffusion and by surface reaction can easily be made by variation of the stirring speed, which will only affect diffusion-controlled rates. The identification of rate limitation due to diffusion through a leached or precipitated surface layer is more difficult.

Mathematically it can be demonstrated that, if diffusion processes through a surface layer are rate controlling, the amount of olivine dissolved is a linear function of the square root of time. This is illustrated by the following equation (2.3):

For diffusion in a semi infinite surface layer the flux of species per surface area (J) at the surface is given by (Cussler, 1984):

$$J = \sqrt{\frac{D}{\pi \cdot t}} \cdot (C_{ol} - C_{\infty}) \quad \textbf{2.1}$$

combined with

$$\frac{dC}{dt} = \frac{J \cdot A}{V} \quad \textbf{2.2}$$

and integration to time (t) yields:

$$C(t) = \frac{2 \cdot (C_{ol} - C_{\infty}) \cdot \sqrt{D} \cdot A}{\sqrt{\pi} \cdot V} \cdot \sqrt{t} \quad \textbf{2.3}$$

With C(t) the concentration of a dissolved species (e.g. Mg or Fe), C_{ol} the "concentration" of that species in olivine and C_{∞} the concentration of the species at the surface of the leached layer. D is the diffusion coefficient of the dissolved species in the leached layer, A the surface area of the olivine, and V the volume of the solution.

Equation 2.3 shows that if the surface area of the olivine and the concentration of the dissolved species at the external edge of the surface layer does not change with time, which is true if only a small fraction of olivine is dissolved, the amount of dissolved olivine is a function of the square root of time. This type of dissolution is sometimes described as parabolic dissolution behavior (e.g. Luce et al., 1972; Lasaga, 1984).
The occurrence of parabolic dissolution behavior can be indicative for the formation of a leached or precipitated surface layer. The formation of a surface layer furthermore implies that dissolution is incongruent, which is indicated by a ratio of olivine constituents in solution being different from that of the solid phase. Another feature that is characteristic for diffusion-controlled dissolution is the development of evenly rounded grains without etch features. It should also be possible to identify some sort of surface layer by micro-analytical techniques.
If the dissolution rate is controlled by surface reactions the amount of dissolved olivine is a linear function of time (for small amounts of olivine dissolved). In contrast to diffusion control the dissolution is congruent and dissolution features such as etch pits and dissolution cracks are developed.
Initial experiments on the dissolution of olivine were conducted by allowing mixtures of unbuffered solutions of varying initial pH and ground olivine to reach equilibrium at room temperature (Keller et al., 1963; Huang and Keller, 1970; Luce et al., 1972) . The dissolution progress was monitored by analyzing one or more solutes at regular time intervals. Luce et al. (1972) performed dissolution experiments of ground olivine in vigorously stirred aqueous solutions with initial pH's ranging from 1.68 to 9.58. They found that at the low pH range a quick exchange of one Mg^{2+} by 2 H^{+} occurred, followed by parabolic dissolution, which changed slowly into linear dissolution. This behavior was explained by the following dissolution sequence: I) rapid exchange of surface Mg ions by H^{+}, ii) formation of a leached/precipitated surface layer leading to the parabolic rate, and iii) continued dissolution stage where the rate of dissolution at the external edge of the surface layer equals the rate of formation at the inside, resulting in a surface layer of constant thickness and a linear dissolution rate. Due to the fact that the Mg-to-Si ratios in solution were higher than stoichiometrically expected, the surface layer was identified as a Mg-depleted silica layer.
As possible causes for the parabolic dissolution behavior Luce et al. suggested two possible diffusion mechanisms: I) a non steady-state diffusion mechanism through the mineral lattice, and ii) a quasi steady-state diffusion mechanism through a distinct leached layer.
Investigation of partly dissolved olivine grains by X-ray diffraction, infrared absorption and mass-spectrometric analysis of mineral surfaces, sputtered by argon ion bombardment, did not reveal the existence of leached layers. Therefore it was concluded that non steady-state diffusion through the mineral lattice was rate controlling. It was furthermore concluded that at low pH levels (<1.68), the initial exchange process is negligible as compared to the surface dissolution process and that parabolic kinetics are not observed.
There are several arguments against the formation of a leached/precipitated surface layer to explain the parabolic dissolution behavior of olivine. First of all it is important to realize that Luce et al. did not buffer the pH during their dissolution experiments, causing significant increases in pH levels during dissolution. Since the dissolution rate of olivine depends on the pH, it is obvious that the rates decreased during the experiments. In addition to that it has been suggested (Schott and Berner, 1983; Murphy and Helgeson, 1987) that during the dissolution of olivine protonated silica tetrahedra can detach rapidly from the mineral surface

due to the fact that no Si-O-Si bonds have to be broken. This mechanism makes the formation of a leached layer highly unlikely. Another feature that may explain the parabolic dissolution behavior is the presence of a large number of very fine particles (<1μm) on the ground olivine used for the dissolution experiments. This was suggested by Holdren and Berner (1979), who compared dissolution rates of untreated ground feldspars and feldspars that were pre-treated with a mixture of HF and H_2SO_4 in order to remove all fine particles. Whereas the untreated feldspar dissolved parabolically, the etched feldspar dissolved linearly from the beginning of the experiment.

Furthermore several authors tried to demonstrate the existence of precipitated or leached surface layers on dissolving olivine grains by micro-analytical techniques. Grandstaff (1978) studied ground olivine grains that had undergone dissolution in a NaAc-HAc buffer of pH 2.6 at room temperature by Scanning Electron Microscopy (SEM). This investigation revealed that no thick, surface covering layers were formed. The specific surface area increased significantly during dissolution, which was confirmed by an investigation by SEM, that revealed extensive formation of etch-pits and other etch features on the crystal planes. Grandstaff concluded that the high initial dissolution rates of parabolic behavior were due to an increase in specific surface area by the formation of etch-pits and other etch-features. He suggested that the dissolution rate of olivine was controlled by surface reactions rather than by diffusion through a surface layer, since no surface layer thicker than 100-200 Å (the resolution of SEM) was formed during dissolution.

Van Herk et al. (1989) investigated ground olivine grains that had undergone dissolution at constant pH of 1-3 at 40-70 °C by SEM. This study also revealed extensive formation of etch-features, such as etch-pits and dissolution cracks. Additionally van Herk found olivine dissolution rates that were first order in olivine concentration. He therefore concluded that, under the conditions investigated, the dissolution rate of olivine is controlled by surface reactions and not by diffusion.

Although investigations by SEM did not identify thick surface layers inhibiting dissolution, two studies with micro-analytical techniques of higher resolution, have shown that very thin altered surface layers might exist on dissolving olivine grains. Schott and Berner (1983) performed an X-ray Photo-electron Spectroscopy (XPS) study on fayalite. The ground fayalite grains were subjected to dissolution in K-H-phthalate buffers of pH 1-6 at room temperature, under both oxygen-free and -containing atmospheres. They found that in the absence of oxygen (preventing oxidation and subsequent precipitation of the olivine-Fe^{II}) or at low pH, the dissolution was congruent after the formation of a thin protonated surface layer. The maximal average thickness of this surface layer was calculated to be 10 Å. Based on long term congruent dissolution Schott and Berner concluded that this protonated surface layer was unstable and did not grow with time.

Recently Wogelius and Fraser (1996) provided evidence that some type of leached surface layer may form. They investigated the surface of olivine crystals that had reacted at pH 4 by Elastic Recoil Detection Analysis (ERDA), which demonstrated the existence of elevated hydrogen concentrations up to a depth of 1000 Å.

Dissolution rate

Several studies have been carried out to quantify the olivine dissolution rate, under natural weathering conditions. In all studies it was assumed that, under the experimental conditions used, the olivine dissolution kinetics were controlled by surface reactions rather than by diffusion through a surface layer (Siegel and Pfannkuch, 1983; Grandstaff, 1986; Blum and

Lasaga, 1988; van Herk et al., 1989; Wogelius and Walther, 1991, 1992). With the surface reaction rate-determining, the olivine dissolution rate is given by the general equation:

$$\frac{d\,[C_{ol}\,]}{dt} = -\,k_T \cdot S_{ol}{}^{m} \cdot A_H{}^{n} \qquad \textbf{2.4}$$

where C_{ol} is the "olivine concentration" in [mole·l^{-1}], S_{ol} the reactive olivine surface area, A_H the hydrogen ion activity, and k_T a constant depending on a.o. the temperature. The rate coefficients m and n are not equal to the stoichiometric coefficients in the reaction equation and have to be determined experimentally. The temperature dependent rate constant, k_T, usually follows an Arrhenius relationship according to:

$$k_T = A \cdot e^{-\frac{E_a}{R \cdot T}} \qquad \textbf{2.5}$$

Where E_a is the activation energy of the reaction, R the gas constant and A a pre-exponential factor. Conventional procedures for the determination of the rate equation coefficients in equation 2.4, involve addition of an excess of one of the reactants or measuring the initial rates (Fogler, 1986). With the first procedure one of the reactants is added in excess in order to keep the concentration effectively constant during the reaction, while the concentration of the other reactant is monitored. The time dependent concentration of the excess reactant can thus be replaced by a constant. Subsequent plotting of the log of the rate versus the log of the monitored concentration yields a straight line with a slope equal to the corresponding rate coefficient. This procedure has to be repeated to find the rate coefficient of the other reactant. For the second method the initial reaction rate is monitored in a series of experiments at different initial concentrations. Subsequent plotting of the log of the initial rate versus the log of the initial concentration of one of the reactants yields a straight line with a slope equal to the rate coefficient of the plotted reactant.

In the studies reported in literature, olivine was allowed to dissolve (to small extents) in aqueous solutions of a constant pH level and temperature. The progress of the dissolution was monitored by analyzing one or more solutes at regular time intervals. The specific surface area of the olivine was usually measured by gas adsorption and calculated according to BET-theory, and the dissolution rates were generally presented as [mole olivine]·[olivine surface area]$^{-1}$·[time]$^{-1}$. In only one study the olivine added was allowed to dissolve almost entirely (van Herk et al., 1989) to establish a relation between the olivine dissolution rate and the "olivine concentration". The measurement of the dissolution rate at different pH levels enabled the authors to determine the rate law coefficient of H^+. In three studies rates of olivine dissolution were measured at different temperatures, to calculate the activation energy of the reaction.

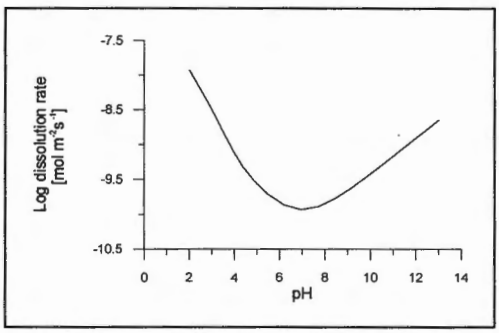

Figure 2.1 Log olivine dissolution rate versus pH (data from Blum, 1988)

Figure 2.1 displays the rate of the dissolution

of olivine as a function of the pH. This curve is typical for the dissolution of silicates: in the acidic range the dissolution rate decreases with increasing pH and in the alkaline range the rate rises with increasing pH. In the following discussion of the literature, dissolution data in the acidic-neutral pH range will be reviewed.
In table 2.1 an overview of the published rate data is presented. Where required, the dissolution rates have been converted to SI-units. In order to compare the rate data the dissolution rate of olivine at 25 °C and pH 4 is calculated and presented in the last column. It can be clearly seen that the rates predicted by Siegel and Grandstaff are lower than the others, which may be due to the fact that the specific surface areas they reported are too high. Murphy and Helgeson (1985) and Wogelius and Walther (1991) have suggested to adjust the specific surface area downward by a factor of 20, with this correction all rates at 25 °C and pH 4 are of the same order of magnitude.

Order in H^+ activity (n)

The dissolution rate depends on the H^+ activity to a fractional power (n in equation 2.1). Table 2.1 shows that powers ranging from 0.33 to 0.56 have been reported. Grandstaff is the only author who found a higher order of 1.09. He suggested that this first order with respect to the hydrogen concentration was due to the fact that the reaction of the first H^+ most likely results in disruption of the mineral structure and, hence, is slower than the subsequent reaction of other H^+ and thus rate limiting. Murphy and Helgeson (1987) stated that the dissolution rates are controlled by the formation of activated complexes at active surface sites and that the stoichiometry of the activated complexes can be inferred from experimental rate data. They explained the first order with respect to hydrogen ions observed by Grandstaff by assuming the formation of an activated complex consisting of a surface species at an active site and a single hydrogen ion. However, all other authors find non-linear pH dependencies. Blum and Lasaga (1986) claim that mineral dissolution rates have a first order dependence on the surface concentration of specific surface species (in the acidic to neutral pH range this is $x\text{-}H_2$, where x represents an active surface site), which can be determined by surface titrations. They conclude that in the acidic range the dissolution mechanism depends on the exchange of 2 H^+ ions for one Mg^{2+} ion at surface active sites. (In the basic pH range a different mechanism dominates; the tetrahedral oxygens are deprotonated, resulting in a negative surface charge. This leads to polarization and inherent weakening of the Si-O bonds. Brady and Walther (1989) confirm this mechanism; at basic pH the proportionality between surface charge and dissolution rates indicates that activated complexes are primarily formed on silica surface sites.)

Temperature dependence

In three studies the activation energy of olivine dissolution was determined, by carrying out experiments at different temperatures. In all studies it was found that the temperature dependent rate constant (k_T in equation 2.1) followed an Arrhenius relationship (equation 2.2). Grandstaff (1986) reported an activation energy of 38.1 $kJ \cdot mole^{-1}$, while van Herk et al. (1989) and Wogelius and Walther (1992) reported higher activation energies. From the data of van Herk et al. (1989) an activation energy of 70±5 $kJ \cdot mole^{-1}$ for olivine dissolution in sulphuric acid and of 58±5 $kJ \cdot mole^{-1}$ in hydrochloric acid was calculated. Wogelius and Walther (1992) reported an activation energy of 79±10 $kJ \cdot mole^{-1}$, determined from experiments carried out at only two different temperatures. These activation energies lie close to the mean activation energy, reported by Lasaga (1984), of 60 $kJ \cdot mole^{-1}$ for the dissolution of silicates. This activation energy is much higher than the activation energy of diffusion

processes in aqueous solutions, which is about 20 kJ·mole^{-1} (Lasaga, 1984; Drever, 1988). The high activation energy of olivine dissolution therefore provides additional evidence that the dissolution rate is controlled by surface reactions.

Author	Conditions: T [°C]	pH	Olivine properties	Solution chemistry	Dissolution rate [mole·m^{-2}·s^{-1}]	Log rate at 22°C and pH 4
Siegel 1983	22	4	FO_{79} 38 - 42 μm S_a = 1.3 m^2·g^{-1} Max. 2.2 % diss.	HNO_3	$R = 10^{-10.4}$	-10.4 Corrected: -9.1
Grandstaff 1986	1 - 49	3 - 5	FO_{81} 74 - 194 μm S_a = 0.93 m^2·g^{-1} Max. 6.6 % diss.	HCl in 0.1 M KCl	$R = k_T \cdot a_H^{1.09}$ k_T : E_a = 38.8 kJ·mole^{-1} $A = 10^{0.27}$	-10.97 Corrected: -9.67
Blum 1986	25 ?	1 - 12	?	?	Acid-neutral range: $R = 10^{-8.88} \cdot a_H^{0.56}$	-9.12 (25 °C ?)
v. Herk 1989	40 - 70	1, 2 & 3	FO_{93} 105 - 125 μm S_a = 0.63 m^2·g^{-1} 80 - 99 % diss.	H_2SO_4&HCl	**H_2SO_4 :** $R = k_T \cdot C_{ol}^1 \cdot a_H^{0.43}$ k_T : E_a = 70 ± 5 kJ·mole^{-1} $A = 10^{7.06}$ **HCl :** $R = k_T \cdot C_{ol}^1 \cdot a_H^{0.33}$ k_T : E_a = 58 ± 5 kJ·mole^{-1} $A = 10^{4.43}$	H_2SO_4 : -9.0 HCl : -9.12
Wogelius 1990	25	2 -12	FO_{100} & FO_{91} 149 - 250 μm S_a = 0.0598 m^2·g^{-1} & 250 - 420 μm S_a = 0.0307 m^2·g^{-1}	HCl	Acid-neutral range: $R = 10^{-7.04} \cdot a_H^{0.54} + 10^{-10.28}$	-9.3
Wogelius 1992	65	2, 6 & 9.8	FO_{91} same fractions as Wogelius 1990	HCl	Acid-neutral range: $R = 10^{-5.46} \cdot a_H^{0.50} + 10^{-9.49}$ combination with 25 °C data yields: k_T : E_a = 79 ± 10 kJ·mole^{-1} $A = 10^7$	

Table 2.1 Overview of literature data on olivine dissolution rates.
FO.=mole-% of forsterite in olivine, S_a=Olivine specific surface area, % diss.=% of mineral dissolved during the dissolution study, R=dissolution rate, C_{ol}=olivine concentration, a_H=H^+-activity, k_T=temperature dependent rate constant, E_a=activation energy and A=preexponential factor of the Arrhenius equation.

Relation between "olivine concentration" and surface area

Only van Herk et al. (1989) attempted to quantify the dependency of the dissolution rate on the 'olivine concentration'. They found a first order dependence of the dissolution rate on the olivine concentration [moles·l^{-1}] (see Table 2.1) which they attributed to a surface reaction being rate controlling. However, if surface reactions are rate-controlling, a first order dependence of the dissolution rate on the surface area of the olivine rather than on the olivine concentration would be expected. For a collection of spherical olivine grains of similar diameters a dependence on the surface area of the olivine would result in a rate proportional to $C_{ol}^{2/3}$.

Effect of olivine composition

It is worthwhile mentioning that some investigations have been carried out to study the effect of compositional variations of olivine on the dissolution rate. Wogelius and Walther (1990) concluded from experiments with olivine containing varying amounts of forsterite that at 25 °C in the pH range 2.0-5.7 the olivine dissolution rate is not significantly influenced by redox reactions, the presence of CO_2 at atmospheric levels, and the compositional variation of olivine from FO_{100} to FO_{91}. Their experiments (1992) with fayalite (FO_6) furthermore showed that in the pH range 2-7 at 25 °C in a deoxygenated atmosphere, the dissolution rate of fayalite is six times higher than that of forsterite ($R=10^{-5.96}\cdot a_H^{0.69} + 10^{-9.49}$). He suggested that dissolution rates of olivines of intermediate compositions can be calculated by assuming a linear relationship between dissolution rate and olivine composition.

Specific Surface Area

Dissolution rates of silicates are generally normalized on the specific surface area of the dissolving silicate. The correct measure of the specific surface area, however, is still under discussion. To illustrate the difficulties a ground sample of a natural silicate is considered. The surface of the particles produced by grinding can be divided in three categories: I) fresh, previously unexposed surface ii) non-fresh surface, that has undergone natural weathering, and is characterized by etch features, such as etch-pits, small dissolution cracks, etc., and iii) internal surfaces in deep dissolution cracks, that has been produced by natural weathering. Generally a distinction between internal and external surface area can be made based on the transport mechanism; at internal surfaces the transport is controlled by diffusion processes, and at external surfaces by convection.

It has to be realized that the surface area is not equally reactive, as illustrated in figure 2.2. In both cases the schematically represented mineral has the same specific surface area. However, grain B has a higher number of reactive sites than grain A. It is clear that the reactive surface area is not a simple function of the total surface area.

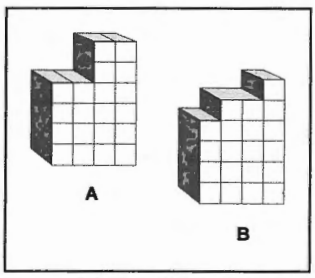

Figure 2.2 Relation between surface area and active sites for two different grains

The easiest method for calculating the surface area is to establish the particle size distribution by a conventional technique, such as sieving or light-scattering, and to calculate subsequently the surface area by assuming that the particles have a distinct (e.g. spherical or cubical) geometry. The thus calculated surface area is usually referred to as the geometrical surface area. It is obvious that the geometrical surface area does not include the area present in superficial etch features and internal surfaces. The geometrical surface can be corrected for the area present in superficial etch features by multiplication with the surface roughness factor. This factor is generally calculated by dividing the surface area measured by gas adsorption according to BET theory by the geometrical surface area. The surface roughness factor has been determined for a number of silicates (White, 1995). The factor appeared to be virtually independent of the particle size for ground silicates with a mean value of 7. For naturally weathered silicates, however, significant higher surface roughness factors were found that showed no relation with the particle size.

In most dissolution studies the specific surface area has been measured by gas adsorption techniques and calculated according to BET-theory, resulting in the so-called BET surface area. With this procedure surface areas of surface features larger than 3-4 Å can be measured;

the reproducibility is generally in the range of 10 to 20 % (Brantley, 1995). In most studies the dissolution rate is normalized on the initial specific BET surface area. Although generally only small percentages of the mineral are dissolved, the specific surface area may change drastically due to the formation of etch features. It was therefore suggested that the final specific surface area should be used to normalize dissolution data (Brantley, 1995). There are, however, several problems that might arise. First there is the possible formation of secondary precipitated (silica) phases, that erroneously increase the measured surface area, resulting in lower normalized dissolution rates. Furthermore it is possible that the dissolution rate in deep etch-features, that contribute significantly to the specific surface area, is controlled by diffusional transport and thus lower than the rate at other surfaces, which will also result in lower normalized dissolution rates.
Two studies have been conducted, indicating that sample preparation methods may also affect the specific surface area. Eggleston et al. (1989) investigated the effect of aging on the specific surface area of ground (< 75 μm) diopside (a pyroxene). He observed a slight decrease in specific surface area within a period of 250 days. This was attributed to the healing of micro cracks, caused by grinding. Anbeek (1992) concluded from his dissolution experiments with ground feldspars that surfaces that contain large numbers of dissolution active surface sites were exposed relatively early in the grinding process. The number of active sites per surface area would then decrease during continued grinding.
Obviously it is difficult to find a measure of the true reactive surface area, which is required to normalize dissolution rate data. Most likely it is not a simple function of the total mineral surface area. As an approximation geometrical or BET surface areas have to be used. The geometrical surface area does not include the area present in superficial etch features. However, this can be incorporated by multiplication with the surface roughness factor, which is independent of the grain size for ground silicates. The use of the BET specific surface area has the disadvantage that the reproducibility varies from 10 to 20 %. Furthermore it is important to measure the specific surface area at an appropriate time, most authors use the initial specific surface area, which may yield overestimated normalized dissolution rates.

Mechanisms of olivine dissolution under Olivine Process conditions
Considering the large differences between 'natural' conditions and 'Olivine Process' conditions, it is unlikely that the same dissolution model can be applied for both cases.
For the dissolution of olivine in 3M sulphuric acid two important points have to be considered in relation to the dissolution conditions studied in literature. First the dissolution rate is much higher, possibly giving rise to diffusion-controlled dissolution due to transport limitations of H^+ to, and Mg^{2+} from the reacting mineral surface. Secondly the silica monomers will start to polymerize as soon as their concentration exceeds 100 $mg \cdot l^{-1}$ (Iler, 1979). The polymerization rate is enhanced at decreasing pH and increasing temperature. In appendix 2.1 the rates of the three important processes, dissolution, diffusional transport, and silica polymerization are assessed by "back of the envelope" calculations. The dissolution-rate determining process can be identified by comparing the calculated rates. For a 100 μm spherical olivine particle the diffusional transport rates of Mg^{2+}, H^+ and $Si(OH)_4$ are not rate-controlling as they are a factor of 10^4 higher than the rates at which these species are released from the mineral surface. However, the silica polymerization rate is 10^{10} times higher than the diffusional transport rate. These calculations suggest that in non-stirred systems silica will precipitate close to the dissolving olivine grains. This is clearly demonstrated in a SEM image, shown in picture 2.1, of an olivine grain that has undergone dissolution in unstirred

3M H_2SO_4 at 25 °C. The olivine grain is entirely covered by a layer of precipitated silica, which exhibits shrinkage cracks due to drying of the hydrous layer of precipitated silica. Electron microprobe studies indicated that the layer consists solely of silica and that the adjacent olivine surface has not been leached. A SEM image of olivine grains that were stirred during dissolution, represented in Picture 2.2, shows that these grains are free of precipitated silica layers.
The continued precipitation of polymerized silica on dissolving olivine grains leads in general to complete solidification of the olivine bed (Jonckbloedt 1995, 1996, 1997). To prevent the solidification the olivine bed has to be agitated continuously. Under these conditions the rate of olivine dissolution is controlled by surface reactions.

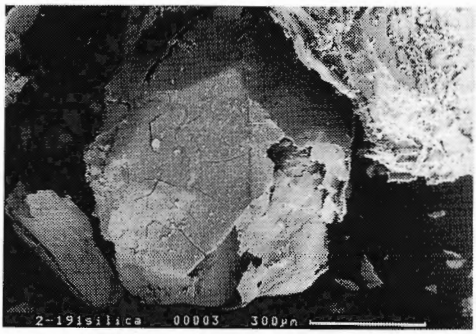

Picture 2.1 Partly dissolved olivine grain, covered by a layer of precipitated silica

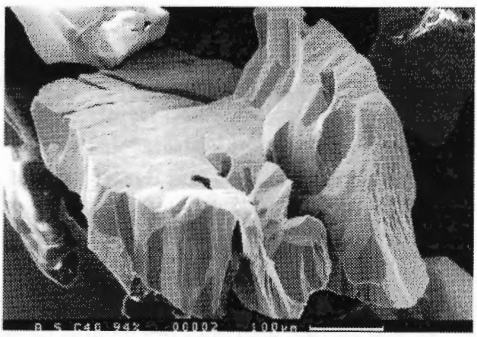

Picture 2.2 Partly dissolved olivine grain, showing etch pits and dissolution cracks

Conclusions

Olivine dissolution under natural conditions

- Under conditions of vigorous stirring, as employed in all experiments on olivine dissolution, no thick, continuous precipitated or leached surface layers are formed on the olivine grains. The dissolution of olivine is therefore kinetically controlled by surface reactions rather than by diffusion processes.
- SEM investigations show that during dissolution extensive etch features, such as etch-pits and dissolution cracks are formed. Continuous surface layers inhibiting dissolution are not observed.
- XPS and ERDA studies have demonstrated the existence of protonated surface layers with thicknesses from 10 to 1000 Å on dissolving olivine grains. It has been demonstrated that these surface layers are unstable and do not grow during dissolution.
- The dissolution rate is proportional to the hydrogen ion activity to a power ranging from 0.33 to 0.56. This has been explained by a dissolution mechanism that depends on the exchange of 2 H^+ ions for one Mg^{2+} ion at active surface sites.
- Activation energies reported for the dissolution of olivine range from 59 to 70 $kJ \cdot mole^{-1}$. This confirms the assumption that the dissolution rate is controlled by surface reactions.
- The dissolution rate of olivine increases with increasing iron content of the olivine.

- A good measure for the true reactive surface area, necessary to normalize rate data, is difficult to obtain. Usually initial BET surface areas are used as an approximation. This may explain the discrepancies between reported rate data.

Olivine dissolution in concentrated acid

- In unstirred concentrated acid, silica polymerizes and precipitates close to the olivine surface, this causes a decrease in reaction rate. Continued precipitation leads in general to complete solidification of the olivine bed.
- In order to prevent the precipitation of silica on olivine grains that dissolve in acid, vigorous stirring of the reaction mixture is required. Under these conditions the dissolution reaction is kinetically controlled by surface reactions.

Appendix 2.1 Olivine Dissolution in 3M H_2SO_4 at 25 °C some "Back of the Envelope" calculations"

Introduction

The dissolution of olivine involves a number of processes, a comparison of the rates of the individual processes yields better insight in the dissolution mechanism. The processes can be divided in transport processes: diffusion and convection, and reaction processes: surface reactions and silica polymerization. In Figure 2.3 the relevant concentrations for the transport processes involved in the dissolution of olivine in acid are displayed. Unfortunately, literature data is not available for these processes in strong acids; diffusion coefficients are generally only available for dilute solutions in water, and rates of olivine dissolution and silica polymerization only at pH > 1. For dissolution in strong acids the rates have to be calculated by extrapolating literature data, and can therefore only be considered as indicative. As a semi-quantitative example the dissolution of an olivine sphere, of a diameter of 100 μm in 3 M H_2SO_4 will be considered. The rates of the processes are estimated by extrapolating literature data on diffusion-, dissolution- and silica-polymerization rates. Since most literature data is only available at room temperature, the dissolution is considered at 25 °C.

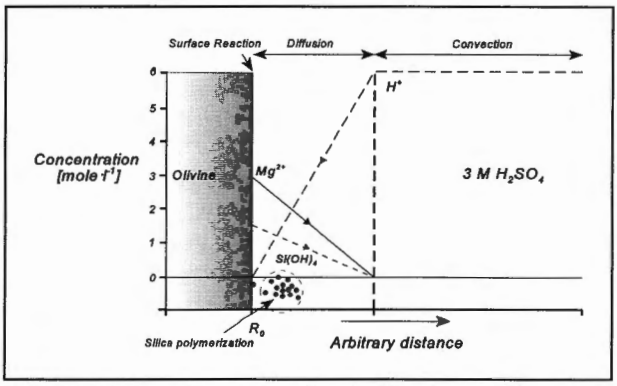

Figure 2.3 Schematic olivine dissolution : transport processes and concentrations of relevant species

1) Transport processes:

The transport process can be described by mass transfer coefficients (k_c), which quantify transport due to stirring. At the sphere surface the flux can be described by the following equation (Fogler, 1986):

$$J_I = k_c \cdot C_{I\,sat} \quad \textbf{2.6} \qquad \text{with :} \qquad k_c = \frac{D_I}{2 \cdot r_0} \cdot Sh$$

Using the following dimensionless numbers :

Sherwood : $Sh = 2 + 0.6 \cdot Re^{1/2} \cdot Sc^{1/3}$

Reynolds : $Re = \frac{2 \cdot r_0 \cdot \rho \cdot U}{\eta}$

Schmidt : $Sc = \frac{\eta}{D_i \rho}$

With J_i the flux of species I [mol·s^{-1}], $C_{i\,sat}$ the saturation concentration [mol·l^{-1}], D_i the diffusion coefficient of that species and r_0 the radius of the dissolving particle. The parameters of the solution are : ρ (density), η (viscosity) and U(flow velocity).

In the schematic dissolution model in Figure 2.3, the diffusional transport of Mg^{2+}, H^+ and the neutral $Si(OH)_4$ is considered. The major difficulty is to find correct diffusion coefficients for these ions in 3 M H_2SO_4 solution. As an approximation diffusion coefficients from the literature, for dilute concentrations of the species in water, were transformed according to Atkins (1990) using the Stokes-Einstein equation in equation 2.7, in order to account for interactions between the different species in solution.

$$D_i = \frac{k_b \cdot T}{6 \cdot \pi \cdot \eta \cdot a_i} \qquad \textbf{2.7}$$

In this equation k_b is the Boltzmann constant, η the viscosity of the medium and a_i the hydrodynamic radius of species I. The hydrodynamic radius was calculated from the diffusion coefficients in water. Subsequently the radii thus obtained were used to calculate the coefficients in the 3 M sulphuric acid solution. There is a possibility that the silica monomers released during dissolution will polymerize to form larger particles. Since the maximum size of soluble silica particles is reported to be about 50 Å (Iler 1979), the diffusion coefficients were also calculated for particles of this size. The results are summarized in Table 2.2.

Species	D [$cm^2 \cdot s^{-1}$] (dilute concentrations in water)	Hydrodynamic radius a [Å]	D [$cm^2 \cdot s^{-1}$] (3 M H_2SO_4)
Mg^{2+}	$7.11 \cdot 10^{-6}$ (1)	3.07	$4.0 \cdot 10^{-6}$
H^+	$9.32 \cdot 10^{-5}$ (1)	0.23	$5.3 \cdot 10^{-5}$
$Si(OH)_4$	$1 \cdot 10^{-5}$ (2)	2.18	$5.7 \cdot 10^{-6}$
Polymerized silica		25	$5.0 \cdot 10^{-7}$

Table 2.2 Diffusion coefficients in water and 3 M H_2SO_4 for relevant species. Data from: (1) Cussler (1984), (2) Wollast and Garrels (1971).

With the dissolution of olivine the transport rate of H^+ is twice as high and in opposite direction to the Mg^{2+} transport. A single 'average' diffusion coefficient can be used to describe this coupled transport. The harmonic average of the Mg^{2+} and H^+ diffusion coefficients at concentrations half-way the diffusion layer was used as a 'mean' diffusion coefficient (equation 2.8, with Z the ion-charge and M the concentration [$mole \cdot l^{-1}$].). This yields a coupled diffusion coefficient (D_e) of $1.1 \cdot 10^{-5}$ $cm^2 \cdot s^{-1}$.

$$D_e = D_{Mg} \cdot D_H \cdot \frac{(Z^2_{Mg} \cdot M_{Mg} + Z^2_H \cdot M_H)}{(D_{Mg} \cdot Z^2_{Mg} \cdot M_{Mg} + D_H \cdot Z^2_H \cdot M_H)} \qquad \textbf{2.8}$$

At zero liquid velocity the flux at the surface of the particle is $2 \cdot 10^{-9}$ $mol \cdot s^{-1}$ for Mg^{2+} and respectively $5.4 \cdot 10^{-10}$ and $4.7 \cdot 10^{-11}$ $mol \cdot s^{-1}$ for silica with hydrodynamic radius of 2.2 and 25 Å (using a C_{sat} of 3 $mol \cdot l^{-1}$ for Mg, and of 1.5 $mol \cdot l^{-1}$ for silica).

2) Surface reaction rate:

According to Blum and Lasaga (1988), the olivine dissolution rate at pH <2, is given as a function of the H^+ activity by : $10^{-6.88} \cdot a_{H^+}^{0.56}$ [$mol \cdot m^{-2} \cdot s^{-1}$] **2.9.**

The hydrogen activity in 3 M H_2SO_4 at 25 °C can be calculated with Pitzer equations. For this purpose the computer program PHREEQPitz (Plummer et al. 1989) was used, which yielded a H^+ activity of $10^{0.78}$.

Using this activity in equation 2.9, a dissolution rate of $1.1 \cdot 10^{-14}$ [$mol \cdot s^{-1}$] for a 100 μm spherical olivine grain is obtained .

3) Rate of silica polymerization:
Okkerse (1961) reported some data on the polymerization rate of silica at pH levels lower than 2. He studied the silica polymerization rate of silica solutions ranging in concentration from 0.01 to 0.08 mol·l^{-1}, at pH 0.6-2.0 and 25 °C. The polymerization rate was determined by monitoring the concentration of silicic acids of low molecular weights (mainly monomeric and dimeric) as a function of time. The polymerization rate was found to rise with increasing initial silica concentration (C_{sil}) and increasing H^+ concentration, below pH 2 the polymerization rate is given by : $(2.73\text{-}0.76 \cdot pH) \cdot C_{sil}^3$ [mol silica·hour^{-1}].
Linear extrapolation of his data to a pH of -0.78 and a silica concentration of 1.5 mol·l^{-1}, yields a polymerization rate of $3.3 \cdot 10^{-2}$ mol silica·s^{-1}.

Discussion and Conclusions
The calculations show that at 25 °C for a 100μm olivine sphere, the diffusional transport rates of Mg^{2+} and silica are much higher (a factor of 10^3-10^4) than their release rates due to dissolution. This indicates that at 25 °C diffusion processes in the aqueous phase are not rate limiting. The silica polymerization rate is, however, a factor of 10^7 higher than the diffusional transport rate of silica, which suggests that silica polymerizes close to the olivine grains. Continued polymerization may lead to the precipitation of a solid silica phase, that will affect the diffusional transport rates of Mg^{2+} and H^+ considerably.

Chapter 3

Olivine Dissolution in Sulphuric Acid at Elevated Temperatures

Abstract

A kinetic model for the dissolution of olivine in sulphuric acid at elevated temperatures is presented. A reliable model is essential for the design of an industrial process for the neutralization of waste acids by olivine or for the production of precipitated silica from olivine. The effects of temperature, grain size fraction and amount of olivine on the neutralization rate have been quantified by carrying out a range of complete neutralization experiments.

For the interpretation of the experimental data a measure of the hydrogen ion activity is required. Since it is not possible to accurately measure pH values in acids at high temperatures, the hydrogen ion activities were calculated using the Pitzer model.

The rate equation coefficients and constants were obtained by fitting an expression for the rate equation to the experimental data. The following equation was obtained, that enables one to calculate the progress of the neutralization as a function of time:

$$\frac{d\,[H^+]}{dt} = - \; e^{-\frac{E_{act}}{R \cdot T}} \cdot 10^8 \cdot (1.92 \pm 0.12) \cdot S_{geom} \cdot A_{H^+}^{0.33} \qquad [mol \cdot minute^{-1}]$$

with E_{act} the activation energy of 66.5±2 kJ·mol^{-1}, S_{geom} the geometrical surface area of the olivine grains calculated from the grain size distribution, and A_{H+} the hydrogen ion activity calculated with the Pitzer model, using the computer program PHRQPITZ. The equation was validated for the dissolution of Norwegian olivine (FO_{93}) with grain sizes from 63-300 μm in sulphuric acid at temperatures ranging from 60-90 °C.

Introduction

For the design of an industrial process for the neutralization of waste acids by olivine, a kinetic model for the dissolution of olivine in acid is necessary. To date only studies on the dissolution of olivine under natural conditions have been published (e.g. Blum and Lasaga 1988, Wogelius and Walther 1991, Wogelius and Walther 1992 and van Herk et al. 1989). In this study the effect of temperature, grain size and quantity of olivine on the dissolution of one type of Norwegian olivine in 3 molar sulphuric acid has been investigated. This is the concentration generated by the production of titanium dioxide, currently the largest industrial waste acid stream. The results of the kinetic study are formulated into a kinetic rate law, that enables one to calculate progress of the neutralization as a function of time.

Experimental Method

The rate for the neutralization of acid by olivine [in mol H^+·time^{-1}] is given by the general equation:

$$\frac{d\,[H^+]}{dt} = -\,k_T \cdot S_{ol}^{\,m} \cdot A_{H^+}^{\,n} \qquad \textbf{3.1}$$

with S_{ol} the reactive olivine surface area, A_{H+} the hydrogen ion activity and k_T a constant depending on a.o. temperature. Conventional methods for the determination of the rate equation coefficients (m and n) in equation 3.1, involve using an excess of one of the reactants or the measurement of initial rates, as discussed in chapter 2. These methods are not suitable for olivine dissolution under Olivine Process conditions. The excess method fails due to the fact that the olivine surface area and H^+ concentration are difficult to monitor or to keep constant in concentrated acids. The initial rates procedure proved to be inaccurate due to analytical errors. Therefore it was decided to extract the rate equation coefficients from a number of complete neutralization experiments. For this purpose the rate equation was rewritten. Generally, the surface area of a distribution of particles is related to the total particle volume, and can be approximated by $Surface = k \cdot Volume^{\,x}$. For a single sphere x is equal to ⅔, for a distribution of particles x is higher than ⅔ and depends on the characteristics (mean, shape, range etc.) of the particle size distribution.
Consequently the olivine surface area can be expressed as:

$$S_{ol} = k \cdot (k_s + \tfrac{1}{4}\,H^+)^{\,x} \quad with\ k_s = (C_{ol\,0} - \tfrac{1}{4}\,H_0^+) \qquad \textbf{3.2}$$

With k a constant and k_s a stoichiometry constant depending on the initial concentrations: H_0 the initial H^+ concentration and $C_{ol\,0}$ the initial amount of moles of olivine per liter acid.
Combining 3.1 and 3.2 yields an equation, which can be fitted to all experiments to estimate the rate equation coefficients.

$$\frac{d\,[H^+]}{dt} = -\,k_T \cdot k \cdot (k_s + \tfrac{1}{4}\,H^+)^{\,m} \cdot A_{H^+}^{\,n} \qquad \textbf{3.3}$$

This equation was fitted by least squares analysis to experimental data that was obtained by monitoring the H^+ concentration in a series of complete neutralization experiments.
In order to determine all constants and coefficients in this equation, (k, k_T, m *and* n) three sets of complete neutralization experiments were conducted (see also Table 3.1): I) to establish the temperature dependence, experiments with stoichiometric mixtures of acid and olivine

with a grain size fraction of 63-150 μm, at temperatures 60, 70, 80 and 90 °C were conducted ii) to fit the stoichiometry factor correctly, experiments were carried out at 80 °C with 0, 10, 20 and 30 % excess quantities of olivine, with a grain size fraction of 150-250 μm. iii) to determine the effect of the olivine grain size, experiments were conducted at 80°C with stoichiometric mixtures of acid and four olivine grain size fractions: 63-106, 106-150, 150-210, 210-300 μm. The upper grain size limit was chosen, since, for the type of olivine used, the largest olivine crystals without internal fractures are about 300 μm. In order to assess the reproducibility of the experiments, the experiment with 0 % excess olivine of set 2 was carried out in triplicate.

For the interpretation of the kinetic rate data it is necessary to have a good estimate of the H^+ activity. However, it is difficult, if not impossible, to measure meaningful and accurate pH values in highly acidic solutions of high ionic strengths at elevated temperatures. For this reason H^+ activities were calculated using the Pitzer model. The calculations were carried out with the computer program PHRQPITZ (Plummer et al. 1988), which was developed for the calculation of chemical equilibria in solutions of high ionic strength using the Pitzer model in the temperature range 0-60 °C. The program offers two possibilities for scaling of the single ion activity coefficients; the simplest option is the direct calculation of unscaled coefficients with the single ion Pitzer formula (e.g. van Gaans (1997). The activity coefficients can also be scaled according to the MacInnes convention which defines that the activity coefficient of Cl^- is equal to the mean activity coefficient of KCl in a pure KCl solution of the same ionic strength. In this study unscaled ion activity coefficients were used, the H^+ activities were calculated as a function of the amount of residual moles H^+ in the neutralization system of 3M H_2SO_4.

Materials and Methods

Experiments were carried out in a vigorously stirred double-walled glass reaction vessel with an inner volume of 800 ml, the temperature was kept constant by circulating water from a thermostat bath through the outer wall, see Figure 3.1. For all experiments 500 ml of 3M sulphuric acid was used, the experiments were continued until at least 95 % of the acid had reacted. At regular time intervals 2 ml samples were taken from the reaction vessel, in which the amount of H^+ was determined (in triplicate) by a titration with a 0.05 M $Na_2B_4O_7$ solution (Vogel, 1953). Titrations were carried out with a 20 ml piston burette from Metrohm A.G. The standard deviation of this H^+ determination is 0.017 [mol H^+]. The ground olivine (0-4 mm) was supplied by Hoogovens B.V. and produced by A.S. Olivine in Norway. The desired grain size fractions were obtained by wet sieving 2 kg loads of ground

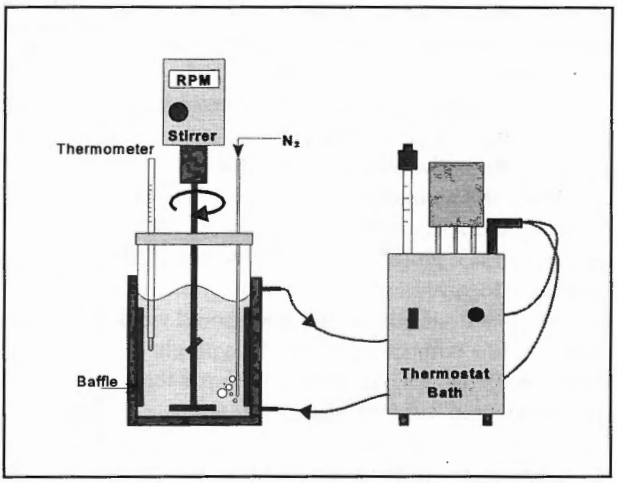

Figure 3.1 Schematic reactor setup.

olivine for 20 minutes, using 20 cm analytical sieves and a Retsch Vibro sieve machine. The sieve fractions were subsequently ultra-sonically treated to remove any adhering fines. The grain size distribution of all fractions was measured with a Malvern 3600D laser particle-sizer.
The chemical composition of the olivine was determined by ICP-analysis: $Mg_{1.86}Fe_{0.13}Ni_{0.006}SiO_4$ (FO_{93}). The ground olivine contained 7.4 weight % other, low reactive minerals (see also chapter 1, Olivine properties).
The 3 M H_2SO_4 solution was prepared from pure 96 % sulphuric acid from Lamers & Pleuger B.V. and demineralized water. The 0.05 M borax solution was prepared from pure, water-free $Na_2B_4O_7$ from Merck and demineralized water.

Results and Interpretation

The triplicate experiment with a stoichiometric amount of olivine, of a grain size fraction 150-250 μm, at 80 °C revealed that the variation between the experiments mainly consists of a small bias between the reaction progress curves. This illustrates that the variation due to analytical errors in the determination of H^+ is small compared to variation from other sources such as the inhomogeneity of olivine, temperature differences, etc.
The standard deviation of the average bias of the three experimental curves is 0.046 [mol H^+]. This estimate of the experimental standard deviation is based on three experiments, the confidence interval of the experimental standard deviation can be calculated using a χ^2-distribution (Koch and Link 1971). With a confidence level of 90 % (and two degrees of freedom) the true experimental standard deviation will be found in the interval of 0.03 and 0.2 [mol H^+]. Considering the fact that each of the three experimental standard deviations is calculated from a large number of observations per experiment, the value of 0.2 [mol H^+] represents, in the worst case, the upper limit of the experimental standard deviation.
A typical neutralization curve, using a stoichiometric amount of olivine (63-150 μm) at 70 °C, is displayed in Figure 3.2. According to equation 3.3, plotting the logarithm of dH^+/dt versus the logarithm of H^+ for a stoichiometric amount ($k_s = 0$) of olivine and acid should yield a straight line with slope ($m+n$). This plot is shown in Figure 3.3, which clearly shows that the relationship between $\log(dH^+/dt)$ and $\log(H^+)$ is not linear. The slope of the line is steeper at higher H^+ concentrations, a transition

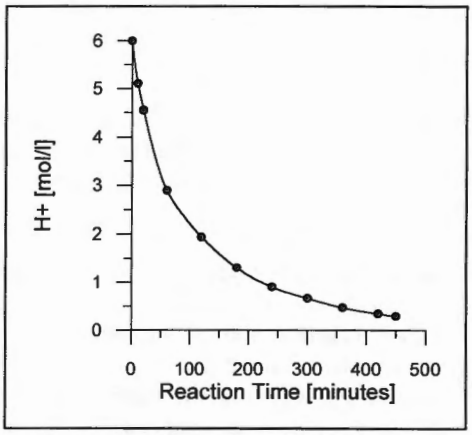

Figure 3.2 Mol H^+ versus reaction time, stoichiometric amount of olivine (63-150 μm) at 70 °C

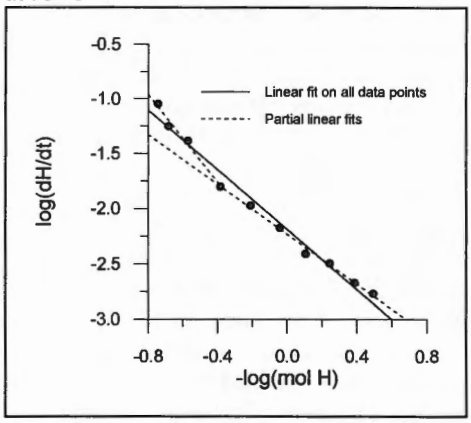

Figure 3.3 log(dH/dt) versus -log(mol H^+)

to gentler slopes is for all experiments approximately situated around -log(H^+) = -0.4. The deviation can be caused by the considerable increase in ionic strength of the reaction mixture during neutralization. This causes a relatively stronger decrease in hydrogen ion activity at increasing extent of neutralization than expected. For the incorporation of the hydrogen ion activity in equation 3.3, the activities were calculated with the Pitzer model, using the computer program PHRQPITZ. The results of these calculations for different temperatures are illustrated in Figure 3.4, where the pH calculated by PHRQPITZ is plotted versus the negative logarithm of the amount of residual moles H^+. Clearly these curves are not straight and have a change of slope in the -log(H^+) range from -0.4 to -0.2, which coincides with the change of the slopes of the experimental log(dH^+/dt) versus log(H^+) curves.

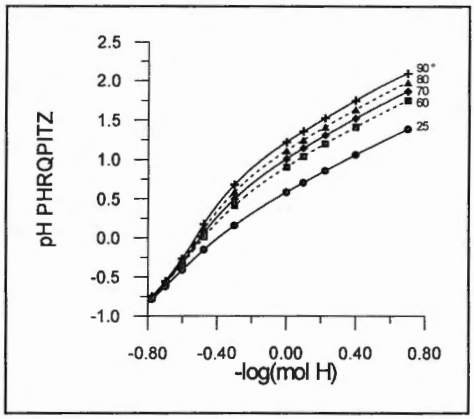

Figure 3.4 pH calculated by PHRQPitz versus -log(mol H^+)

Consequently, dH^+/dt in equation 3.3 is a function of both the H^+ activity (H^n) and of the H^+ concentration ($(k_s+k_4H^+)^m$). A plot of the logarithm of dH^+/dt versus a linear combination of the log of the H^+ concentration and the pH, calculated from the PHRQPITZ curves (Figure 3.4) indeed can, within the limits of the precision of the data, be described by a straight line (Figure 3.5). By fitting equation 3.3 to the experiments with the excess amounts of olivine, the order with respect to the H^+ activity (n) can be determined. Subsequent fitting to the other sets of experiments yield values for the other parameters. In appendix 3.1, the fit results for the set of experiments with excess amounts of olivine, those at temperatures from 60-90 °C and those with the various olivine grain size fractions are displayed. The figures show that straight lines could be obtained by fitting equation 3 to the experimental data. Table 3.1 summarizes the fitted rate equation coefficients and constants.

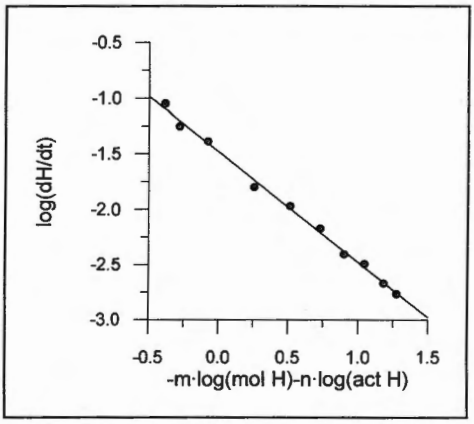

Figure 3.5 Log(dH/dt) versus a combination of -log(mol H^+) and pH calculated by PHRQPitz

Experiment			m	constant $\log(k_T \cdot k)$
Grain size	Temperature	Excess olivine	n = 0.33	
150-250 μm	80 °C	0 % 10 % 20 % 30 %	0.81	-1.41
63-150 μm " " "	60 °C 70 °C 80 °C 90 °C	0 % " " "	0.94 " " "	-1.79 -1.48 -1.23 -0.92
63-105 μm 105-150 μm 150-210 μm 210-300 μm	80 °C " " "	0 % " " "	0.91 0.83 0.81 0.77	-1.18 -1.29 -1.41 -1.53

Table 3.1 Fitted rate equation coefficients and constants for all experiments.

The set of constants derived from the temperature varied experiments was used to determine the activation energy of the reaction, using the Arrhenius relation. The Arrhenius plot of the natural logarithm of the rate constant versus the inverse temperatures (in $^\circ K^{-1}$) is shown in Figure 3.6. The activation energy was determined from the slope of the curve to be 66.5±2 kJ·mole^{-1}. Finally the relationship between the expression for the olivine surface area (the factor $k \cdot (k_s + \frac{1}{4}H^+)^m$ in equation 3.3) and the grain size fractions used in the experiments was evaluated. For this purpose the surface area factor, calculated as a function of the residual volume of olivine using the fitted parameters (m and k), was first compared with the geometrical surface area (S_{geom}). The geometrical surface area was calculated as a function of olivine volume for each grain size fraction, using the initial grain size distributions and assuming a spherical particle geometry. It was found that the relation between surface area factor and geometrical surface area is linear for all experiments with similar slopes. No relation between differences in slope and grain size fraction were observed. See Figure 3.7 for an illustration of this relationship for the experiment with a stoichiometric amount of olivine (63-150 μm) at 70 °C.

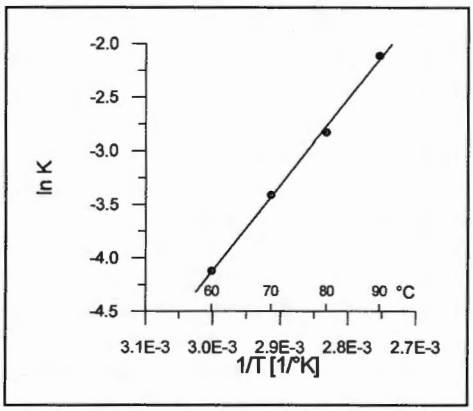

Figure 3.6 Arrhenius plot

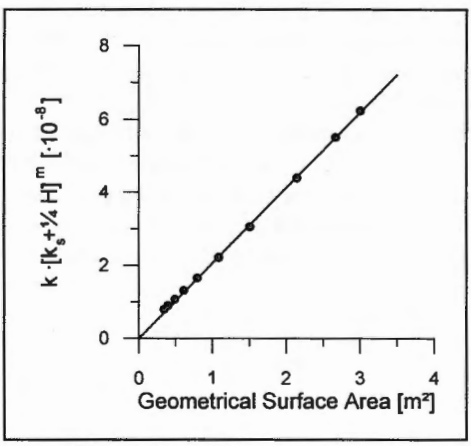

Figure 3.7 Olivine surface area factor versus geometrical surface area

The linear relationship calculated from all experiments is summarized by:

$$S_{ol}^{m_l} = 10^8 \cdot (1.92 \pm 0.12) \cdot S_{geom}$$

Discussion

The hydrogen ion activity, required for the interpretation of the kinetic rate data, was calculated using the Pitzer model. For this purpose the calculations had to be extrapolated from the temperature range 0-60 °C, used in the computer program PHRQPITZ, up to 90 °C. At present it is not possible to quantitatively verify these extrapolations.

Nevertheless, the rate equation coefficients derived from the fit procedure using the extrapolated pH-calculations, are comparable with coefficients reported in literature, see table 2.1 in chapter 2. For their dissolution experiments in sulphuric acid, van Herk et al. (1989) found an order in H^+ activity (*n* in equation 3) of 0.43, while in this study a value of 0.33 was obtained. The difference is possibly due to different experimental conditions (van Herk et al. performed experiments in dilute acid solutions). On the other hand, there is some variation in reported rate coefficients, see Table 2.1. For the dissolution of olivine in hydrochloric acid the H^+ dependence ranges from 0.56 (Blum and Lasaga 1988), 0.54 (Wogelius and Walther 1991), 0.5 (Wogelius Walther 1992) to 0.33 (van Herk et al. 1989).

The activation energy of 66.5±2 kJ·mole^{-1}, found in this study, is comparable with the activation energy calculated from the data of Herk et al. (1989) of 70±5 kJ·mole^{-1}. It is also, within the limits of precision, comparable to the activation energy determined by Wogelius and Walther (1992), who found 79±10 kJ·mole^{-1} based on experiments at only two temperatures.

It is surprising that the dissolution rate depends linearly on the geometrical surface area of the olivine grain size fraction. It can be expected that by extensive formation of etch features, as illustrated in picture 2, the reacting olivine surface area is not in a simple way related to the olivine volume. The results of this study indicate, however, that for the bulk dissolution rate the reacting olivine surface area can be satisfactorily approximated by the geometrical surface area multiplied by a factor 1.92. These findings are not in accordance with those of van Herk et al.(1989), who found that the olivine dissolution rate was first order with respect to the olivine volume. They conclude that this is caused by the fact that the dissolution rate is controlled by surface reactions. It is, however, more appropriate to state that the dissolution rate, when surface reactions are rate controlling, depends on the olivine surface rather than the olivine volume. It is unlikely that the surface area is exactly linearly proportional to the volume.

The results of this study can be summarized by the following rate equation, that enables one to calculate reaction curves as a function of time for mixtures of olivine and sulphuric acid:

$$\frac{d\,[H^+]}{dt} = - e^{-\frac{66.5 \cdot 10^3}{R \cdot T}} \cdot 10^8 \cdot 1.92 \cdot S_{geom} \cdot A_{H^+}^{0.33} \qquad [mol \cdot minute^{-1}] \qquad \textbf{3.4}$$

with S_{geom} the geometrical surface area in m^2 and A_{H+} the hydrogen ion activity calculated with the Pitzer model, using the computer program PHRQPITZ. The equation was validated for the dissolution of Norwegian olivine, with grain sizes from 63-300 μm, in sulphuric acid at temperatures ranging from 60-90 °C. The experimental neutralization curves could be reproduced, with maximum deviations of 4 % (neutralized H^+), by numerical integration of equation 3.4.

Conclusions

- Conventional methods are not applicable to study the kinetics of olivine dissolution in sulphuric acid at elevated temperatures. Therefore complete neutralization experiments have to be performed to determine the coefficients and constants of rate equations.
- A measure of the hydrogen ion activity is required for the kinetic interpretation of experimental dissolution data. Since it is not possible to carry out accurate pH-measurements, the hydrogen ion activity was calculated with the Pitzer model, using the computer program PHRQPITZ. It was possible to satisfactorily fit calculated data to all experimental data using the calculated H^+ activities.
- The order with respect to calculated H^+ activity for the dissolution of olivine in sulphuric acid was found to be 0.33.
- The bulk dissolution rate is linearly proportional to the geometrical surface area of the olivine grain size fraction used.
- The results of this kinetic study can be summarized by the following rate equation, that enables one to calculate progress of the reaction as a function of time for a range of olivine grain sizes and temperatures

$$\frac{d\,[H^+]}{dt} = - \; e^{-\frac{E_{act}}{R \cdot T}} \cdot 10^8 \cdot 1.92 \cdot S_{geom} \cdot A_{H^+}{}^{0.33} \qquad [mol \cdot minute^{-1}]$$

with E_{act} the activation energy of $66.5 \cdot 10^3$ kJ·mol^{-1}, S_{geom} the geometrical surface area and A_{H+} the calculated H^+ activity. The equation was validated for the dissolution of Norwegian olivine, with grain sizes from 63-300 μm, in sulphuric acid at temperatures ranging from 60 to 90 °C.

Appendix 3.1 Fit Results

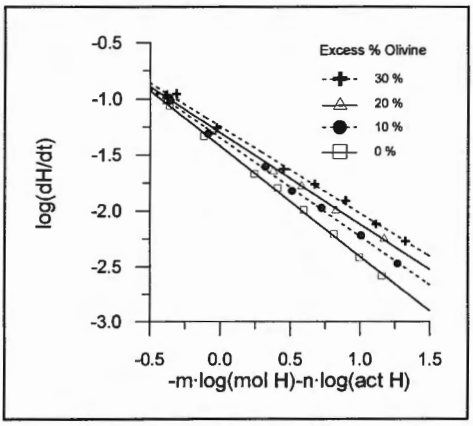

Figure 3.8 Fit curves for experiments with excess amounts of olivine

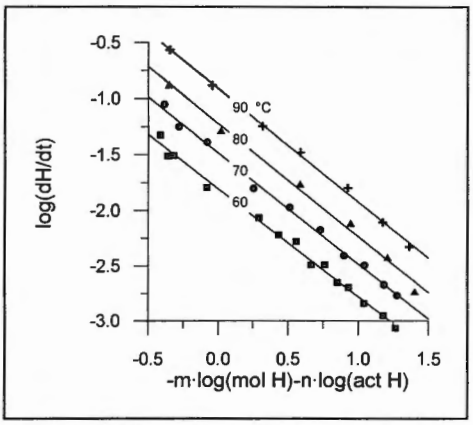

Figure 3.9 Fit curves for experiments at different temperatures

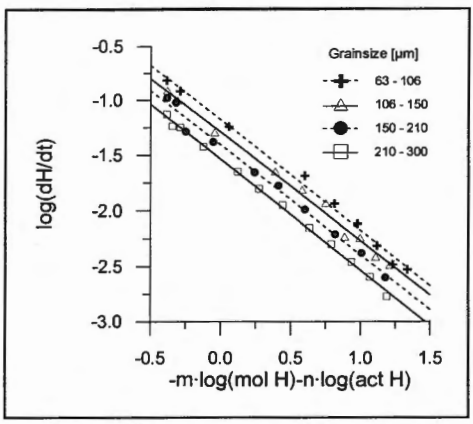

Figure 3.10 Fit curves for experiments with different grain size fractions

The curves in figures 3.8 to 3.10 were obtained by fitting the rate equation (3.3) to experimental data.

$$\frac{d\,[H^+]}{dt} = -\,k_T \cdot k \cdot (k_s + ¼\,H^+)^{m} \cdot A_{H^+}^{n} \qquad 3.3$$

The fitted rate-equation constants and coefficients are displayed in Table 3.1. In order to plot the fitted curves, the constant ($\log(k_T \cdot k)$) was set to zero, otherwise the curves would all overlap each other.

Chapter 4

Dissolution Rates of Olivine Grain Size Fractions larger than 300 μm

Abstract

The occurrence of internal fractures in olivine grains from ultramafic rocks is common. Dissolution takes place preferentially along these fractures, leading to breaking-up of the olivine grains. The disintegration results in a higher available olivine surface area and consequently in a higher dissolution rate.

For the Norwegian olivine that was used in chapter 3 the largest grain size without internal fractures is about 300 μm. Investigations of the dissolution rate of larger grain sizes revealed that the observed rate of the larger fractions is indeed higher than the expected rate. The measurement of grain size distributions of partly dissolved olivine fractions, confirms the process of fragmentation of large olivine grains.

For the calculation of the progress of the neutraization with time, it is necessary to know the olivine surface area as a function of the olivine volume. Since it is difficult to assess the extent of the fragmentation of olivine grains with internal fractures as a function of time, the relation between surface area and olivine volume has to be determined by experiments.

Introduction

In chapter 3 a rate equation was derived for the dissolution of olivine of grain sizes ranging from 63 to 300 μm. The upper grain size limit of 300 μm was chosen, since microscopic investigations revealed that the largest olivine crystals without internal fractures are about 300 μm. Qualitative dissolution experiments showed, that dissolution preferentially proceeds place along these internal fractures, causing break-up of the grains. The fragmentation results in a higher available olivine surface, and may consequently increase the dissolution rate. The occurrence of internal fractures in olivine grains from ultramafic rocks is common (e.g. Nockolds (1979) and Ehlers (1982). It is therefore interesting, for industrial applications, to study the mechanism and the rate of dissolution of larger olivine grain sizes.

In order to determine the dissolution rate, a set of complete neutralization experiments was carried out with four Norwegian olivine (FO_{93}) grain size fractions larger than 300 μm, according to the procedure described in chapter3.

To gain quantitative insight in the process of break-up of the olivine grains during dissolution, another set of experiments was conducted. In these experiments small amounts of olivine were partly dissolved, followed by measurement of the grain size distribution of the remaining olivine fractions.

Experimental method

The dissolution experiments were carried out in vigorously stirred double-walled vessels at 80°C according to the procedure described in Chapter 3. All experiments were performed with Norwegian olivine (FO_{93}) and 3 M technical grade sulphuric acid. Four grain size fractions larger than 300 μm were used: 300-355, 355-500, 500-630, and a fraction of a wider range of 355-630 μm.

The experimental neutralization curves were compared with curves calculated by the reaction rate equation, which was derived in Chapter 3.

$$\frac{d\,[H^+]}{dt} = - \; e^{-\frac{66.5 \cdot 10^3}{R \cdot T}} \cdot 10^8 \cdot 1.92 \cdot S_{geom} \cdot A_{H^+}{}^{0.33} \qquad [mol \cdot minute^{-1}] \qquad \textbf{4.1}$$

The hydrogen ion activity (A_{H+}) was calculated by PHRQPITZ and the geometrical surface area (S_{geom}) of the dissolving olivine fractions was calculated as a function of the olivine volume, assuming a spherical particle geometry.

For the preparation of the partly dissolved olivine samples, used to determine the grain size distribution, samples of 5 g of olivine were dissolved in 20 ml 3M sulphuric acid at 80°C. All reactions were stopped before the viscous stage was reached (Chapter 1.), since it is not possible to separate all residual olivine from the reaction mixture, when too much silica has precipitated. Therefore only the effects of limited degrees of dissolution can be studied. For the experiments five grain size fractions were used: 63-150 μm and the four fractions larger than 300 μm, which were also used for the complete dissolution experiments. After reaction, the mixtures were cooled down to room temperature, the acid was subsequently decanted and the olivine residue was washed four times with demineralized water. The extent of neutralization was determined by analyzing the amount of residual H^+ in the decanted acid by titration with a borax solution. All olivine grain size distributions were measured with a Malvern 3600D laser particle-sizer, all analyses were duplicated. In order to assess the accuracy of the grain size distribution measurements, at least two replicates of each unreacted olivine fraction were analyzed.

Results and Interpretation

From the analyses of replicates of the unreacted olivine fractions the accuracy of the grain size distribution measurement was assessed. The accuracy can be expressed in standard deviation of the surface areas calculated from the measured grain size distributions. The duplicated analyses of the replicates reveal that the analytical variation due to the measurement is small as compared to the variation between replicates. The relative standard deviation of measurements between replicates is 5.5 %.

Figures 4.1 to 4.4 compare the experimental and calculated neutralization curves of residual moles H^+ versus reaction time for the four olivine grain size fractions larger than 300 μm. The figures clearly show that the larger fractions reacted faster than predicted by the dissolution model. The lack of fit of calculated and experimental curve rises at increasing grain size.

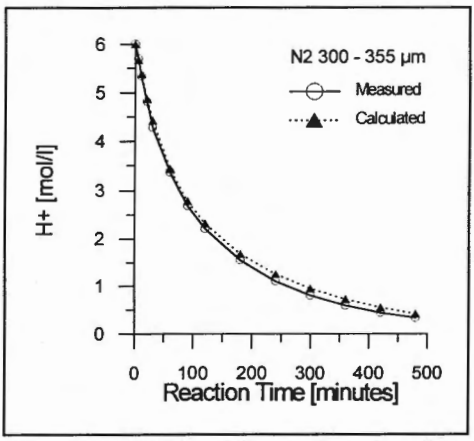

Figure 4.1 Moles/liter H^+ versus reaction time Grain size fraction 300-355 μm

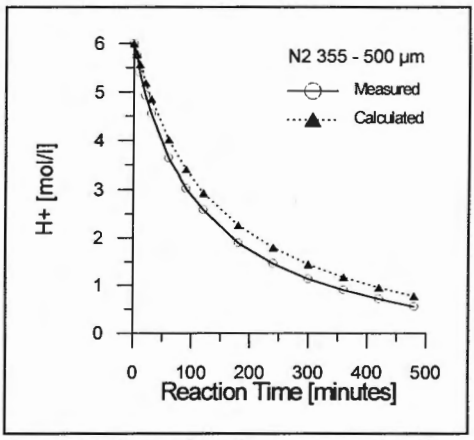

Figure 4.2 Moles/liter H^+ versus reaction time Grain size fraction 355-500 μm

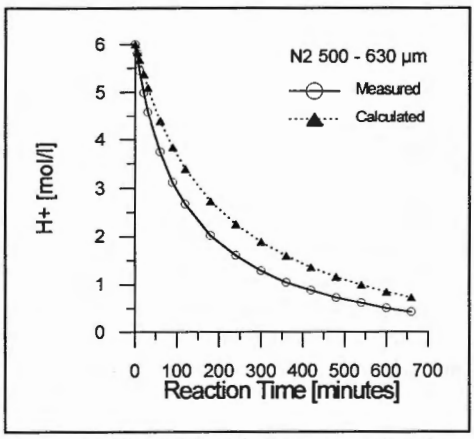

Figure 4.3 Moles/liter H^+ versus reaction time Grain size fraction 500-630 μm

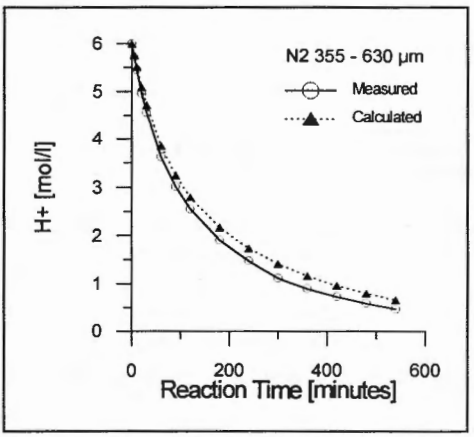

Figure 4.4 Moles/liter H^+ versus reaction time Grain size fraction 355-630 μm

In order to assess the difference in reaction rate the general rate equation from chapter 3 (equation 3.3) was fitted to the experimental data by adjusting the olivine surface area factor ($k \cdot (k_s + {}^1\!/_4 H^+)^m$). The fit results for all fractions used are displayed in figures 4.5 to 4.8, which clearly show that it is possible to fit straight lines to the experimental data using equation 3.3.

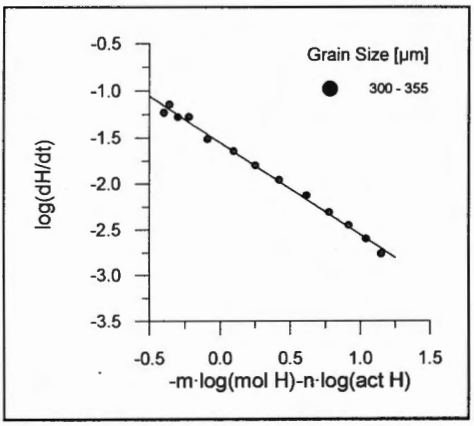

Figure 4.5 Fit curves for grain size fraction 300-355 µm

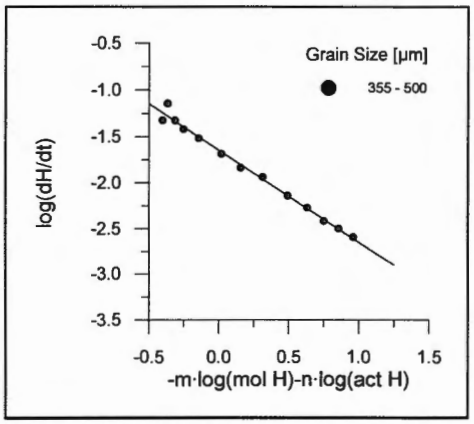

Figure 4.6 Fit curves for grain size fraction 355-500 µm

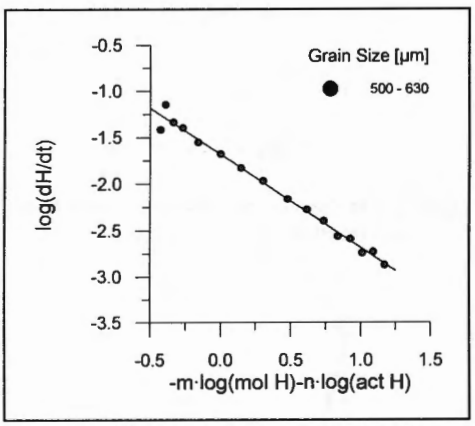

Figure 4.7 Fit curves for grain size fraction 500-630 µm

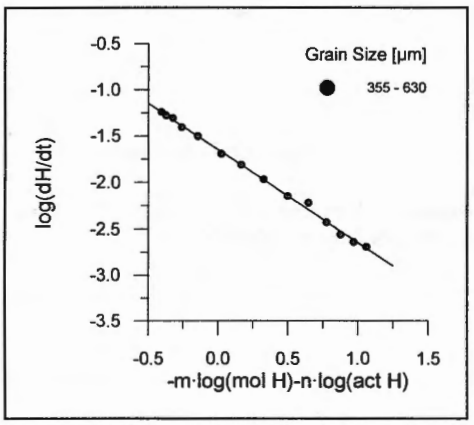

Figure 4.8 Fit curves for grain size fraction 355-630 µm

The olivine surface area factors resulting from the fitting procedure were compared with the geometrical surface area calculated as a function of the residual olivine volume from the initial olivine grain size distribution. The results are displayed in figures 4.9 and 4.10 that, most remarkably, show that the relation between surface area factor and calculated geometrical surface area is linear for all fractions. The slopes of the linear relation increase with increasing grain size fraction. Table 4.1 lists the slopes (k_r) of the curves in figures 4.9 and 4.10.

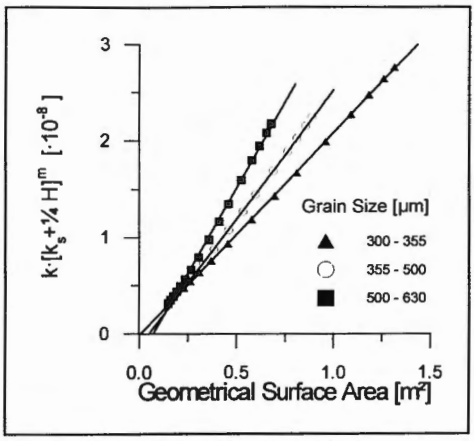

Figure 4.9 Olivine surface area factor versus geometrical surface area for several grain sizes

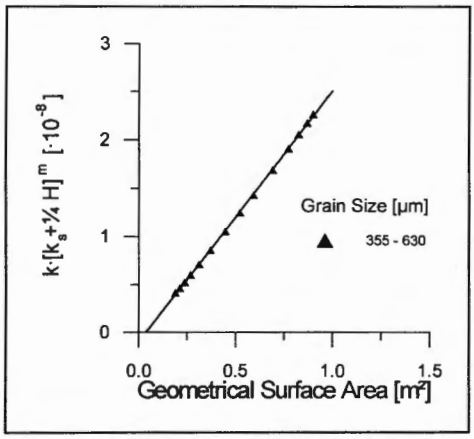

Figure 4.10 Olivine surface area factor versus geometrical surface area for fraction 355-630 μm

The measured grain size distributions of the partly dissolved olivine fractions are displayed in figures 4.11 to 4.15 for all fractions used. For the two broad fractions 63-150 and 355-630 μm the grain size distributions after partial dissolution were also calculated from the initial distribution, assuming a spherical grain morphology. These calculated distributions are displayed for dissolution percentage of 28 % of the fine fraction (in Figure 4.11), and of 24 % of the coarse olivine fraction (in Figure 4.15).

Grain size fraction [μm]	k_r: [Ratio of surface area factor and geometrical surface area]
300 - 355	2.10
355 - 500	2.66
500 - 630	3.56
355 - 630	2.60

Table 4.1 Geometrical surface area constants for several grain size fractions (see text).

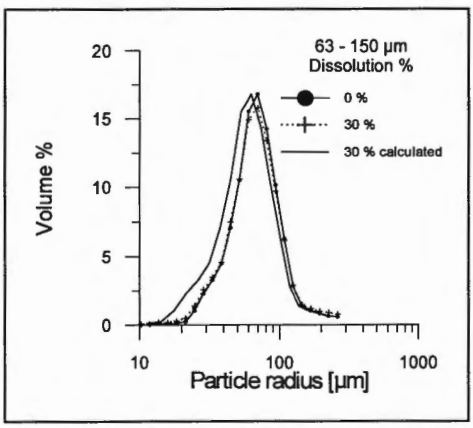

Figure 4.11 Grain size distributions of initial and partly dissolved olivine. Fraction 63-150 μm.

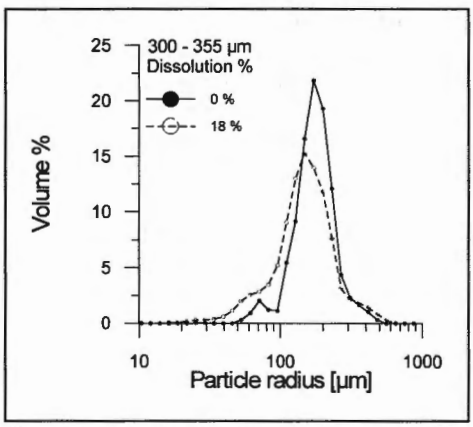

Figure 4.12 Grain size distributions of initial and partly dissolved olivine. Fraction 300-355 μm.

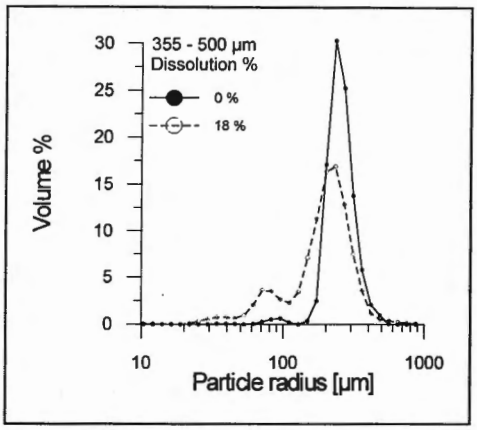

Figure 4.13 Grain size distributions of initial and partly dissolved olivine. Fraction 355-500 μm.

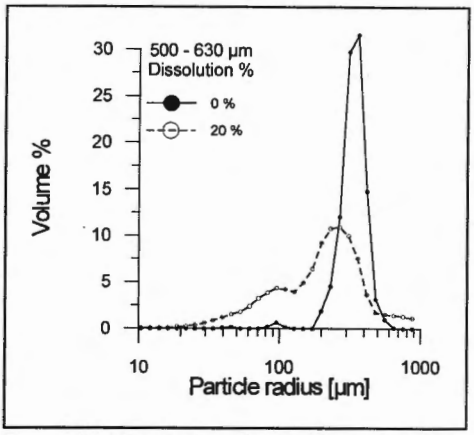

Figure 4.14 Grain size distributions of initial and partly dissolved olivine. Fraction 500-630 μm.

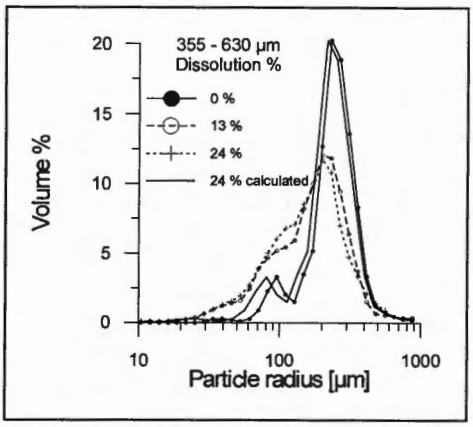

Figure 4.15 Grain size distributions of initial and partly dissolved olivine. Fraction 355-630 μm.

In Table 4.2 reaction data on the partial dissolution experiments is presented, together with the geometrical surface areas of olivine calculated from the measured and modeled grain size distributions. The geometrical surface areas are expressed as total m^2 of olivine surface area present in the reactor. Figure 4.11 shows that the shape of the grain size distribution of the fine (63-150 μm) fraction is hardly affected by dissolution. The measured distribution after dissolution is slightly broader and only slightly shifted to the left (towards smaller grain sizes) as compared to the initial distribution. The shift to smaller grain sizes is very small compared with the expected shift, as illustrated by the calculated distribution. Table 4.2 shows that despite this difference in shape of measured and calculated grain size distributions, the geometrical surface areas, calculated from the grain size distributions, are similar.
The grain size distributions of the coarse olivine fractions (larger than 300 μm) are considerably affected by dissolution. Figures 4.12 to 4.15 show that the initial bimodal grain size distributions are broadened and shifted towards smaller grain sizes during dissolution. The broadening indicates that the amount of relatively finer particles increases with respect to larger particles. Furthermore the distributions after partial dissolution all appear to be trimodal. For the olivine fractions larger than 300 μm there is, in contrast to the fine olivine fraction, a difference between the olivine surface areas calculated from the measured and the modeled distributions. This is illustrated by the ratio of both surface areas (k_a) in Table 4.2. The surface area calculated from the measured distributions is larger than the one calculated from the modeled distributions. The difference between both surface areas rises with increasing olivine grain size fraction.

Grain size Fraction [μm]	Reaction time [minute]	Dissolution percentage [%]	Geometrical surface area of measured distribution [$\cdot 10^{-2}$ m^2]	Geometrical surface area of calculated distribution [$\cdot 10^{-2}$ m^2]	k_a: [Ratio of measured and calculated geometrical surface area]
63 - 150	6 12	17 28	6.05 5.36	6.10 5.29	0.99 1.01
300 - 355	15	18	2.90	2.28	1.27
355 - 500	18	18	2.50	1.55	1.61
500 - 630	20	20	2.62	1.15	2.28
355 - 630	9 15 18	13 19 24	3.11 2.87 2.79	1.86 1.72 1.63	1.67 1.67 1.71

Table 4.2 Experimental data on partial dissolution experiments and geometrical surface areas of measured and calculated grain size distributions after partial dissolution.

The same trend has been observed for the complete neutralization experiments, where the difference in observed and predicted reaction rate increases with increasing grain size fraction. The data from the partial dissolution experiments and the complete neutralization experiments can be combined. Table 4.3 presents the ratio of k_r (ratio of surface area factor and calculated geometrical surface area, from Table 4.1) and k_a (ratio of the surface area calculated from measured and modeled distributions, from Table 4.2). Considering the precision of the data, this ratio is remarkably similar for all grain size fractions.

Grain size Fraction [μm]	Ratio of k_r and k_a
300 - 355	1.65
355 - 500	1.65
500 - 630	1.56
355 - 630	1.55

Table 4.3 Ratio of k_r (from Table 4.1) and k_a (from Table 2.2).

Discussion

Dissolution experiments with olivine fractions of a grain size smaller than 300 μm, described in Chapter 3, revealed that the dissolution rate is linearly related to the geometrical surface area, calculated from the initial grain size distribution. The rate was found to be proportional to a constant of 1.92 (±0.12) times the geometrical surface area, independent of the grain size fraction. The results from the experiments with olivine grain sizes larger than 300 μm indicate that the dissolution rate of these larger grain sizes is also linearly related to the calculated geometrical surface area. However, the constant depends on the grain size fraction, and increases with larger grain size fractions. Qualitatively the dependance of the constant can be explained by a mechanism where larger olivine grains dissolve preferentially along existing micro cracks, and break up into a number of smaller fragments. The disintegration causes an increase in reacting surface area, resulting in a higher dissolution rate. The dependence of the surface area constant on the grain size fraction shows that for larger grain

sizes the difference between the actual olivine surface area and the surface area modeled from the initial grain size distribution is larger.
It is highly remarkable that the dissolution rate of the larger fractions is linearly proportional to the geometrical surface area calculated from the initial grain size distribution. It can be expected that by fragmentation of large particles, the grain size distribution of the dissolving olivine changes drastically. This is substantiated by the experiments, in which the grain size distribution of partly dissolved olivine fractions was measured.
For the fraction of a grainsize of 63-150 μm, the distribution after dissolution of 28 % is slightly broadened and shifted towards smaller grain sizes. However, the shift is less than expected on the basis of calculations (Figure 4.11). This may be explained by a dissolution mechanism where initially olivine is mainly dissolved by the formation of extensive etch features, leaving the macroscopic morphology of the grains intact. The geometrical surface areas calculated from the measured and modeled distribution are, on the other hand, comparable. This illustrates that despite the fact that the calculated geometrical surface area can be used to model the dissolution rate, the calculated grain size distribution is not representative for the actual grain size distribution of the dissolving olivine.
There is a clear change in grain size distribution after partial dissolution for the olivine fractions larger than 300 μm. The broadening of the grain size distribution indicates that the amount of relatively finer particles increases relatively to larger particles, which corroborates the mechanism of fragmentation of large particles during dissolution. After partial dissolution, the surface area calculated from the measured grain size distributions is higher than the surface area calculated from the modeled distribution, and the difference increases for a larger grain size fraction. This is in accordance with the results from the complete neutralization experiments. Division of the surface area constants obtained from the complete neutralization experiments by the ratio of surface areas calculated from measured and modeled grain size distributions yields similar values for all fractions, with an average of 1.6. This suggests that the bulk dissolution rate of the coarse fractions is proportional to 1.6 times the actual, and not the modeled, geometrical surface area. This value of 1.6 is lower than the surface area constant of 1.92 ($\pm$0.12) that was obtained for olivine fractions smaller than 300 μm, in Chapter 3. However, both surface area constants are of comparable magnitude, considering the precision of the data, and the fact that the actual geometrical surface areas could only be determined after limited degrees of dissolution. Another possible explanation for a lower surface area constant for coarser fractions might be the fact that all surface area exposed by fragmentation of large grains is not equally reactive.
With these data it is possible to model the dissolution rate of any olivine grain size distribution if the relationship between geometrical surface area and olivine volume is known. For olivine fractions smaller than 300 μm it has been demonstrated that the geometrical surface area, calculated from the initial grain size distribution, can be adequately used. For fractions of a size larger than 300 μm, however, fragmentation of the grains has to be taken into account. At present it has not been possible to calculate grain size distributions dealing with this fragmentation process as a function of the extent of dissolution, since it is impossible to assess the extent of fragmentation as a function of dissolution time. Therefore, the relationship between surface area and olivine volume has to be determined by experiments.

Conclusions

- During dissolution of olivine grains with internal fractures, dissolution proceeds preferentially along the micro cracks, causing break-up of the grains. The fragmentation increases the available surface area of the olivine, resulting in higher dissolution rates.
- The rate equation that was used for the fractions of Norwegian olivine of a size smaller than 300 μm used in Chapter 3 can also be satisfactorily fitted to complete neutralization experiments of coarser fractions. The resulting surface area constants increase with fractions of a larger size.
- After partial dissolution, the change of the grain size distribution of the fine fraction 63-150 μm is smaller than expected. This might be explained by the formation of extensive etch features, leaving the macroscopic morphology of the grains intact. The geometrical surface areas calculated from measured and modeled grain size distributions are, however, similar.
- For the fractions larger than 300 μm there is a clear change in grain size distribution. The distributions are broadened and shifted towards smaller grain sizes during dissolution. This broadening indicates that the amount of relatively finer particles increases with respect to larger particles.
- Division of the surface area constants from complete neutralization experiments by the ratios of surface areas calculated from measured and modeled distributions yields similar values for all grain size fractions, with an average of 1.6.
- It is possible to calculate the extent of dissolution as a function of time if the geometrical surface area is known as a function of olivine volume. For fractions of a size smaller than 300 μm of the Norwegian olivine used in the experiments the geometrical surface area can be calculated as a function of volume from the initial grain size distribution. For fractions of a larger size the surface area has to be determined as a function of olivine volume by experiments, since it is not possible to assess the extent of fragmentation of the grains as a function of the time of dissolution.

Chapter 5

Olivine Type, Implications for the Olivine Process

Abstract
The properties of natural raw materials are in general variable. For industrial processes using natural raw materials it is essential to know the influence of the varying properties on the perfomance of the process.
For the neutralization of waste acids with olivine, the following olivine properties are of importance, the mineralogical composition and the deformation/alteration history of the olivine source rock, as well as the chemical composition of the olivine.
This study investigates the dissolution behavior of olivine from three different potential sources in sulphuric acid. One of the olivine comes from Norway (FO_{93}) and three from Greece (FO_{92}- FO_{90}). The dissolution behavior of these olivines is compared with the Norwegian olivine used in chapters 3 and 4. The main difference in dissolution behavior is the higher dissolution rate of the three olivines from Greece. A possible explanation for the higher dissolution rate is the presence, or formation during dissolution, of more abundant etch-features as compared to the Norwegian olivines.
It is shown that differences in the rate of neutralization due to varying olivine properties are small as compared to, e.g., the effect of temperature on the reaction rate.

Introduction

The chemical and physical properties of natural materials are in general subject to considerable variation. The suitability of an olivine type for the neutralization of waste acids is determined by several factors. The most important factors are the mineralogical composition of the olivine source rock, the degree of deformation and the alteration of the source rock, and the chemical composition of the olivine. Evidence for the importance of the degree of deformation has been given in Chapter 4, where relative higher dissolution rates of coarse olivine fractions were explained by the presence of micro cracks. Wogelius and Walther (1991) established the dependance of the olivine dissolution rate on the chemical composition by observing that the dissolution rate of olivine increases with the iron content. In order to investigate the suitability for the neutralization of industrial waste acids, olivine from three potential sources was tested, by carrying out a set of complete neutralization experiments.

Another set of experiments was carried out to compare the dissolution behavior of the olivine types tested in this study with that of the Norwegian olivine that was tested in chapter 3. In these experiments small amounts of olivine were partly dissolved, followed by measurement of the grain size distribution of the remaining olivine fractions.

Materials and Method

For the experiments four types of olivine were used, one type from Norway and three from Greece. The Norwegian sample was produced by A.S. Olivine, and was provided by Holland Mineraal B.V. (code AFS50). The Greek olivine rock samples were provided by IGME, two samples came from the Gerakini magnesite mine, currently exploited by Grecian Magnesite S.A. (codes GN1 & GN2), and one from the Vavdos magnesite mine, operated by Magnomin (code AN1). The samples were taken from unaltered parts of the ultramafic bodies that host the magnesite mineralisations. The rock samples were, if necessary, crushed to a size smaller than 2mm with a jaw crusher. From all samples a grain size fraction of 63-150 μm was separated by wet-sieving, according to the method described in chapter 3.

The resulting grain size distribution of the olivine samples was measured with a Malvern 3600D laser particle sizer. The chemical composition of all olivine samples was determined by ICP-ES. Microscopical studies revealed that the Greek samples contained small amounts of magnesite ($MgCO_3$). Since this carbonate is very reactive in acid, it is important to know the exact concentration. Therefore carbonate analyses of all samples were carried out with a NA 1500 NCS analyzer from Fisons Instruments. Small amounts (± 40 mg) of a sample were heated in tin sample holders to 1010 °C, followed by "dynamic flash combustion" of the sample holder, which increases the temperature up to 1800 °C. The CO_2, produced by decomposition of carbonates in the sample, is measured with a thermal conductivity detector. Carbonate analyses could be performed with a relative standard deviation of 3 %.

Dissolution experiments were carried out in vigorously stirred double-walled vessels at 80 °C, according to the procedure described in chapter 3. For all experiments technical grade 3 M sulphuric acid was used.

The curves of the H^+ concentration versus the reaction time obtained for all olivine types were subsequently compared with curves calculated with the reaction rate equation that was derived in Chapter 3 (for Norwegian olivine, code N2). For the calculations, the exact weight of olivine, used in each experiment, and the measured grain size distribution of each olivine type was used.

The partly dissolved olivine samples for the grain size distribution measurements were

prepared according to the method described in chapter 4. All olivine samples were allowed to dissolve for 12 minutes in 3 M H_2SO_4 at 80 °C.

Results and Interpretation

In tables 5.1 and 5.2 the mineralogical composition and the chemical composition of the olivine samples that were tested are listed.

Sample	Wt % olivine	Wt % magnesite	Wt % inerts
N2 (Norwegian)	92.6	0.0	7.3
AFS 50 (Norwegian)	94.8	0.0	5.2
AN1 (Greek, Vavdos)	95.6	3.1	1.3
GN1 (Greek, Gerakini)	97.2	1.4	1.4
GN2 (Greek, Gerakini)	94.2	2.0	3.8

Table 5.1 Mineralogical composition of olivine types tested

Sample	Molar weight [g]	# of atoms per SiO_4			
		Mg	Fe	Ni	Mn
N2	145.2	1.86	0.13	0.006	0.0007
AFS 50	145.1	1.86	0.13	0.006	0.0007
AN1	145.4	1.85	0.14	0.007	0.0009
GN1	146.4	1.82	0.17	0.006	0.0013
GN2	146.5	1.82	0.18	0.004	0.0015

Table 5.2 Molar weights and chemical composition of olivines, expressed in number of atoms per SiO_4

In figures 5.1 to 5.4 the experimental curves of the H^+ concentration versus the reaction time are compared with the calculated neutralization curves. In Chapter 3 it was demonstrated that experimental neutralization curves could be reproduced with a precision of 4 % by using the derived reaction rate equation. (The precision of 4 % corresponds with a maximum difference between calculated and measured curve of 0.24 mol H^+.)

Figure 5.1 shows that, considering the above precision, there is no significant difference between the experimental and calculated neutralization curve of Norwegian olivine AFS 50 (there is a small, insignificant deviation at 20 and 30 minutes reaction time).

For the Greek olivine AN1 the experimental curve cannot be satisfactorily reproduced. Figure 5.2 shows that the Greek olivine reacts significantly faster than predicted by the rate equation. The difference is large during the initial stages and diminishes towards the end of the reaction. The maximum difference between observed and calculated H^+ concentration is 0.5mol·liter^{-1}.

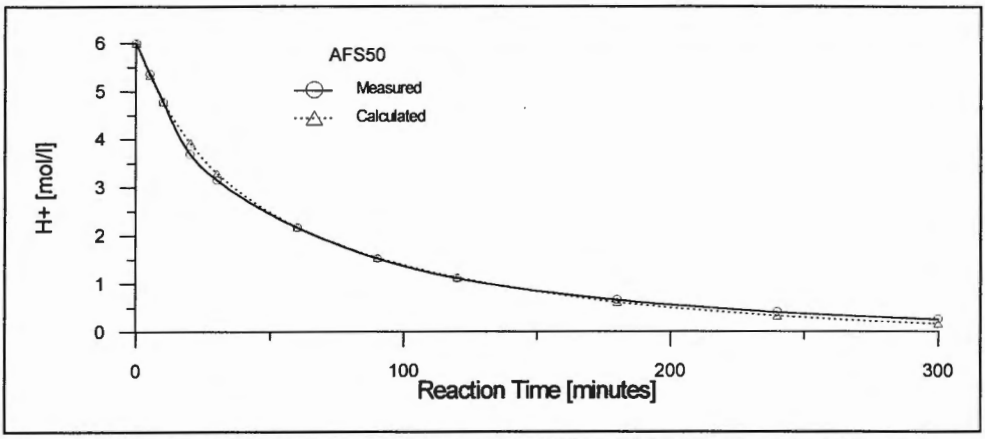

Figure 5.1 Calculated and measured concentration of H^+ as a function of reaction time for olivine type AFS 50.

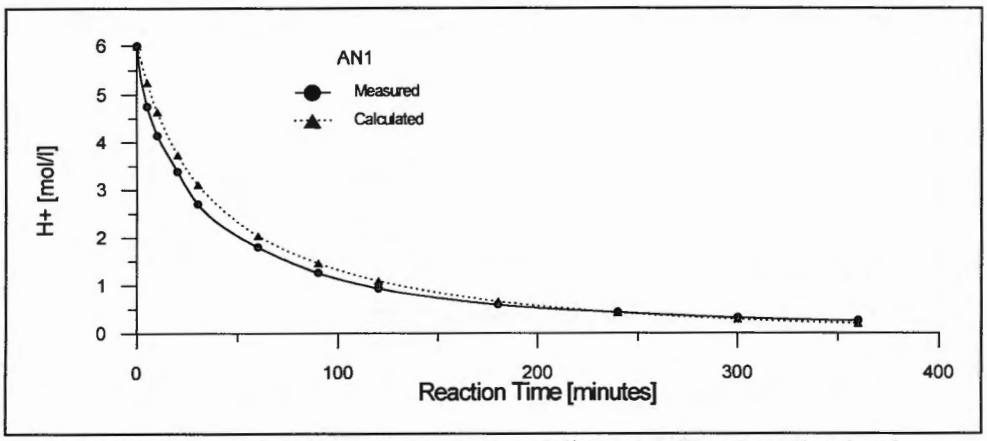

Figure 5.2 Calculated and measured concentration of H^+ as a function of reaction time for olivine type AN1.

The two other Greek olivines GN1 and GN2 give the same results, Figures 5.3 and 5.4 illustrate that initially also these Greek olivines react faster than predicted. The maximum differences between the experimental and the calculated H^+ concentration are 0.6 and 0.7 mol·liter^{-1} for GN1 and GN2, respectively. Near the end of the neutralization, ($[H^+] < 1$ mol·liter^{-1}), the predicted H^+ concentration is lower than observed. However, for both types of olivine the difference is smaller than 0.24 mol·liter^{-1}, and thus barely significant.

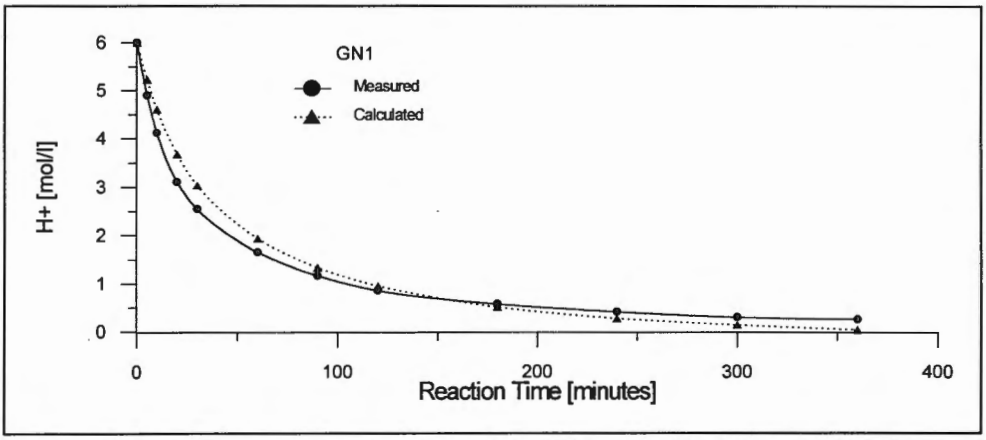

Figure 5.3 Calculated and measured concentration of H^+ as a function of reaction time for olivine type GN1.

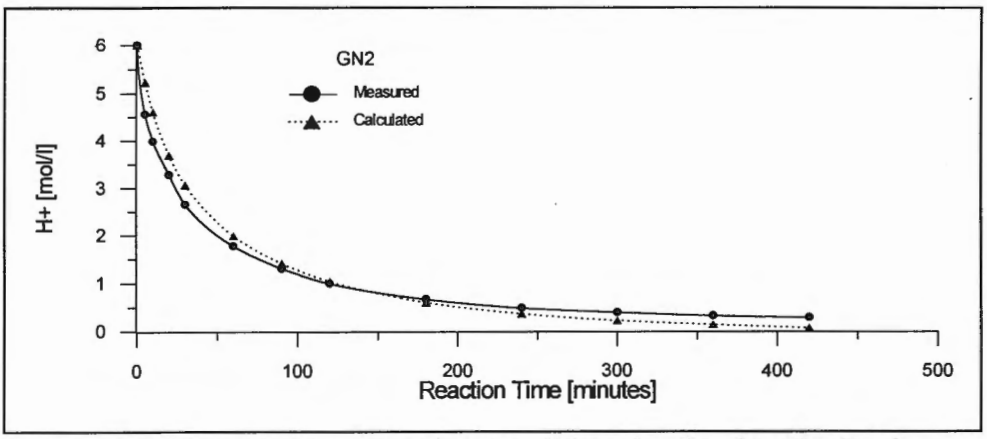

Figure 5.4 Calculated and measured concentration of H^+ as a function of reaction time for olivine type GN2.

For the grain size distribution measurements after partial dissolution, all samples were allowed to react for 12 minutes. This resulted in a dissolution of 28 % for the Norwegian olivine AFS 50 and of about 40 % for the three Greek samples. The grain size distributions before and after partial dissolution are compared for all samples in Figures 5.5 to 5.8. The figures show that for all olivines the grain size distribution after dissolution is slightly broader and slightly shifted to the left (towards smaller grain sizes) as compared to the initial distributions. The change of the distribution is the same as was observed in chapter 3b for the Norwegian olivine N2 that was used to derive the reaction rate equation. Apparently the grains of the olivine types tested do not break-up significantly during dissolution, as compared to olivine N2.

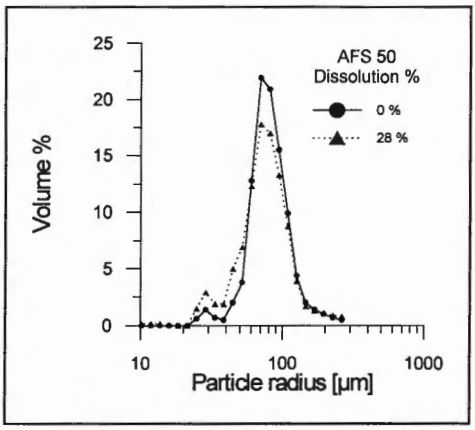

Figure 5.5 Grain size distributions of initial and for 28 % dissolved olivine. Sample AFS 50 .

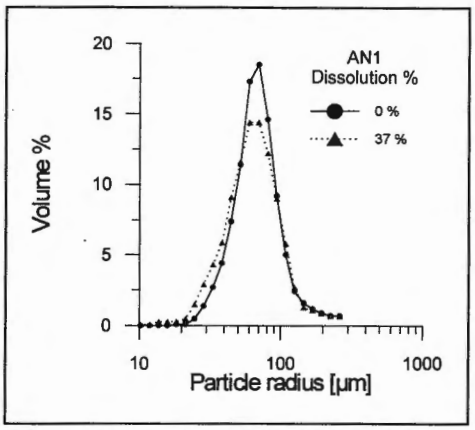

Figure 5.6 Grain size distributions of initial and for 37 % dissolved olivine. Sample AN1.

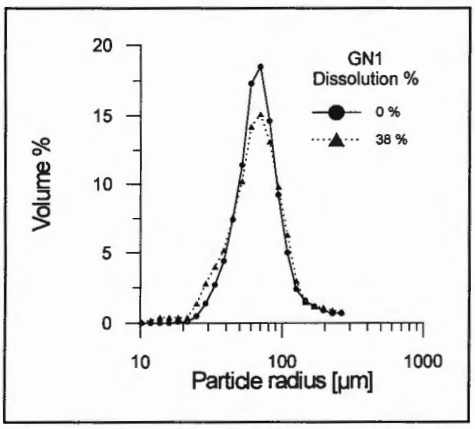

Figure 5.7 Grain size distributions of initial and for 38 % dissolved olivine. Sample GN1.

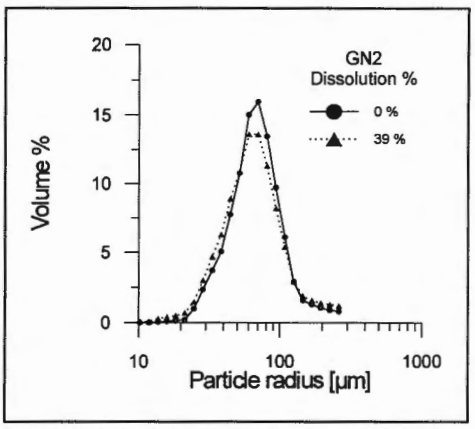

Figure 5.8 Grain size distributions of initial and for 39 % dissolved olivine. Sample GN2.

Discussion

The measured neutralization curve of the Norwegian olivine AFS 50 could be satisfactorily reproduced by calculations using the reaction rate equation derived in chapter 3. This illustrates the robustness of the dissolution model. Despite the fact that olivine AFS 50 and the olivine used to derive the rate equation (N2) were produced from the same olivine deposit, they were processed differently and provided by different companies.

The small, non-significant, difference between the calculated and the observed H^+ concentration after a reaction time of 20 and 30 minutes, might be due to the fact that at this time the reaction mixture had reached the viscous stage.

Unfortunately, the reaction rate equation from chapter 3 fails to reproduce the experimental

neutralization curves of the three Greek olivines. The Greek olivines initially react faster than predicted by the rate equation. Part of the difference in reaction rate can be attributed to the presence of small amounts of magnesite, which will react immediately with hot acid. For olivine AN1 this implies that the maximum difference of 0.5 mol·liter^{-1} between the calculated and the observed H^+ concentration would be 0.33 mol·liter^{-1}. Considering the reproduction precision of the rate equation of 0.24 mol·liter^{-1} (chapter 3), this is a significant difference. For the olivines GN1 and GN2 the maximum differences, corrected for the presence of magnesite, are respectively 0.48 and 0.62 mol·liter^{-1} H^+, which are also significant.

The differences cannot be explained by a mechanism, in which olivine grains break-up during dissolution, thereby creating additional surface area and increasing the reaction rate. This was demonstrated by the similarity of the grain size distributions measured after partial dissolution of the Greek and Norwegian olivines.

A possible explanation for the higher dissolution rates of the Greek olivines might be their higher iron contents. Comparison of the iron content of the olivines with the maximum difference between the observed and the calculated H^+ concentration shows a positive relationship. However, when the rate constant would be adjusted to compensate for the initial difference between measured and observed rates, the predicted H^+ concentration near the end of the neutralization ($[H^+] < 1M$) would be significantly lower than the observed concentration. This is especially the case for the Gerakini olivines GN1 and GN2.

Another explanation for the higher reactivity of the Greek olivines might be the presence, or formation during dissolution, of more abundant etch-features as compared to the Norwegian olivine. This seems likely considering the fact that the Greek olivine samples came from deformed and altered ultramafic bodies.

The higher reaction rate of the Greek olivines is an advantage with their application in the neutralization of industrial waste acids. The presence of magnesite in the ground olivine is only expected to be a problem if emission of CO_2 is unwanted or the interest of performing the dissolution process is more focussed on the production of silica than on the neutralization of waste acids. Furthermore it has to be realized that the higher iron content of the Greek olivines will increase the consumption of chemicals during further processing of the residual solution of the Olivine Process.

Despite the higher reactivity and the presence of some magnesite in the Greek olivines, the actual difference in reaction rate between Norwegian and Greek olivine is small as compared to, e.g., the effect of temperature on the reaction rate.

Conclusions

- The grain size fraction of 63-150 μm of Norwegian olivine AFS 50 reacts similarly with acid as the same fraction of Norwegian olivine N2, that was used in chapter 3 to derive a rate equation. This is illustrated by the fact that the measured neutralization curve of AFS 50 can be satisfactorily reproduced by calculations using the reaction rate equation for Norwegian olivine N2. This also illustrates the robustness of the dissolution model.
- The same grain size fractions of three Greek olivines react differently as compared to Norwegian olivine N2. The Greek olivines react initially faster than predicted by the model. Furthermore, for the two olivines from Gerakini the predicted H^+ concentration is near the end of the neutralization ($[H^+]<1$ mol·liter^{-1}) lower than the observed concentration.
- The higher initial dissolution rate can only in part be explained by the presence of small amounts of magnesite.
- Grain size distribution measurements of partly dissolved olivine fractions indicate that compared to the Norwegian olivine N2 the Greek olivines do not break-up significantly.
- A possible explanation for the higher dissolution rate may be the higher iron content of the Greek olivines. However, a simple adjustment of the rate constant to compensate for the higher initial rates will increase the difference between the predicted and the observed H^+ concentration at the end of the neutralization. Another explanation is the presence, or formation during dissolution, of more abundant etch-features as compared to the Norwegian olivine.
- The differences in reaction rate of the olivine types tested in this study are small ascompared to, e.g., the effect of the temperature on the reaction rate.
- The high reaction rate of the Greek olivines is an advantage with their use for the neutralization of waste acids.

Chapter 6

Heat of Reaction of the Dissolution of Olivine in Sulphuric Acid

Abstract

One of the main advantages of the Olivine Process is the low energy consumption due to the exothermic reaction of olivine and acid. Accurate heat of reaction data are necessary for the industrial design of the Olivine Process.

The heat of reaction was measured for the dissolution of three olivine types in 3 molar sulphuric acid with a LKB 2277 bio-activity monitor. Two Norwegian olivines were used, both FO_{93}, and one from Greece, FO_{92}. With the analytical method used no significant differences in heat of reaction between the three olivine types, could be detected. The average value of the heat of reaction of the dissolution of olivine in sulphuric acid was determined at (223 ± 2.9) kJ· mole^{-1}.

The dissolution behavior of the three olivine types is discussed by comparing the heat of reaction curves with the geometrical surface areas calculated as a function of olivine volume. The comparison shows that the Greek olivine reacts faster than the Norwegian olivine.

Introduction

The dissolution of olivine in sulphuric acid is exothermic. Schuiling et al. (1986) suggested that, after initial heating, the reaction will sustain itself. Van Herk and Pietersen (1987) calculated a heat of reaction of 351.3 kJ ·mole^{-1} for the dissolution of pure Mg_2SiO_4. Due to the exothermic reaction, the energy consumption of the Olivine Process is low, which is one of the main advantages of the process (Chapter 1).

For the industrial design of any process it is necessary to have accurate data on the heat of reaction. Since no literature data providing accurately measured heat of reaction for the dissolution of olivine in acid is available, a study was carried out to determine the heat produced during dissolution of olivine in 3 M H_2SO_4.

Furthermore, monitoring the heat of reaction produced during reaction can be used to gain information on the dissolution behavior of olivine.

Materials, Methods & Data Treatment

The heat of reaction was measured with a LKB 2277 bio-activity monitor. The monitor measured the heat flow from a small reaction vessel containing the dissolving olivine. The output in μW was recorded at 60 seconds time intervals, using the computer program Digitam 2. The measurements were carried out with small, 5-10 mg, samples of olivine, which were allowed to dissolve in 2.5 ml 3 M H_2SO_4 at 63 °C. The small reaction vessels consisted of tightly sealed glass bottles of a volume of 3 ml. The amounts of olivine were chosen so as to not exceed the upper measurement limit of 1000 μW. Consequently the maximum amount of acid consumed was only 2% of the initial amount.

Three types of olivine were used, two samples from Norway and one from Greece. The Norwegian samples were both produced by A.S. Olivine. One sample, with grain sizes from 0-4mm, was provided by Hoogovens B.V.(code N3); the other, with grain sizes from 0.1-0.3 mm by Holland Mineraal B.V.(code AFS 50). The Greek olivine rock sample was provided by the Greek geological survey, IGME, and came from the Magnomin magnesite-mine in Vavdos (code AN1). The rock-samples were crushed to < 2mm with a jaw crusher if necessary. The chemical composition of the olivine samples was determined by ICP-ES:

Norwegian samples N3 & AFS 50: $Mg_{1.86}Fe_{0.13}Ni_{0.006}Mn_{0.0007}SiO_4$ (FO_{93})

Greek Olivine sample AN1: $Mg_{1.85}Fe_{0.14}Ni_{0.007}Mn_{0.0009}SiO_4$ (FO_{92})

For the experiments a narrow grain size fraction of 90-106 μm was selected with all olivine types. In order to study any effects of grain size, a coarser fraction of 200-250 μm was used for the two Norwegian olivine samples. The desired grain size fractions were obtained by wet-sieving for 20 minutes. Subsequently the olivine was separated from the other minerals by magnetic separation using a Frantz isodynamic separator (operating conditions: 15° forward slope, 20° side tilt, fraction 0.73-0.80 Amp.). Finally the olivine fractions were ultrasonically treated to remove any adhering fines.

The 3 M H_2SO_4 solution was prepared from concentrated (95-97 %) technical grade sulphuric acid from Lamers & Pleuger B.V. and demineralized water.

Measurement procedure:

The olivine and sulphuric acid were added at room temperature in 3 ml glass bottles, that were immediately sealed with aluminum caps. After weighing, to detect any leakage during reaction, the bottles were put into the monitor in pre-heating position, where they were allowed to reach the exact measurement temperature (63 °C) for 20 minutes. Recording software was started 1 minute after placement into the pre-heating position. The samples were monitored for 24 hours. For calibration purposes a pulse of 300 μW was generated for 60

minutes, after 16 hours recording, during all analyses. All analyses were carried out in duplicate.

Data treatment:
First the background signal, measured at the beginning and end of each analysis, was subtracted. After subtraction only analyses where the calibration pulse was within ± 2% of 300 μW were further processed. Next the heat of reaction data was re-scaled in order to make the calibration pulse exactly equal to 300 μW. Subsequently the heat of reaction curves were linearly extrapolated from the start of the measurement over the 20 minutes pre-heating interval. The heat of reaction was obtained by integration of the reaction heat curves.

Results and Interpretation
In Figure 6.1 the heat of reaction, calculated with respect to the initial amount of olivine, is plotted versus time for both the fine and coarse fraction of the Norwegian olivine. From these curves it can be clearly seen that the fine fraction reacts faster than the coarse fraction. In Figure 6.2 the scaled heat of reaction data of the fine fractions of the Norwegian (N3) and the Greek olivine are compared. The Greek olivine reacts faster than the Norwegian olivine. The heat of reaction data of all experiments was integrated in order to determine the heat of reaction of each olivine sample. In Table 6.1 the results are summarized.

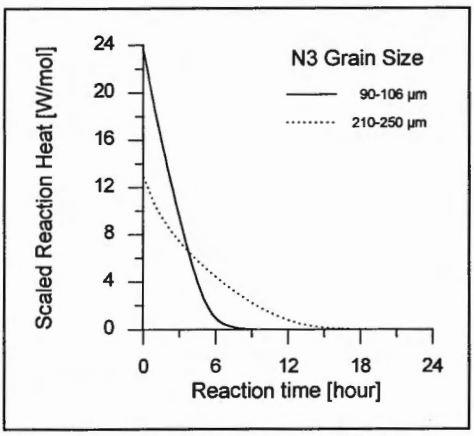

Figure 6.1 Heat of reaction scaled to initial amount of olivine versus reaction time. Fine and coarse fraction of Norwegian olivine N3.

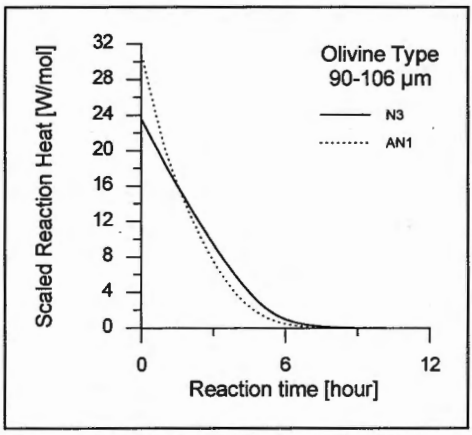

Figure 6.2 Heat of reaction scaled to initial amount of olivine versus reaction time. Fine fraction of Greek AN1 and Norwegian olivine N3.

From the duplicate experiments a standard deviation of 2.9 was calculated. Taking this standard deviation into account, only the difference in heat of reaction of the fine fraction of the Greek olivine (217 kJ/mole) and of the coarse fraction of AFS50 (229 kJ/mole) is significant. Within the limits of the analytical accuracy, no significant differences exist between the other measurements.

Olivine type	Grain size [μm]	Olivine amount [mg]	Total energy [J]	Heat of reaction [kJ/mole]	Average heat of reaction
N3	90-106	5.70 4.91	8.85 7.53	225 223	224
	210-250	9.66 8.30	14.93 12.47	224 218	221
AFS50	90-106	4.78	7.33	223	(223)
	210-250	8.76 9.71	13.88 15.27	230 228	229
AN1	90-106	5.11 5.04	7.69 7.43	219 214	217

Table 6.1 Experimental heat of reaction data.

Under the assumption that during the reaction heat measurements the dissolution rate is controlled by surface reactions, the curves of heat production versus time can be used to extract information on the reacting olivine surface. The assumption seems to be justified, since during the experiments no silica was precipitated on the dissolving grains and the diffusional transport rates of Mg^{2+} and H^+ are expected to be higher than the olivine dissolution rates.

Since it is not possible to measure the reacting olivine surface area during dissolution, the reaction heat data is compared with a calculated geometrical surface area. The geometrical surface area is calculated by assuming a lognormal grain size distribution of spherical particles, between the minimum and maximum grain size of the sieve fractions used. The surface area is calculated as a function of the residual amount of olivine by assuming that the rate of decrease of the particle radii is independent of the particle radius. In Figure 6.3 the reaction heat of the fine fractions of both Norwegian olivines is plotted versus the calculated geometrical surface areas. Both curves are approximately linear.

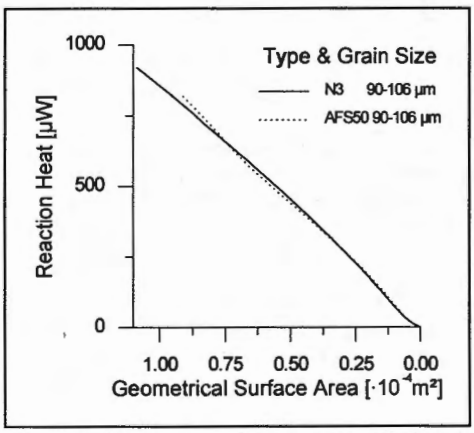

Figure 6.3 Heat of reaction versus calculated geometrical surface area. Fine fraction of Greek AN1 and Norwegian N3 olivine.

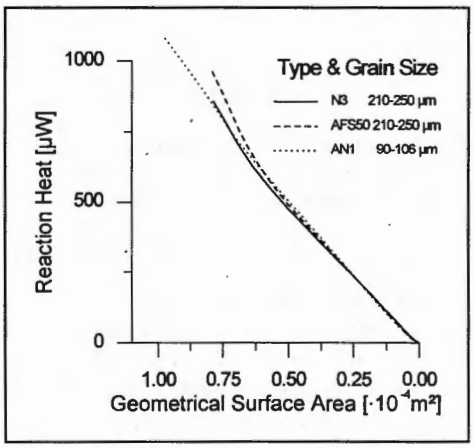

Figure 6.4 Heat of reaction versus calculated geometrical surface area. Coarse fraction of Norwegian N3 & AFS50 and fine fraction of Greek AN1 olivine.

Figure 6.4 represents the curves of the reaction-heat versus the geometrical surface area for the coarse fractions of the Norwegian olivine and the fine fraction of the Greek olivine. These three curves appear to consist of two linear parts, of which the initial part has a slightly higher slope than the later part, which coincides with the curves for the fine fractions of the Norwegian olivines.

Discussion

A large possible source of error in the analytical procedure is the extrapolation of the heat of reaction over the initial 20 minute pre-heating period. During this period the sample is allowed to reach the exact measuring temperature, which is required for an accurate measurement. However, already about 8% of the coarse fractions and 15 to 20% of the fine fractions is dissolved during that period. The use of the heat of reaction data for the study of the reacting olivine surface area may therefore be insensitive for any initial dissolution features. However, for the determination of the reaction heat the effect of the extrapolation is expected to be of minor importance. The heat of reaction of the dissolution of olivine (AFS50) in sulphuric acid was also estimated by monitoring the temperature increase during the initial reaction stages of a neutralization experiment performed on a scale of 10 liter. The heat of reaction was subsequently calculated using the measured temperature and the experimentally determined heat-loss of the reactor. This yielded an estimation of 234 kJ/mole olivine, which is close to the above mentioned heats of reaction.

The current analytical procedure enables one to measure the heat of reaction with a standard deviation of 2.9 kJ/mole. With this precision no significant effect of the grain size on the heat of reaction could be found. The only slightly significant difference in heat of reaction was measured between the fine fraction of the Greek olivine and the coarse fraction of AFS50. Despite the slight difference in chemical composition of the olivine, the heat of reactions measured for the Greek AN1 and Norwegian N3 olivine are similar. The heat of reaction, averaged over all experiments is 223±2.9 kJ/mole.

Comparison of the reaction heat data with the calculated geometrical surface area revealed that the heat of reaction of the fine fractions of both Norwegian olivines is linearly proportional to the geometrical surface area. For these olivine fractions the geometrical surface area can thus be satisfactorily used to model the reaction heat curves. For the coarse fractions of the Norwegian olivines and the fine fraction of the Greek olivine the relationship is not simply linear. The curves of heat of reaction versus the geometrical surface area appear to consist of two linear parts. The slope of the final part coincides with the curves for the fine fractions of the Norwegian olivines, where that of the initial part is higher. A possible explanation for this is that initially the reacting olivine surface area is larger with respect to the geometrical surface area. This can be caused by the formation of extensive etch features. The higher initial dissolution rate of the Greek (AN1) olivine as compared to the Norwegian, is in accordance with the bulk dissolution experiments presented in Chapter 5.

The dissolution rates for the N3 Norwegian olivine found in this study can be compared to the dissolution rates calculated by the dissolution model, that was dealt with in chapter 3. The dissolution rate, calculated from the heat of reaction data, was averaged over the two grain size fractions used. This yielded a dissolution rate of $(1.02 \pm 0.01)\cdot10^{-2}$ [mole $H^+\cdot minute^{-1}\cdot m^{-2}$ olivine surface area]. The dissolution rate calculated with the dissolution model is $(1.6 \pm 0.1)\cdot10^{-2}$ [mole $H^+\cdot minute^{-1}\cdot m^{-2}$ olivine surface area]. These dissolution rates are of the same order of magnitude, despite the fact that they were determined by completely different methods.

Conclusions

- The heat of the dissolution reaction in 3M sulphuric acid was measured for three types of olivine. With the current measurement procedure no significant effect of the type of olivine and the grain size on the heat of reaction could be detected. The average heat of reaction of all olivine types is 223±2.9 kJ/mole olivine.
- For a good reaction heat measurement it is required to pre-heat the sample, for 20 minutes, to the exact measurement temperature. The use of heat of reaction data for a quantitative study of the reactive olivine surface area is not possible during this period of time.
- The heat of reaction of the fine fractions of both Norwegian olivines is linearly proportional to the calculated geometrical surface area. For the coarse fractions of the Norwegian olivines and the fine fraction of the Greek olivine the curves of heat of reaction versus the geometrical surface area appear to consist of two linear parts The initial part has a slightly steeper slope than the later part, which coincides with the curves for the fine fractions of the Norwegian olivines. A possible explanation for this is the formation of extensive etch features during the initial stages of dissolution.

Chapter 7

The Olivine Process for the Neutralization of Waste Acids

Abstract

Since each waste acid has a characteristic composition it is important to assess whether specific adaptations have to be made to the Olivine Process to optimize the reaction progress and the properties of the reaction products. The use of olivine for the neutralization of three different waste acids is investigated by comparing the neutralization behavior with technical grade sulphuric acid.

One of the waste acids is a sulphuric acid (2.9 M H_2SO_4) with inorganic contaminants from the production of titanium dioxide. The two other waste acids contain organic contaminants; a concentrated sulphuric acid (12.8 M H_2SO_4), and a concentrated hydrochloric acid (9.7 M HCl). The concentrated sulphuric acid has to be diluted to 3 M H_2SO_4 in order to prevent the precipitation of magnesium sulphate after neutralization. Dilution is not necessary for the hydrochloric acid. As compared to pure sulphuric acid, the neutralization rate of the titanium dioxide waste acid is slightly lower, which is attributed to the higher ionic strength of the waste acid. The presence of organic compounds increases the rate of neutralization.

The neutralization of the three waste acids yields white precipitated silicas. In order to prevent the precipitation of heavy metals on the silica from the titanium dioxide waste acid, the neutralization must be stopped at a pH level below 1, and the silica has to be separated and washed as rapidly as possible. Typically, the resulting silica contains about 2 wt % TiO_2. The surface areas of silicas from the waste sulphuric acids are comparable to those from pure sulphuric acid. The silica from the hydrochloric waste acid has a significant lower surface area.

By raising the pH with magnesium oxide, most of the contaminating metals can be separated from the residual solution of the titanium dioxide waste acid. The use of magnesium oxide has the advantage that no new cations are introduced in the residual (magnesium) sulphate solution.

Introduction

The success of the application of the Olivine Process for the treatment of industrial waste acids is not only determined by the neutralization reaction. Further processing of the neutralized solution and production of usefull by-products are equally important. As each waste acid has its own characteristic composition, specific adaptions may have to be made to the Olivine Process to achieve a rapid reaction and to control the properties of the reaction products.

The suitability of the Olivine Process for the neutralization of three different waste acids has been tested. One of the waste acids was a sulphuric acid with inorganic contaminants from the production of titanium dioxide, and the two other waste acids, one sulphuric and one hydrochloric acid, contained organic contaminants.

After separation of the silica the neutralized solution of the sulphuric waste acid from the titanium dioxide production was further processed according to the concise process description, that has been presented in Chapter 1.

Materials and Methods

The sample from the titanium dioxide industry was provided by Tioxide Calais. Table 7.1 presents a chemical analysis, combined with data from Tioxide.

Analysis	Concentration [ppm] unless indicated otherwise	Data from Tioxide	Analysis	Concentration [ppm] unless indicated otherwise	Data from Tioxide
density [kg/l]	1.25		Zn	22	
H_2SO_4 [%]	22.5	21.4	Cd	1.1	
Mg [%]	0.49	0.49	V	481	
Fe [%]	1.36	1.34	Cr	187	197
Al [%]	0.19	0.23	Si	23	
Ti [%]	0.24	0.24	K	39	
Na [%]	0.08	0.14	Ca	140	320
Ni	2.1		Li	1.3	
Co	50		Sr	0.9	
Mn	244	262	B	19	

Table 7.1 Analysis of Tioxide Calais waste acid, combined with data from Tioxide Calais.

It is important to realize that the total sulphate concentration is 3.7 M, which is higher than the H_2SO_4 concentration of 2.9 M. The Tioxide Calais waste acid also contained about 39 mg per liter of suspended white titanium dioxide. Before neutralization the solid matter was removed by filtration to prevent contamination of the silicagel.

The two waste acids with organic contaminants were provided by AKZO, one sulphuric waste acid of 78 % and a hydrochloric acid of 31 %. AKZO analyses of the acids are represented in Tables 7.2 and 7.3. Due to analytical difficulties it was not possible to analyze the exact

composition of the acids. The sulphuric waste acid had to be diluted by a factor of 4 to a concentration of about 3M H_2SO_4, in order to prevent precipitation of magnesium sulphate after neutralization. The dilution caused precipitation of a considerable fraction of the dissolved organic compounds, which could be removed by filtration. Approximately 83 wt % of the organic contaminants was thus removed.

Property	Unit	Producer's Specification	Range	Measured
Density	kg/cm^3	1670 (15 °C)	1640-1710	1727
Viscosity	m·pa·s	15 (15 °C)		
Colour		Black		
Strength (H_2SO_4)	wt %	75	72-78	80
Water	wt %	20	17-23	
Fe	mg/kg	70		50.1
Cd	mg/kg	max 0.01		
Hg	mg/kg	Max 0.05		
Al	mg/kg	Max 2		
Cl	mg/kg	max 5		
HCl	mg/kg	700		
Organic Chlorine (as Cl)	mg/kg	max 1000		
C	wt %	max 1.5		
SO_2	mg/kg	20		
Volatile Organic (as benzene)	mg/kg	max 100		
Aromatic Hydrocarbon (non volatile)	mg/kg	max 1000		
Sulfonates and derivatives	wt %	1		
Suspended organic matter	wt %			3
Dissolved organic matter	wt %			0.5

Table 7.2 Analysis of AKZO sulphuric waste acid.

The hydrochloric waste acid did not have to be diluted, since the solubility of magnesium chloride is higher than the solubility of magnesium-sulphate. However, in order to compare the neutralization rate with the rates of sulphuric acids, an experiment was also conducted with a hydrochloric waste acid sample that was diluted to a concentration of 6 M HCl. Table 7.3 shows that the hydrochloric waste acid contains a small amount of acetic acid.

Property	Unit	Producer's Specification	Measured
Density	kg/cm^3		1.15
HCl	wt %	30.9	
Acetic acid	wt %	0.6	
Monochloro-acetic acid	wt %	0.2	
Total acidity (as HCl)	M/l		9.66

Table 7.3 Analysis of AKZO hydrochloric waste acid.

For reasons of comparison, neutralization experiments were also executed with 3 M technical grade sulphuric acid.

All neutralization experiments were carried out in 1 liter vigorously stirred double walled glass reaction vessels at 70 °C (according to the method described in Chapter 3).

Stoichiometric amounts of Norwegian olivine (N2) were used for all experiments; for the sulphuric acids, fractions of grain sizes of 63-150 and of 355-630 μm and for the hydrochloric waste acid a fraction of a grain size 355-630 μm were employed.
The precipitated silica was separated from the neutralized solutions by filtration in a pressure filter at 5 bar nitrogen pressure. Nitrogen gas was used for the filtration to prevent the oxidation of Fe^{II} and subsequent precipitation of the resulting Fe^{III} on the silica. Subsequently the silica was washed four times by resuspension in demineralized water, followed by filtration in the pressure filter. The silica was dried overnight at 100 ° and the specific surface area was measured by using the BET procedure.
The experiments to investigate further processing of the residual solution of the Tioxide waste acid were performed with samples of 100 ml of solution in 200 ml vigorously stirred beakers. The beakers were placed in a water-bath of constant temperature of 70 °C. For the precipitation of heavy metals, such as Ti, Al, V, Cr and Fe^{III}, the pH was increased to 4.5 by the addition of MgO. The heavy-metal precipitate was subsequently separated by filtration. The metals remaining in solution, like Fe^{II}, Ni and Mn, were precipitated in a second step by increasing the pH and simultaneously oxidizing the Fe^{II}. This was accomplished by the addition of MgO and bubbling air through the solution. The amount of MgO added was calculated to be exactly sufficient to raise the pH from 4.5 to 7 and to neutralize the acid that was formed by oxidation of ⅔ of the Fe^{II}. The resulting precipitate was also filtered.
All chemical analyses were carried out with ICP-ES. For good analyses the sulfur concentration must be below 1000 ppm, therefore all samples of the solutions from the experiments with sulphuric acid were diluted 100 times. Solid samples were analyzed by dissolving 0.1 g in 10 ml 9 M HCl, followed by addition of demineralized water to a total volume of 100 ml.
The chemical composition of the precipitated silica produced from the Tioxide waste acid was analyzed by XRF.

Results

Neutralization experiments

In Figures 7.1 to 7.3 results of the neutralization experiments with the three waste acids are compared with the experiments with technical grade sulphuric acid.
The extent of neutralization is expressed as the percentage neutralized of initial amount of H^+, in order to facilitate the comparison of the different acids.
Figure 7.1 shows that the rate of neutralization of the Tioxide sulphuric waste acid is slightly lower than the rate with technical grade acid, for both olivine grain size fractions used.
During the neutralization experiments with the Tioxide waste acid it was observed that if the pH of the reaction mixture increased above about 1.7, the color of the mixture changed from light green to black, and a brown precipitate of heavy metals resulted. Furthermore it was noted that if the reaction suspension was kept at a pH of 1 for several hours, a white precipitate (most likely a Ti/Al(hydr)-oxide) was slowly formed. In order to produce a pure silica product from the reaction suspension, the neutralization was stopped before a pH of 1 was reached and the neutralization and subsequent filtration were carried out as rapidly as possible. Inspite of the precautions the silica had a light-brown color, that could not be entirely removed by subsequent washing.

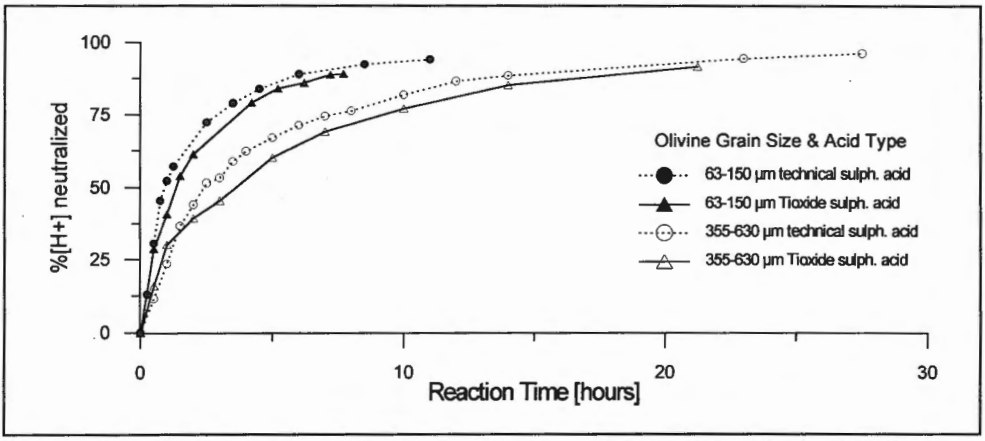

Figure 7.1 Neutralization degree [%] versus reaction time for technical grade- and Tioxide waste sulphuric acid and two olivine grain size fractions.

The rate of neutralization of the sulphuric acid with organic contaminants from AKZO is higher than the rate of technical grade sulphuric acid, for both olivine grain size fractions used. This is illustrated by the neutralization curves of Figure 7.2. The silica that was precipitated during neutralization had a gray color after separation from the neutralized solution. After washing, however, a bright white silica was obtained.
The rate of neutralization of the hydrochloric waste acid was found to be slightly higher than that of the technical grade sulphuric acid. It was important to maintain a nitrogen atmosphere over the reaction suspension, both during neutralization and silica filtration, in order to prevent the rapid oxidation of Fe^{II}.
After separation of the precipitated silica by filtration, the silica cake typically retains about 30 volume % of (neutralized) solution, which has to be removed by washing.
Table 7.4 represents the results of the BET specific surface area measurements of the washed and dried silicas, produced by the neutralization of the three waste acids and the technical grade sulphuric acid.

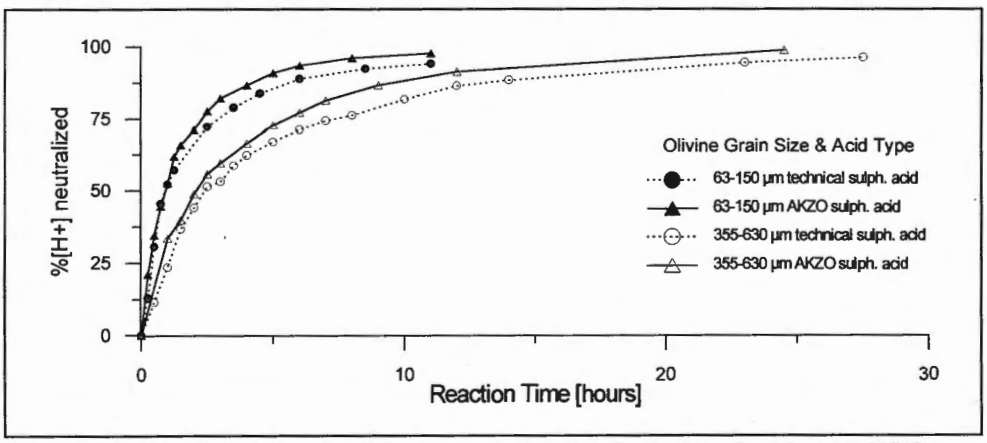

Figure 7.2 Extent of neutralization [%] versus reaction time for technical grade- and AKZO waste sulphuric acid and two olivine grain size fractions.

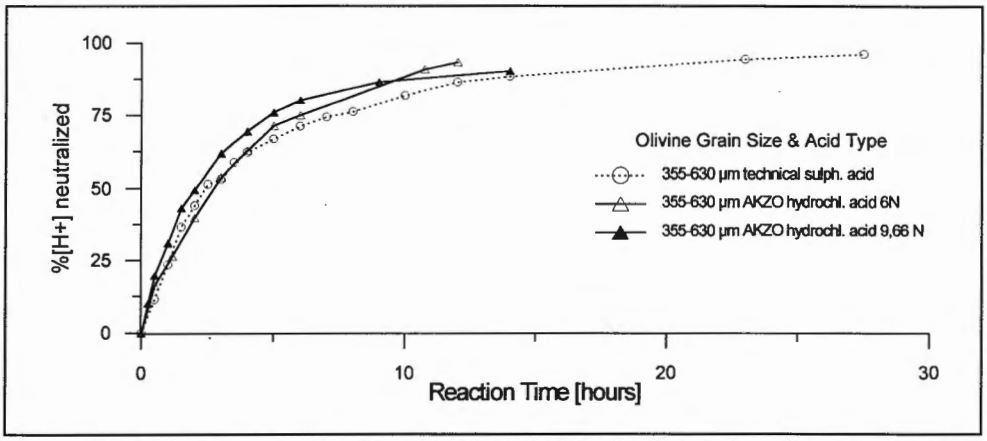

Figure 7.3 Extent of neutralization [%] versus reaction time for technical grade sulphuric acid and AKZO hydrochloric waste acid. Olivine grain size fractions 355-630 μm.

Sample	Olivine grain size fraction [μm]	BET specific surface area [m^2/g]	Micropore area [m^2/g]
3 M technical sulphuric acid	63-150 355-630	410 240	170 170
Tioxide waste sulphuric acid	63-150 355-630	360 220	190 80
AKZO waste sulphuric acid	63-150 355-630	323 320	97 100
AKZO waste hydrochloric acid	355-630	97	18

Table 7.4 Overview of the specific surface areas and micropore areas of silicas produced by neutralization of waste acids and technical grade sulphuric acid.

Since the neutralization experiments have not been duplicated, the surface areas of Table 7.4 have to be considered as mainly indicative. The table shows that the specific surface areas of the silica produced with the Tioxide sulphuric waste acid are comparable to those produced with technical grade sulphuric acid. The AKZO waste hydrochloric silica has a significantly lower specific surface area.
Table 7.5 shows a XRF analysis of a silica produced with the Tioxide waste acid, the concentrations are in wt-%. This analysis shows that the silica is not pure, apart from some magnesium, it contains some titanium and iron are present.

SiO_2	Al_2O_3	Fe_2O_3	MnO	MgO	CaO	Na_2O	K_2O	TiO_2	P_2O_5	LOI
78.5	<0.22	0.19	<0.006	0.30	<0.13	0.21	<0.05	2.09	0.01	11.94

Table 7.5 Analysis in wt % of a silica produced with Tioxide waste acid. LOI = Loss On Ignition, weight loss after heating to 1100°C

Processing of the Residual Solution

Only the residual solution of the neutralization of the Tioxide Calais waste acid was further processed. An ICP analysis of the solution is presented in Table 7.6.

In the first heavy-metal precipitation step the pH was raised from 1.5 to 4.5 by the addition of MgO. This required an averaged 12.2 g of MgO per liter of residual solution. It took about 3 hours at 70 °C before the precipitation was completed. Separation of the resulting heavy metal precipitate by filtration was difficult. Filtration of 250 ml of the reaction suspension in a pressure filter, with a filtration surface area of 19.6 cm^2, at 3 bars nitrogen pressure and a temperature of 45 °C, took more than 23 hours. The resulting filtercake thickness was 1.2 cm. It was found that the filterability of the precipitate improved slightly with increasing synthesis temperature.

Per liter of residual solution typically 17.7 g of heavy metal precipitate was formed. An analysis of the heavy metal precipitate is shown in Table 7.7, an analysis of the solution after separation of the first precipitate can be found in Table 7.6.

Element concentrations in ppm (mg/l) or g/l where indicated	Tioxide waste acid Residual solution after neutralization	Residual solution after first precipitation at pH 4.5	Residual solution after second precipitation and air oxidation at pH 7
Mg [g/l]	70	74	74
Fe [g/l]	30	25	1.1
Ni	505	477	52
Co	119	61	7
Mn	431	306	413
Zn	37	61	2
Cd	2.3	-	-
Al g/l	2.3	-	-
Ti	417	-	-
V	497	-	-
Cr	211	-	-
Si	156	61	104
Na [g/l]	1.0	1.3	1.0
K	76	-	127
Ca	213	-	356
Li	1.9	-	1.8
Sr	2.1	-	2

Table 7.6 Analyses of Residual Solutions of the Tioxide waste acid, after neutralization and separation of first and second metal precipitate.

The second precipitate, a magnetic ferrite, was generated at 70 °C by partial oxidation of Fe^{II}, by bubbling air through the solution. Per liter residual solution 23 g of magnesium oxide was added to neutralize the H^+ remaining in solution after the first precipitation and the H^+ formed by oxidation and precipitation of the iron. It was not possible to raise the pH higher than 7, due to the limited dissolution of MgO in the concentrated magnesium sulphate solution. During the addition of MgO to the residual magnesium sulphate solution, the color of the solution changed quickly from light-green to gray to dark-green, and subsequently gradually into greenish-black. After one day a black magnetic precipitate resulted. During the oxidation the pH was checked at regular time intervals, and the reaction was stopped after 6 days, when the pH had decreased from 7 to 6. During this period demineralized water was added regularly to compensate for water losses due to evaporation. The magnetic precipitate was

separated from the solution by filtration in the pressure filter. Filtration of 200 ml reaction suspension at 25 °C, under 4 bars nitrogen pressure, took approximately 4 hours. The resulting ferrite-cake thickness was 3 mm. Per liter of residual solution about 41 g of magnetic ferrite is formed in the second precipitation step.Tables 7.6 and 7.7 show chemical analyses of the magnesium sulphate solution after the second precipitation, and the magnetic ferrite precipitate. From the analyses a mass balance of all elements over the three reaction products was calculated, which is displayed in Table 7.8. It is important to note that the final residual solution still contains some Fe, Ni, Mn and Co.

Element [mg/g]	1st Heavy metal precipitate	2nd Magnetic ferrite precipitate
Mg	1.25	15.6
Fe	16.4	627
Ni	1.69	11.7
Co	0.08	2.6
Mn	0.04	1.0
Zn	0.24	0.9
Cd	0	0.1
Al	143	0.2
Ti	27.4	0.04
V	32.8	0.04
Cr	14.6	0.03
Si	4.5	0.75
Na	0.3	0.45
K	0.02	0.07
Ca	0	0.14
Li	0	0
Sr	0	0

Table 7.7 Analyses of the first heavy metal precipitate and the magnetic ferrite synthesized from Tioxide waste acid.

Element	1st Heavy metal precipitate [%]	2nd magnetic ferrite precipitate [%]	'clean' rest solution [%]	Amount present in system of 1 l waste acid [mg]
Mg	0.01	0.8	99.2	79.1 g
Fe	0.6	94.9	4.55	28.3 g
Ni	5.6	84.3	10.12	512
Co	1.3	92.2	6.6	105
Mn	0.14	8.4	91.4	424
Zn	10.6	84.7	4.7	39
Cd	0.1	99.9	0	1.8
Al	99.8	0.2	0	2438
Ti	99.3	0.3	0.4	2954
V	99.7	0.3	0	602
Cr	99.6	0.4	0	234
Na	0.5	1.7	97.8	986
K	0.3	2.0	97.7	60
Ca	0	1.5	98.5	194
Li	0.3	1.9	97.8	1.7
Sr	0.3	0.7	99.0	1.7

Table 7.8 Distribution [in %] of elements, present in the neutralization system of 1l waste acid, over the reaction products.

Discussion

Neutralization reaction

As compared to the neutralization of 3 M technical grade sulphuric acid, the neutralization rate of the Tioxide waste acid was lower. This is most likely due to a lower H^+ activity, caused by the higher ionic strength of the waste acid.

With the current experiments the solid TiO_2 present in the Tioxide Calais waste acid was separated by filtration in order to prevent contamination of the silica. For some applications the presence of this finely divided TiO_2 might be advantageous, as it will improve the white color of the silica (e.g. in special concretes or filler applications). In those cases the filtration step can be omitted. The silica that was produced from the neutralization of the waste acid contained a considerable amount of metals, such as Ti and Fe, despite the fact that the neutralization and silica separation were carried out as quickly as possible. The presence of these metals will affect the possible applications of the silica thus obtained.
The silica wash-water was not used for further processing, but it has to be realized that it can not be dumped, considering the high concentration of heavy metals.
It has to be remarked that the composition of the Tioxide Calais waste acid is not representative for the sulphuric waste acids produced by all titanium dioxide industries. Rothe (1987) published an average composition. The main difference with the Tioxide Calais acid is the higher iron content of 4 wt %.
The neutralization rate of the two waste acids with organic contaminants, especially the sulphuric waste acid, are higher than the rate for technical grade sulphuric acid. This might be due to the presence of organic compounds. Several studies on the effects of organic ligands on the dissolution rate of olivine have been conducted under natural weathering conditions (Grandstaff, 1986; Wogelius and Walther, 1991 and 1992). Generally it was found that the presence of organic compounds increases the olivine dissolution rate, which has been attributed to the formation of Mg-organic ligand complexes at the olivine surface. Grandstaff (1986) found that at pH 4.5 the relative order of the effect on the dissolution rate was: fulvic acid≈EDTA≈citrate>oxalate>tannic acid >>succinate>phthalate>acetate, which is the same relative order as the strength of the Mg-ligand complexes. Wogelius and Walther (1992) found that the effects of organic ligands on the olivine dissolution rate are only important in the near neutral pH region. At pH 2 the presence of small amounts of ascorbic acid (10^{-3} M) or phthalate (0.05 M) did not have any influence.
The current results show that the presence of organic compounds increases the olivine dissolution rate, even in solutions of a high acidity.
Differences in the reaction rate of olivine with sulphuric and hydrochloric acid have been investigated by van Herk and Pietersen (1987), who measured the neutralization rate of 3M sulphuric- and 6M hydrochloric acid. Van Herk et al. (1989) determined the dissolution rate of olivine in both acids in the pH range 1-3. The investigations revealed that the reaction rate is much lower for hydrochloric acid. Therefore, the slightly higher neutralization rate of the AKZO hydrochloric acid, (diluted to 6 M H^+), as compared to 3 M technical sulphuric acid, is most likely due to the presence of organic compounds.

Processing of the residual solution

A possible solution for the difficult suspension of light MgO powder in the residual solution is to add the MgO as a slurry in water for the first precipitation of heavy metals.
The time necessary for the oxidation of ⅔ of the Fe^{II} and the precipitation of a magnetic ferrite at 70 °C is 6 days, when oxygen from the air is used as oxidant. This long reaction time is most likely due to the fact that it is difficult to dissolve gases in concentrated solutions at elevated temperatures. The required reaction time for air oxidation is too long for industrial application, other methods for the synthesis of magnetic ferrites from the residual solution of the Olivine Process will be described in chapter 8.
Furthermore, a complete removal of all heavy metals is unfortunately not possible by the use

of magnesium oxide for pH conditioning. Magnesium oxide can only raise the pH of the magnesium sulphate solution to 7, which is not sufficiently high. Therefore a stronger base, such as sodium hydroxide, has to be used, which has the disadvantage that a new cation is introduced into the magnesium sulphate solution.

Conclusions

- Olivine can successfully be used for the neutralization of sulphuric waste acid from Tioxide Calais, and of both hydrochloric and sulphuric acid with organic contaminants from AKZO.
- The concentrated sulphuric waste acid from AKZO has to be diluted to a concentration of 3M H_2SO_4, to prevent the precipitation of magnesium sulphate after neutralization. Dilution causes the precipitation of a large amount (about 83 wt %) of the organic compounds, which can be separated easily by filtration. Dilution is not necessary for the waste hydrochloric acid, due to the higher solubility of magnesium chloride.
- The rate of neutralization of the sulphuric waste acid from Tioxide is lower as compared to that of technical grade sulphuric acid. This difference in neutralization rate is probably due to the lower H^+ activity, caused by the higher ionic strength of the waste acid.
- The neutralization rates of both waste acids with organic contaminants are higher compared to clean sulphuric acid. The higher neutralization rate is probably caused by the organic compounds.
- The silica produced by neutralization of the Tioxide waste acid is white with a brownish tint, typically it contains about 2 wt % TiO_2. In order to keep the metal concentration in the silica as low as possible, the neutralization has to be stopped at a pH lower than 1, and the silica must be separated and washed as quickly as possible. The silicas produced from the AKZO waste acids are bright white. The surface areas of the silicas produced from waste sulphuric acids are comparable to those from clean (technical grade) sulphuric acid. The silica from the hydrochloric waste acid has a significantly lower surface area.
- The use of magnesium oxide to raise the pH of the residual solution of the Olivine Process has the advantage that it does not introduce new cations in solution; unfortunately it reacts slowly. Furthermore, it is only possible to raise the pH of the solution to 7, which is not high enough for complete removal of all heavy metals. The use of a stronger base, such as sodium hydroxide, is necessary.

Chapter 8

Review of the Synthesis and Magnetic Properties of Magnetic Ferrites

Abstract
Regardless of the composition of the acid neutralized by olivine, the residual magnesium salt solution always contains iron, nickel and other metals, which are present in olivine. The solution presents the largest quantity of by-product, and it is essential that it is pure, irrespective of its application.
The best method for removal of contaminating metals from the residual solution is the precipitation of a magnetic ferrite, followed by magnetic separation. A large number of divalent metals can be incorporated in the ferrite structure.
A review of the synthesis methods of ferrites, described in literature, is presented. In solutions containing Fe^{II}, magnetic ferrites can best be produced by slow oxidation, e.g. by air or nitrate, at pH ≥ 8 and temperatures > 50 °C. For the residual solution from the Olivine Process, the use of nitrate as an oxidant has several advantages. Nitrate can be added exactly stoichiometrically and does not cause abundant evaporation.
Finally, the magnetic properties of iron-oxides are discussed. The measurement of magnetic properties of ferrites can be used as an analytical tool for grain size and chemical composition.

Introduction

The residual magnesium salt solution represents the largest quantity of by-product generated by the Olivine Process. Regardless of the application of the residual solution, e.g. raw material for MgO or $MgSO_4$ or even disposal by dumping, it is necessary that the solution is clean. To use a residual magnesium sulphate solution as raw material for the production of epsomite ($MgSO_4 \cdot 7H_2O$), for instance, the iron concentration must be lower than 0.8 mg/l. Metals such as iron, nickel and manganese, have to be removed. For this separation several processes are available. The best process is the precipitation of iron in the form of a magnetic ferrite, which can easily be removed from the residual solution by magnetic separation.
In literature several procedures have been described for the synthesis of magnetic ferrites in dilute solutions. These studies are reviewed in order to facilitate the development of a synthesis process in the concentrated residual solution of the Olivine Process, which will be dealt with in the next chapter.
Finally a concise description of the magnetic properties of ferrites is presented, to assess their use as analytical tools.

Process Selection: Long Reaction Time or Long Filtration Time ?

The easiest way to separate metals such as iron, nickel and manganese, from the residual solution is to increase the pH above 7 and to oxidize the iron with a quick oxidant like hydrogen-peroxide. An amorphous Fe^{III}-hydroxide is thus formed, which is known for its effective scavenging properties for other metals. The amorphous precipitate can subsequently be separated from the solution by filtration. However, the precipitate is difficult to filter. Compared to the precipitated silica the amorphous iron precipitate has a much higher cake resistance, typically about a factor of 9, resulting in long filtration times.
The synthesis of a crystalline iron oxide, that also can incorporate other metals, and can be rapidly separated from the solution by magnetic methods is therefore appealing. However, the synthesis of magnetic ferrites requires a much longer reaction time. In chapter 7 the formation of magnetic ferrite in the residual solution of Tioxide sulphuric waste acid has been described. For these experiments iron was oxidized by oxygen from air, that was bubbled through solution. The minimum required reaction time at 70 °C was 6 days ! Such long reaction times are a disadvantage for industrial applications of the process, therefore another synthesis procedure was developed.

Synthesis of Magnetic Ferrites, Literature Review

The experiments for the synthesis of magnetic ferrites, described in literature, were generally carried out with solutions containing less than 1 M SO_4^{2-}. Furthermore, with the experiments performed to study the incorporation of other metal cations in the ferrites, the molar ratio of iron to the other metal cations in solution was in general higher than 2. Such conditions are very different as compared to the high (3M) SO_4^{2-} concentration in the residual solution of the Olivine Process and the low iron-to-magnesium ratio (e.g. 0.08 and 0.19 for residual solutions from technical grade sulphuric acid and Tioxide Calais waste acid, respectively). Therefore synthesis methods described in literature cannot be applied directly to the residual solution.

Magnetite structure

Magnetite (Fe_3O_4) is a magnetic ironoxide with an inverted spinel structure. The spinel structure is usually described as a double oxide AB_2O_4, where A is a divalent metal, such as Fe, Mg, Zn, Mn, Ni etc., and B is a trivalent metal, like Fe, Al, Cr etc. The spinel group is

divided into three groups depending on the type of trivalent metal: i) magnetite with mainly Fe^{III} ii) spinel with Al, and iii) chromite with mainly Cr^{III} as B atom. In the minerals of each group extensive solid solution occurs. In natural ferrites complete solid solution between the end members magnetite $Fe^{II}Fe^{III}_2O_4$ and magnesioferrite $MgFe^{III}_2O_4$ occurs. In the spinel structure the oxygen atoms exhibit approximately a cubic closest packing, see figure 8.1 (from Deer et al. 1975). The spinel unit cell contains 32 O-atoms and 24 cations. The 8 A atoms are in fourfold coordination between a tetrahedral group of oxygen atoms and the 16 B atoms are in sixfold coordination between an octahedral group of oxygens. Each oxygen atom is thus linked to one A and three B atoms. In the inverted spinel structure of magnetite, 8 Fe^{III} occupy the A positions, and the B positions are filled with 8 Fe^{II} and 8 Fe^{III}. Maghemite, γ-Fe_2O_3, is another magnetic iron oxide. It has the same structure as magnetite, with the same amount of oxygen atoms, but some iron positions are vacant (□). A possible structural formula is $Fe^{III}[Fe^{III}_{5/3}\square_{1/3}]O_4$; some structural OH can also be present. Maghemite is metastable and transforms to hematite (α-Fe_2O_3) at high temperatures (> 200 °C).

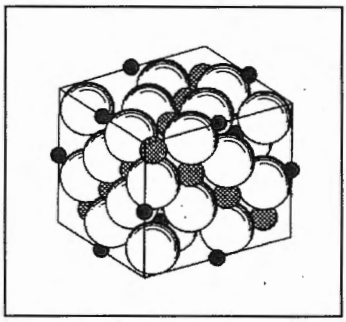

Figure 8.1 Spinel structure: large spheres= oxygen, black=A and gray= B positions. (From Deer et al. 1975)

Relevant iron oxides and oxyhydroxides, and their relations

The synthesis of magnetite by oxidation of Fe^{II} in solution is a complex process. Depending on the reaction conditions, a number of iron oxides and oxyhydroxides can be produced. Possible reaction products are goethite (α-FeOOH), lepidocrocite (γ-FeOOH), feroxyhyte (δ'-FeOOH) and magnetite (Fe_3O_4). The type which is formed depends on reaction conditions such as pH, rate of oxidation, suspension concentration, temperature and concentration of other elements (Feitknecht 1959). Figure 8.2 illustrates the relations between the iron oxides, and oxyhydroxides, and the synthesis conditions. According to Schwertmann and Cornell (1991) goethite and lepidocrocite can be formed by oxidation with air in the pH range 6-7, goethite is formed by slow, and lepidocrocite by faster oxidation.

The presence of carbonate inhibits the formation of lepidocrocite. Goethite is, furthermore, formed at extremely high pH (≈14). Magnetite is formed by slow oxidation (Feitknecht, 1959) at pH ≥ 8. By extreme fast oxidation of Fe^{II} (e.g. with H_2O_2) feroxyhyte is formed. During the synthesis of these ironoxides and oxyhydroxides, intermediate precipitates are formed when SO_4^{2-} or Cl^- ions are present (pH < 13) . Due to their green color and the fact that they occur as anaerobic corrosion products of steel, these precipitates are called Green Rusts. The green rust formed in the presence of Cl^- is called green rust I, with SO_4^{2-} green rust II (GRII) is formed. Tamaura (1984) determined the composition of GRII to be $Fe^{III}Fe^{II}_2SO_4(OH)_{5-2n}O_n$. Green rust II is only stable under a N_2 -atmosphere at temperatures below 10 °C. The transformation of GRII to magnetite is believed to take place through a dissolution-precipitation process.

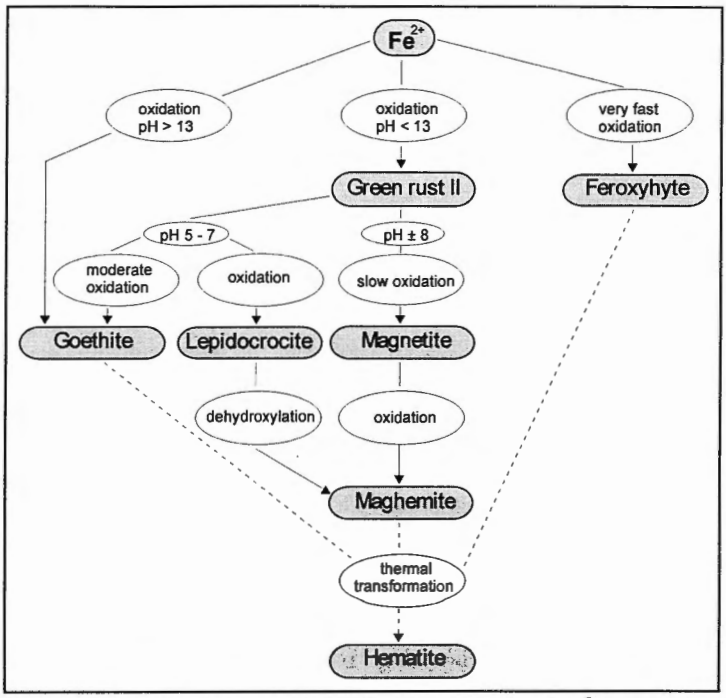

Figure 8.2 Relation between the oxidation products of Fe^{2+} in solution and the reaction conditions (sulphate containing solutions).

Reaction equations 1 and 2 illustrate the formation of magnetite, through the formation of GRII, by the oxidation of Fe^{2+}.

$$3Fe^{2+} + 4OH^- + \tfrac{1}{2} H_2O + \tfrac{1}{4} O_{2\,(g)} + SO_4^{2-} \rightarrow Fe^{III}Fe^{II}_2SO_4(OH)_{5-2n}O_n + nH_2O \qquad (1)$$

$$2Fe^{III}Fe^{II}_2SO_4(OH)_{5-2n}O_n \rightarrow Fe_3O_4 + 3Fe^{2+} + 2SO_4^{2-} + 2(2-n)H_2O + 2OH^- \qquad (2)$$

Combination of reaction equations 1 and 2 yields:

$$3Fe^{2+} + 3H_2O + \tfrac{1}{2} O_{2\,(g)} \rightarrow Fe_3O_4 + 6H^+ \qquad (3)$$

By further oxidation magnetite is transformed into maghemite (γ-Fe_2O_3).

Synthesis procedures for magnetic ferrites

The most important procedure for the synthesis of magnetite is the slow oxidation with air of $Fe(OH)_2$ suspensions at temperatures above 50°C. The pH of the solution is kept high (>8) by addition of a strong base, such as NaOH. This procedure has been applied in numerous studies, e.g. Takada and Kiyama (1970), Kiyama (1978), Kaneko and Katsura (1979), Robbins (1980), Tamaura et al. (1980). According to Takada and Kiyama (1970), ferrite particles of grain sizes from 0.05 to 1μm can be synthesized by air oxidation. The authors found that above pH 10, the ferrite particle size rises at increasing temperature, lower

oxidation rates and an increasing concentration of other cations. The ferrite particle size was not affected by the reaction conditions in solutions of a pH less than 9, when a constant particle size of 0.1 μm was obtained.
Sung and Morgan (1980) have studied the oxidation kinetics of Fe^{II} in solution. In their study the authors investigated the effect of the ionic strength of the solution (I = 0.1-0.33), the temperature (5-30 °C) and the type of anion (SO_4^{2-}, Cl^-, and ClO_4^-) on the oxidation rate. They found that the rate decreased in the order $ClO_4^- > Cl^- > SO_4^{2-}$ and with increasing ionic strength. The oxidation rate increased with increasing temperature.
The oxidation times that have been reported range between 1 and 30 hours.
Tamaura et al. (1984) found that magnetite could also be formed by spontaneous transformation, at temperatures higher than 50°C, of GRII that was prepared at room temperature. Tamaura (1985) has described a method for the formation of magnetite by the adsorption of Fe^{2+} onto γ-FeOOH in sulphate-free solutions.
Instead of oxygen from air, nitrate has also been used as an oxidant, e.g. Sugimoto and Matijević (1979), Tamaura et al. (1980), and Schwertmann and Cornell (1991). Reaction equation (4) illustrates the oxidation of Fe^{2+} by nitrate to form magnetite. A synthesis procedure for uniformly distributed magnetite crystals of 100-200 nm, has been described by Schwertmann and Cornell (1991). In this procedure a 0.36 M $FeSO_4$ solution is oxidized with a solution containing a stoichiometric amount of KNO_3, mixed with KOH at 90 °C for 60 minutes. The reaction mixture is subsequently allowed to cool down slowly, during 24 hours.

$$9Fe^{2+} + 2NO_3^- + 8H_2O \rightarrow 3Fe_3O_4 + 2NO_{(g)} + 16H^+ \quad (4)$$

Divalent metal incorporation
The incorporation of other divalent metals into magnetite has been studied by numerous authors, e.g. Takada and Kiyama (1970), Kiyama (1978), Kaneko and Katsura (1979), Robbins (1980), Tamaura (1985) and (1986). In most of the studies a mixed hydroxide precipitate of Fe^{II} and the divalent metals was prepared, which was subsequently transformed into a magnetic ferrite by slow air-oxidation at temperatures higher than 50 °C. From their experiments with Co, Zn and Mn, Takada and Katsura (1970) concluded that the final metal composition of the ferrite was equal to the metal composition of the intermediate hydroxide precipitate. Kiyama (1978) showed that the divalent metal concentration (Mn and Co) in the ferrite increased during the precipitation. The synthesis of magnesioferrites at 65°C was studied by Kaneko and Katsura (1979), they found that the incorporation of Mg depends on the pH level. At pH 9, all magnesium is incorporated in the ferrites if the molar ratio Mg^{2+}/Fe_{total} is lower than 0.1. Only a small amount of magnesium is incorporated at pH 8. It was therefore suggested that the Mg must be hydrolyzed before it can be incorporated.
Tamaura (1986) produced Ni -ferrites by the spontaneous transformation of Ni bearing GRII. He found that at most only one of the two Fe^{2+} ions in GRII could be replaced by Ni^{2+}. During the subsequent spontaneous transformation, only 20 % of the Ni in the GRII was incorporated in the Ni bearing ferrites. Tamaura (1985) synthesized Zn, Cd, Ni and Co bearing ferrites by the transformation of GRII, that had been produced by reaction of the divalent metal ions, Fe^{2+} and γ-FeOOH (pH 8.5). The concentrations of the divalent metals in the ferrites was different, despite the fact that their concentrations were equal in the starting solutions. The relative order of increasing metal content in the resulting ferrite was Cd<Ni≈Co<Zn, which is the same order as the first hydrolysis constant of these metals. This suggests that the divalent

metal has to be hydrolyzed before it can be incorporated in the ferrite structure, this corroborates the findings of Kaneko and Katsura (1979) for the incorporation of Mg.

Magnetic Properties

The magnetic properties of a material originate from the motions of electrons. Two types of electron motion can be distinguished; the rotation of electrons around the atomic nucleus (orbital moment) and the spin of an electron about its own axis (spin moment). In solids the spin moments are able to allign to an external magnetic field; the orbital moment can usually change its orientation to a very limited extent only due to the surrounding atoms.

The orientation energy of an atomic magnetic moment in an external magnetic field is low. In a magnetic field of, e.g., 1T, the orientation energy is about 10^{-23} J, which is small relatively to the thermal energy, which is at 100 °K about 10^{-20} J. As a result the magnetization of a system of individual magnetic atoms in which the magnetic moments do not interact is low, unless an external magnetic field is applied at temperatures below 10 °K. Within some solids the atomic magnetic moments are ordered due to electrostatic forces. In ferromagnetic materials, such as iron, nickel and cobalt, the atomic magnetic moments are oriented parallel. When the temperature of a ferromagnetic solid is raised, a temperature level is reached where the thermal energy becomes equal to that of the electrostatic coupling of the atomic magnetic moments. The temperature at which the atomic magnetic moment is disordered is the Curie temperature. The Curie temperature can be used to characterize ferromagnetics.

Electrostatic interactions between magnetic atoms, especially through oxygen ions, can also lead to an antiparalel orientation of the atomic magnetic moments. In antiferromagnetic solids the atomic magnetic moments are of equal magnitude, and the resulting magnetization is zero. When the magnetic moments oriented antiparalel have a different magnitude, the solid exhibits a considerable magnetization. Ferrimagnetic solids, such as ferrites, are having magnetic moments of different magnitude in opposite directions.

The temperature at which the ordering is destroyed is the Néel temperature with antiferromagnetic and ferrimagnetic solids.

Hysteresis and magnetic parameters

With large ferromagnetic bodies the magnetic volume is split up in smaller domains in which the atomic magnetic moments are aligned. The magnetization within the different domains is oriented so as to lead to a negligible external magnetic field. In the region between two adjacent domains, the domain wall, the orientation of the atomic moments rotate from the orientation of the first domain into that of the adjacent domain. Depending upon the contribution of the orbital magnetic moments the thickness of the domain walls varies. A high contribution of the orbital magnetic moments, leading to a high magnetocrystalline anisotropy, leads to wide domain walls.

Magnetization of ferromagnetic materials proceeds by migration of domain walls. The growth of domains the magnetization of which is directed against the external magnetic field proceeds until the external field is compensated within the magnetic material. The migration of the domain walls results in the typical magnetization curves of ferromagnetic materials. When the domains with the magnetization not alligned to the external magnetic field have disappeared, the magnetization does not increase further strongly and is said to be saturated. The magnetization of a magnetic material is determined by the magnetic field that is applied and the magnetic history of the material. The relation between magnetization and applied field is characterized by hysteresis.

Figure 8.3 presents an example of a hysteresis curve together with an initial magnetization curve, the different magnetic parameters that characterize magnetic behavior are indicated. The dependence of magnetization on the applied field, in a previously unmagnetised material, is illustrated by the initial magnetization curve. Initially the magnetization is reversible; the magnetization increases slowly on application of a small magnetic field, and reduces to zero if the field is removed. The gradient between initial magnetization and applied field is called initial susceptibility (κ). However, above a critical applied field the magnetization does not reduce to zero, and a remanent magnetization is developed. On application of stronger fields the magnetization increases up to a maximum that is called the saturation magnetization ($\mathbf{M_s}$). The remanent magnetization that remains after removal of the field is called saturation remanence ($\mathbf{M_{rs}}$). By applying a magnetic field in the opposite direction the magnetization can be reduced to zero, the reverse field necessary to achieve this, measured in the presence of this field, is called the saturation coercivity $\mathbf{(B_0)_c}$.

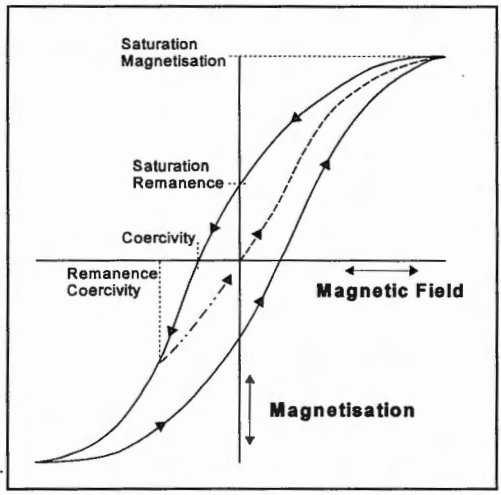

Figure 8.3 Relation between magnetization and applied magnetic field. The dashed line represents the initial magnetization curve.

A larger field is necessary to reduce the remanent magnetization (after removal of the applied field) to zero, the magnetic field to achieve this is called the coercivity of remanence $\mathbf{(B_0)_{cr}}$.

A widely used technique is the measurement of the remanence as a function of the strength of the applied field. This is illustrated by Figure 8.4, first a material is magnetized to its saturation remanence (point a) by application of a very strong magnetic field (> 1T). Subsequently the remanence is measured repeatedly after application of increasing magnetic fields in opposite direction (points b to e). The coercivity of remanence can be determined by plotting the measured remanences versus the applied fields.

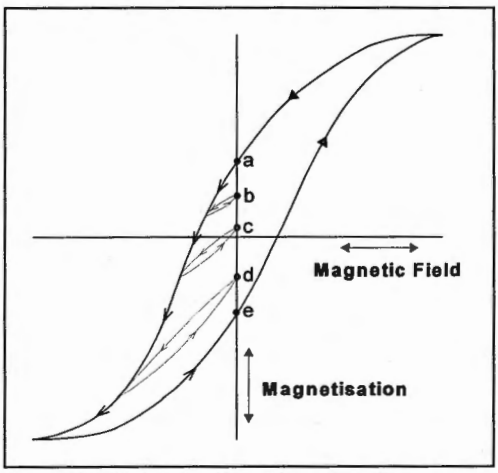

Figure 8.4 Magnetization versus applied magnetic field, illustrating the determination of remanence (b to e) after repeated application of magnetic fields of increasing strength.

Effects of grain size

When the size of ferro- or ferrimagnetic crystallites are decreased to a level which is of the same order of magnitude as the thickness of the domain wall, formation of domains is no longer favorable. The gain in magnetostatic energy by the formation of domains is lost by the rise in energy involved in the establishment of domain walls. As a result sufficiently small ferromagnetic grains are single domain. Since migration of domain walls does not proceed with single domain particles, magnetization calls for higher magnetic fields. However, also demagnetization is much more difficult. When ferrimagnetic grains are very small (0.001-0.01 μm) the magnetic anisotropy energy becomes smaller than the thermal energy. Now the moments of the atoms of magnetic particles perform rotation according to a Brownian rotation, though the magnetic moments remain aligned and exhibit a coherent rotation. The magnetic behavior is now that of paramagnetic atoms with a magnetic moment that is equal to the number of magnetic atoms within the particles times the atomic magnetic moment. Since such magnetic particles can easily contain 10^3 to 10^5 atoms, the apparent moment is much larger than that of paramagnetic atoms. Accordingly , small ferro-or ferrimagnetic particles are exhibiting super paramagnetic behavior. Superparamagnetic grains do not have a remanence and thus do not display hysteresis. Compared to equal amounts of samples of single- or multidomain grains, the initial susceptibility of superparamagnetic grains is much higher.

For samples containing ferrite grains larger than a few hundred angstroms, the ratio of saturation remanence and susceptibility can be used as a rough estimate of the grain sizes. According to Day et al. (1977) a classification of magnetic materials can be made using the relation between the ratios of the saturation remanence and the saturation magnetization (M_{rs}/M_s), and the ratio of coercivity of remanence and saturation coercivity ($(B_0)_{cr}/(B_0)_C$). In Figure 8.5 these two ratios are plotted, and the regions of single-domain, pseudo-single-domain and multidomain grains are indicated. There is a difference in magnetic properties of large, multidomain and small, single-domain grains.

In samples where magnetic grains are closely packed, the magnetic properties are changed, the coercivity decreases and it is easier to magnetize the sample. However, demagnetization of the sample is more difficult.

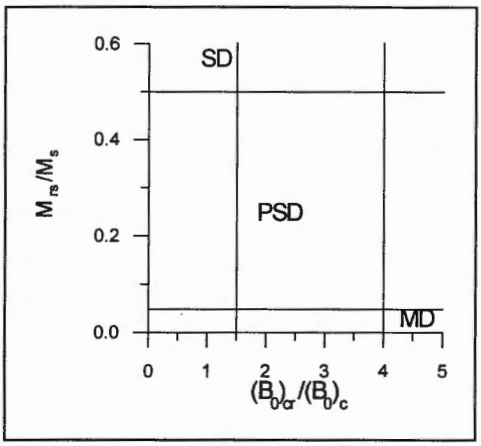

Figure 8.5 Day-plot : ratio of M_{rs}/M_s versus ratio $(B_0)_{cr}/(B_0)_c$. SD=Single-Domain, PSD=Pseudo-Single-Domain and MD=Multidomain.

Effects of ferrite composition

Replacement of Fe^{II} in the ferrite structure by other divalent metals causes changes in Curie temperature, initial susceptibility and saturation magnetization. Table 8.1 shows values of these parameters for some iron oxides and iron oxyhydroxides.

Iron-oxide / -oxyhydroxide		Curie temperature [°C]	Initial magnetic susceptibility [$\cdot 10^{-8}$ $m^3 kg^{-1}$]	Saturation magnetization at 20 °C [A $m^2 kg^{-1}$]
Fe_3O_4	Magnetite	585 [1] 578 [3] 585 [4]	$5 \cdot 10^4$ [4]	92 [1] 93 [4]
$MgFe_2O_4$	Magnesioferrite	440 [1] 440 [4]		27 [1] 21 [4]
$NiFe_2O_4$	Trevorite	585 [1]		50 [1]
$CoFe_2O_4$		520 [1]		80 [1]
$MnFe_2O_4$	Jacobsite	300 [1] 310 [4]		77 [1]
γ-Fe_2O_3	Maghemite	620 [2] ±740 [4]	$4 \cdot 10^4$ [4]	85 [4]
γ-FeOOH	Lepidocrocite	-196 [4]	70 [4]	
α-FeOOH	Goethite	60-170 [3] 120 [4]	70 [4]	10^{-3}-1 [3] ±1 [4]

Table 8.1 Curie temperature, Initial magnetic susceptibility and Saturation magnetization at 20 °C, for some iron-oxides and -oxyhydroxides. Data from: [1] Smit and Wijn (1959), [2] Lax and Button (1962), [3] O'Reilly (1984) and [4] Thompson and Oldfield (1986).

Considering the large variation of these parameters for the different ferrites listed in the table, measurement of these parameters might be used as a tool for characterizing the ferrite composition.

Discussion

The oxidation of the Fe^{2+} in the residual solution of the Olivine Process to a magnetic ferrite has the advantage that the ferrite can be easily removed from the solution by magnetic separation. However, as compared to the alternative; precipitation of a completely oxidized iron oxyhydroxide, the period of time involved in the synthesis of magnetic ferrites is very long. A procedure for the synthesis of magnetic ferrites that has been frequently described in literature is the oxidation of Fe^{II} solutions with air. In chapter 7 it was shown that with the residual solution of Tioxide waste acid this procedure takes at least 6 days. Therefore air-oxidation is not a feasible option for the treatment of the residual solution of the Olivine Process. The use of nitrate as an oxidant seems a better option. It has the advantage that it can be added in exactly stoichiometric amounts and that it causes no abundant evaporation. Unfortunately the procedures described in literature cannot be applied directly, due to the great compositional differences between the residual solution and the solutions studied in literature. In chapter 9 a procedure for the synthesis of magnetic ferrites in the residual solution, using nitrate as oxidant, will be presented.

Kaneko and Katsura (1979) and Tamaura (1985) suggested that divalent metals have to be hydrolyzed in order to be incorporated in ferrites. When magnesium oxide is used to raise the pH of the residual solution, it is highly likely that apart from the hydroxides of Fe^{II}, Ni, Mn and other divalent metals, that have to be incorporated in the ferrites, magnesium hydroxide is present. It can therefore be expected that magnesium will be incorporated in the ferrites formed in the residual solution.

Conclusions

- For the removal of iron and other metals from the residual solution of the Olivine Process, the synthesis of magnetic ferrites is a favorable option. The magnetic ferrites can be easily removed from solution by magnetic separation.
- The general procedure for the synthesis of magnetic ferrites is the slow oxidation of solutions containing Fe^{II} at pH ≥ 8 and at temperatures $\geq$ 50 °C. The use of oxygen from air and nitrate as oxidants has been reported. With this synthesis method ferrite crystals with sizes ranging from 0.01 to 1 μm can be produced.
- For the residual solution the use of nitrate as oxidant has the advantage that it can be added exactly stoichiometrically and will not cause abundant evaporation like air.
- The measurement of magnetic properties, such as susceptibility, saturation magnetization, Curie temperature and coercivity can be used as tools for characterizing the grain size and the chemical composition of the ferrites.

Chapter 9

Synthesis of Magnetic Ferrites in Concentrated Magnesium Sulphate Solutions by Oxidation with Nitrate

Abstract

Standard procedures for the synthesis of magnetic ferrites cannot be applied directly to the residual solution of the Olivine Process. The reaction time required for the oxidation with oxygen from air is, for example, five times higher for the residual solution than the maximum reaction time reported in literature.

A set of experiments was conducted to optimize the ferrite synthesis in Fe^{II} containing concentrated sulphate solutions, using a mixture of magnesium nitrate and magnesium oxide. The main objectives were the synthesis of magnetic ferrite of a good quality and the production of a pure magnesium sulphate solution.

Three types of solution were used, a Mg/Fe-sulphate solution prepared from pure chemicals and the residual solutions of the neutralization with olivine, of technical grade sulphuric acid and of waste sulphuric acid from a titanium dioxide plant. The effects of temperature (80-150 °C), reaction time (2-10 hours), addition of magnetite seed crystals, and amount of nitrate were investigated. The precipitates were studied by ICP, XRD, TEM, and the magnetic properties were measured.

Generally it can be concluded that the synthesis is favored by increasing temperature, increasing reaction time, higher initial Fe^{II} concentration, and the presence of magnetite seed crystals. These parameters mainly influence the crystallinity of the ferrite precipitate, the grain size range of the ferrites (50-750 nm) remains approximately constant.

After ferrite precipitation in the residual solution from clean sulphuric acid, typically about 1 % of the total amount of Ni, and 3 % of the total amount of Mn remains in solution. For a more complete removal of these metals, a second precipitation step has to be carried out, using a strong base, such as sodium hydroxide.

Introduction

After the neutralization of sulphuric acids with olivine and subsequent separation of the precipitated silica, a residual magnesium sulphate solution is produced. This solution contains besides the contaminants originally present in the acid, some iron, nickel and manganese from the olivine. The best method for removing these metals is the synthesis of a magnetic ferrite, that can incorporate most of the other divalent metals, and can be easily removed from the solution by magnetic separation.

In chapter 8 some methods for the synthesis of magnetic ferrites in solution, published in literature were reviewed. In general magnetic ferrites can be produced by slow oxidation, e.g. by air or nitrate, of solutions containing Fe^{II} at pH ≥ 8 and at temperatures higher than 50 °C. Unfortunately the methods described in literature cannot be applied directly to the residual solution of the Olivine Process due to its extreme chemical composition. In chapter 6 a ferrite synthesis, by air-oxidation of the residual solution from Tioxide Calais waste acid, was dealt with. In contrast to a maximum period of time for air-oxidation of 30 hours reported in literature, this synthesis took more than 6 days.

Therefore a set of experiments was conducted to investigate the possibility of producing magnetic ferrites in concentrated magnesium sulphate solutions using nitrate. The aim of the experiments was to find a cost-effective method for both the production of good-quality ferrites, and the production of pure magnesium sulphate solutions.

For the experiments, solutions prepared from pure chemicals were used, as well as residual solutions from olivine-neutralization experiments of technical grade- and waste sulphuric acid. The reaction temperature was varied between 80 and 150 °C, and the reaction time between 2 and 10 hours. The effect of the addition of small amounts of magnetite seed crystals was studied. Furthermore, a set of experiments was executed to study the effect of excess amounts of nitrate on the ferrite synthesis.

Materials and Methods

Ferrite synthesis experiments

A large number of indicative experiments was conducted to investigate the possible use of combinations of NaOH, KOH, MgO and $MgCO_3$ (magnesite) as base and H_2O_2, KNO_3 and $Mg(NO_3)_2$ as oxidant. The use of $Mg(NO_3)_2$ to oxidize the Fe^{II} and MgO to neutralize the H^+ formed during precipitation of the ferrite turned out to be the best combination. In the residual solution of the Olivine Process magnesium nitrate reacts more slowly than potassium-nitrate, but its use has the advantage that no new cations are introduced into solution.

Three types of solutions were used for the production of magnetic ferrites. One solution, containing 2.0 M $MgSO_4$ and 0.5 M $FeSO_4$, was prepared by dissolving pure $MgSO_4 \cdot 7H_2O$ and $FeSO_4 \cdot 7H_2O$ (from E.Merck, Darmstadt, Germany) in demineralized water that had been flushed with CO_2. The other two solutions were prepared by neutralization with olivine of 3M technical grade sulphuric acid and waste sulphuric acid from Tioxide Calais, followed by separation of the silica by filtration. The residual solution from the waste acid was pretreated with MgO to remove Ti, Al, V and Fe^{III}, according to the procedure described in chapter 6.

The formation of ferrites by oxidation of Fe^{II} with nitrate is illustrated by the following reaction equation for the synthesis of Fe_3O_4 (magnetite):

$$9\ Fe^{2+} + 2\ NO_3^- + 8\ H_2O \rightarrow 3\ Fe^{II}Fe^{III}{}_2O_4 + 2\ NO_{(g)} + 16\ H^+ \qquad (1)$$

The reaction equation illustrates that in order to precipitate a stoichiometric magnetite, ⅔ of the Fe^{II} must be oxidized. For all experiments an amount of pure $Mg(NO_3)_2 \cdot 6H_2O$ (from Merck) necessary for the oxidation of exactly ⅔ of the iron present was used. Pure MgO (from OPG Farma, Utrecht, The Netherlands) was used to increase the pH to 7 and to neutralize the H^+ formed during ferrite precipitation.

The reaction set-up for experiments under 100 °C is illustrated in figure 9.1, the experiments were carried out in a glass beaker of 1 liter, that was placed in a bigger beaker containing water. Both were placed on a magnet-stirrer with heating element, the temperature of the water-bath was kept constant with a thermostat-thermometer. During the experiments the reaction vessel was flushed continuously with N_2. Reacting chemicals were added through the drop funnel.

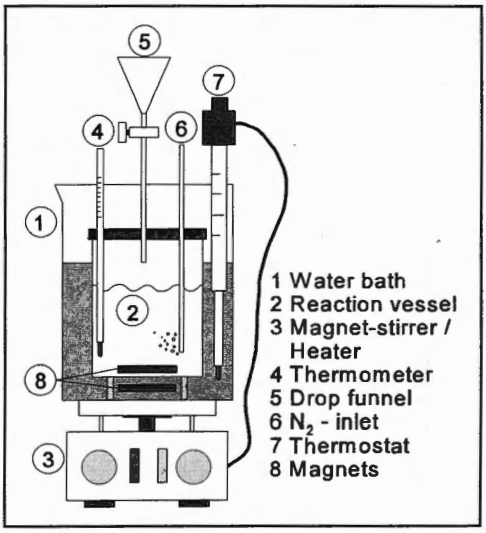

Figure 9.1 Reaction set-up for ferrite synthesis

The reaction was carried out by heating 560 ml of magnesium sulphate solution to the reaction temperature (80-90 °C), followed by the addition, within 5 minutes, of stoichiometric amounts of magnesium nitrate and magnesium oxide in 240 ml demineralized water. In some experiments about 5 g of magnetite seed crystals was added, this magnetite was mixed with the magnesium oxide / magnesium nitrate suspension. The mixture was vigorously stirred during the desired reaction time (8-10 hours) and after that the mixture was allowed to cool down slowly for 12 hours. Subsequently the precipitate was removed from the solution either by magnetic separation or filtration. The magnetic separation was carried out by placing the beaker containing the magnetic suspension on an electromagnet, and after the magnetic precipitate had settled down, the clear supernatant was decanted and filtered to remove any remaining magnetic particles. The filtration was carried out with a 250 ml pressure filter, using 0.45 μm filters and an operating pressure of 4 bar N_2. The ferrite precipitate was washed to remove all magnesium sulphate, a $BaCl_2$ solution was used to check for the presence of sulphate in the wash-water. The washed ferrites were dried at 65 °C.

The reaction conditions used are listed in Table 9.6 (in appendix 9.1). The experiment code is composed of the reaction time [hours] followed by the type of solution [PC=pure chemicals, RSC=residual solution of technical grade sulphuric acid and RSW=residual solution of waste sulphuric acid] and finally the reaction temperature [°C], when magnetite seed crystals were used, "s" is added to the sample code.

Experiments at 150 °C

The ferrite syntheses at 150 °C were carried out in 40 ml Teflon vessels, that were put in stainless steel pressure-vessels. Stoichiometric amounts of magnesium oxide and magnesium nitrate were directly added to the reaction vessels. Subsequently the pressure vessels were rotated continuously in an oven at 150 °C for two hours. The reaction products were separated and treated according to the method described above.

Mass balance experiments

In order to calculate a mass balance of all elements of interest, ferrite syntheses were carried out with volumes of 1 liter residual solution from the neutralization of technical sulphuric acid. The experiments were conducted at 90°C for 10 hours. Stoichiometric amounts of magnesium oxide and magesium nitrate were suspended with 0.75 g of ferrite seed material in 40 ml demineralized water. After separation of the magnetic ferrite, the magnesium sulphate solution was treated with H_2O_2 and MgO, in order to oxidize any remaining Fe^{II} and precipitate a Fe^{III}-oxyhydroxide. The Fe^{III} precipitate was subsequently separated from the solution by filtration in a pressure filter, using 0.45 μm filters and 4 bars pressure. The reaction products were treated according to the method described above. The wash waters of the two precipitates was also analyzed by ICP-ES.

Nitrate excess experiments

In order to investigate the possibility to synthesize ferrites containing more magnesium, three experiments were carried out with excess amounts of nitrate. Volumes of 1 liter residual solution from the neutralization of technical sulphuric acid were used. Experiments were conducted at 90°C for 10 hours. The magnesium oxide and magnesium nitrate were added directly to the solution. The amount of reactants used for the three experiments was enough to oxidize respectively 67, 80 and 100 % of the Fe^{II}. The reaction products were treated according to the method described under Ferrite synthesis.

Analyses

The chemical composition of the reaction products was analyzed by ICP-ES (model Perkin Elmer optima 3000). Solution samples were diluted 50 and 2500 times for the analysis of trace and major elements, respectively. Ferrite samples were prepared by dissolving 0.1 g of the dried ferrite in 5 ml 6 M HCl. After dissolution demineralized water was added to a volume of 100 ml. The chemical analysis of the iron precipitates can be used as an indication for the type of oxide/oxyhydroxide formed; the iron contents [in mg/g] decrease in the order Fe_3O_4 (724) γ-Fe_2O_3 (636) FeOOH (629), $MgFe_2O_4$ (558) and $Fe(OH)_3$ (523).
Table 9.6 (in Appendix 9.1) lists the samples that were selected for the other analysis techniques. The crystallinity and mineralogy of the ferrite precipitates was investigated by X-ray diffraction (XRD, model Philips PW 1700). The XRD spectra were used for a qualitative identification of the iron compounds present in the precipitates. Due to the overlapping of ferrite ($M^{II}Fe_2O_4$) peaks, it is almost impossible to determine which M^{II}-bearing ferrite is present. The particle size, morphology, crystallinity and microchemical composition were analyzed by transmission electron microscopy (TEM, model Philips CM200 FEG with EDAX).
The Curie temperature of the magnetic samples was measured with a modified horizontal translation type Curie balance, which uses a cycling instead of steady field (Mullender et al. 1993). For the measurements about 0.4 mg of sample was put in a glass sample tube, which was closed at the top with quartz wool. The samples were heated up to 700 °C, with a heating rate of 10°C/minute and a cooling rate of 20 °C.
For the measurement of the other magnetic properties, special cylindrical epoxy-resin samples, (⌀ 2.4 x 1.5 cm) were prepared. About 40 mg of ferrite was put on top of 0.6 g calcite in a small cylindrical tube, next the epoxy-resin was added and the content of the tube was mixed thoroughly. The samples were allowed to harden for 24 hours in a shielded room. The initial susceptibility was measured with a Jelinek KLY-2 susceptibility bridge.

The magnetic remanences of the samples were induced by a PM4 pulse magnetizer, with a maximum field intensity of 2.5 T. The remanences were subsequently measured with a digitized spinner magnetometer, based on a Jelinek JR-3 drive unit.
Hysteresis curves were measured with a maximum applied field of 200 mT.

Results and Discussion
The chemical composition of the three starting solutions is displayed in Table 9.1. Note that the iron concentration of the solution prepared from pure chemicals is higher than the iron concentration of the two residual solutions.

Solution	Fe [g/l]	Mg [g/l]	S [g/l]	Ni	Mn	Co	Zn	Na	Si
PC Pure chemicals	28.8	48	80	<1.5	<0.5	<1	<1.5	<3	<1
RSC Residual solution technical grade sulphuric acid	10.4	65.3	92	518	130	73	10	300	100
RSW Residual solution waste sulphuric acid	20.3	60.9	92	500	300	120	50	1000	100

Table 9.1 Chemical composition of the three starting solutions [mg/l] or [g/l] where indicated.

Ferrite chemistry
The color and magnetism, that was qualitatively determined by a bar-magnet, of the iron-precipitates are listed in Table 9.7 (in appendix 9.1), combined with the Fe, Mg and S concentrations. The data show that the formation of a good magnetic ferrite is favored by: a higher temperature, longer reaction time and the presence of magnetite seed crystals. The table shows, furthermore, that the iron content of the ferrites depends on the type of the initial solution; the ferrite iron concentration increases in the order RSC<RSW<PC. The magnesium and sulphur concentrations follow the opposite trend.
The conditions for synthesizing good magnetic ferrites, with iron contents of about 600 mg/g, are different for the three initial solutions. With pure chemicals (PC), seed crystals are required at 80 °C, whereas at 90°C, a reaction time of 6 hours without seed crystals is already sufficient. It has not been possible to synthesize good magnetic ferrites with an iron content of about 600 mg/g from the residual solution of technical grade sulphuric acid (RSC). Magnetic precipitates of lower iron contents resulted with seed crystals at 80°C after 10 hours, and at 90°C after at least 7 hours. From the residual solution of waste sulphuric acid (RSW) good ferrites were formed within 6 hours at 90°C.
Table 9.8 (in appendix 9.2) lists the Ni, Co and Mn concentrations of the ferrites from the RSC and RSW solutions. The Ni and Co contents are higher in the stronger magnetic ferrites.

XRD analyses
All measured XRD spectra exhibit sharp diffraction maxima, indicating that the iron precipitate samples are crystalline. The peaks were used to qualitatively identify the iron compounds present. The following compounds were found: ferrite (MFe_2O_4), maghemite (γ-Fe_2O_3), and goethite (α-FeOOH). Table 9.2 presents the results for the samples analyzed; the peak intensity of the highest magnetic ferrite peak is indicated.
The XRD-results show that almost all samples analyzed consist of mixtures of magnetic

ferrites and maghemite. Only the samples 6PC90S and 8PC90 contain exclusively magnetic ferrites.

Experiment code	Ferrite MFe_2O_4	Maghemite γ-Fe_2O_3	Goethite FeOOH	Maximum ferrite-peak [counts]
8PC80	y	y		650
6PC90	y	y		600
6PC90S	y			620
8PC90	y			750
10RSC80		y	y	-
10RSC80S	y	y	y	300
7RSC90	y	y		290
6RSW90	y	y		310
2RSW150	y	y		320

Table 9.2 Results of XRD analysis.

In the samples of low iron contents, 10RSC80 and 10RSC80S, goethite is present. Furthermore, there seems to be a positive relation between the iron content of the samples and the maximum intensity of the diffraction profile of the ferrite.

TEM-study

In appendix 9.3, TEM and SEM images of the following ferrites are represented: 8PC80, 8PC90, 6PC90, 6PC90S and 6WRS90. The images allow one to evaluate of the effect of temperature, reaction time and presence of magnetite seed crystals on the particle sizes and morphology of the resulting ferrites. The images show that the ferrites prepared from the PC solution have grain sizes of a wide range. For all reaction conditions the grains range in size from 50 to 750 nm. The only visible effect of an increase of reaction time, of temperature and of addition of magnetite seeds is the development of sharper crystal faces (more facetted crystals).

A microanalytical line-scan over the ferrite crystals of sample 6PC90S revealed the presence of sulphur. However, magnesium was not significantly present.

Comparison of the ferrites 6PC90 prepared from the pure chemical solution and 6RSW90 prepared from the residual solution of the waste acid yields remarkable differences. The ferrite grains of 6RSW90 have a more homogeneous grain size distribution of an average size of about 300 nm. The grains have a rounded appearance and are not as well developed as the 6PC90 grains. A microanalytical line-scan revealed the presence of Co and S.

Magnetic parameters

Tables 9.9 and 9.10 in (appendix 9.2), list the measured magnetic parameters. In the following section the parameters will be discussed and compared with literature data that was reviewed in chapter 8.

Curie Temperature

The Curie temperature of pure magnetite is 580 °C, higher temperatures can indicate the presence of maghemite (T_c=620), while lower Curie temperatures can be caused by the presence of ferrites bearing other metals (e.g. Mg, Co & Mn).

The Curie temperature of the ferrites prepared from the PC-solution varies from 570 to 600 °C, which is close to the Curie temperature of pure magnetite of 580 °C. Sample

6PC90S is the only sample with a Curie temperature lower than 580 °C, suggesting that maghemite is not present. This is in accordance with the XRD results, that showed that it does not contain a significant amount of maghemite.
The ferrites prepared from RSC-solutions, have generally lower Curie temperatures (520-550 °C). This can be caused by a higher content of metal bearing ferrites, which is confirmed by the chemical analyses, and by the presence of goethite, as indicated by the XRD-analyses.
One sample, 10RSC80S has a high Curie temperature of 610 °C, which is most likely caused by the presence of maghemite.
The Curie temperatures of the ferrites from RSW-solution exhibit a similar range of 550 to 610 °C.

Initial Susceptibility

Since the samples appear to consist of mixtures of magnetic ferrites and maghemite, the initial susceptibility is expected to vary from $4 \cdot 10^{-4}$ (maghemite) to $5 \cdot 10^{-4}$ [$m^3 \cdot kg^{-1}$] (magnetite).
The initial susceptibilities of the ferrites analyzed range from $4.6 \cdot 10^{-4}$ to $8 \cdot 10^{-4}$ $m^3 \cdot kg^{-1}$. An approximate, positive linear relationship exists between the initial susceptibility and the iron content of the sample. This is illustrated in Figure 9.2 for the ferrites produced from the three different solutions. The scatter of the data seems to be too high to enable one to accurately assess the iron content of the ferrite, by measuring the susceptibility.

Saturation Magnetization

The saturation magnetization of the ferrites prepared in this study is approximately within the expected range of 24 [$A \cdot m^2 \cdot kg^{-1}$] (for $MgFe_2O_4$) to 85 (for γ-Fe_2O_3) and 93 [$A \cdot m^2 \cdot kg^{-1}$] (for Fe_3O_4).
The relatively low saturation magnetization of the RSC-ferrites (ranging from 47-55 $A \cdot m^2 \cdot kg^{-1}$) agrees with the relatively high Mg content of the ferrites.
Similarly to the initial susceptibility, the saturation magnetization exhibits an approximately linear relationship with the iron content of the ferrites, as illustrated in Figure 9.3.
The relationship between the initial susceptibility and the saturation magnetization of the ferrites is linear.

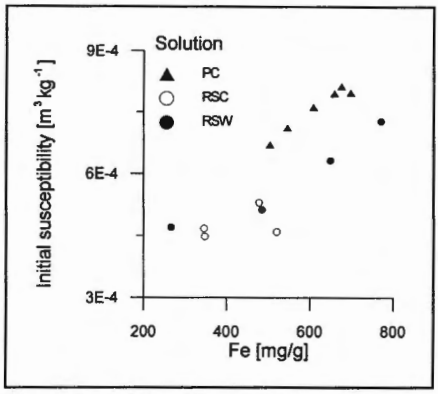

Figure 9.2 Initial susceptibility versus iron content of the ferrites produced from the three different solutions.

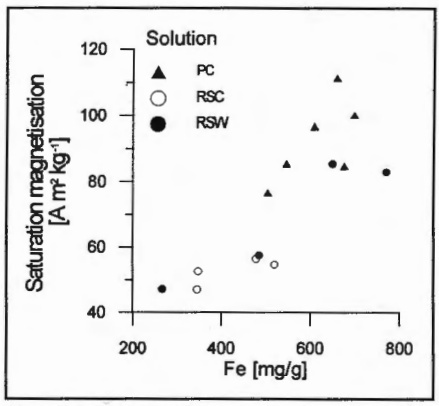

Figure 9.3 Saturation magnetization versus iron content.

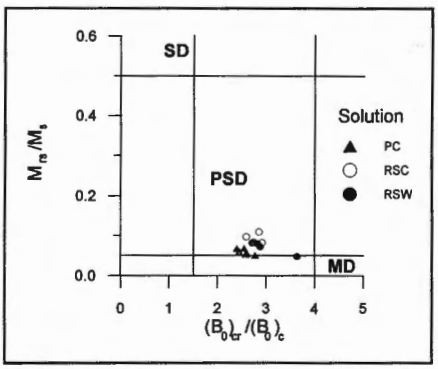

Figure 9.4 Ratio of saturation remanence and magnetization versus ratio of remanence coercivity and coercivity, according to Day et al. (1977)

Coercivity

In chapter 8 it was mentioned that according to Day et al. (1977), information on the ferrite grain size can be obtained by comparing the ratio of saturation remanence and magnetization with the ratio of remanence coercivity and coercivity. This is illustrated for the ferrites analyzed in this study in Figure 9.4. The figure shows that the ferrites all plot in the pseudo-single domain region, close to the border with the super paramagnetic region. According to Thompson and Oldfield (1986), magnetite grains that plot in this region, are typically larger than 80 nm and smaller than 1000 nm. This agrees with the range of grain sizes, that were determined by TEM.

Mass balance experiments

From the ferrite synthesis experiments with RSC-solutions a mass balance of all elements of interest was calculated. The mass balance was calculated for the reaction system of 1 liter solution, including the amount of elements present in the chemicals added. A bulk mass balance of the reactants and products is represented in Table 9.3. Table 9.4 presents the distribution [in percent] of the elements over the three reaction products, magnetic ferrite, 2nd amorphous Fe^{III} precipitate, and residual magnesium sulphate solution. The element concentrations in the wash waters were insignificant and are therefore not included in the mass-balance. The table shows that Ni and Co are mainly incorporated in the magnetic ferrite and that Mn is concentrated in the 2nd Fe^{III} precipitate. It is, furthermore, clear that by using MgO to raise the pH, it is not possible to entirely remove Ni and Mn from the final residual solution.

Total input		Total output	
RSC-solution	1 liter (=1.28kg)	Magnetic ferrite	15 g
$Mg(NO_3)_2 \cdot 6H_2O$	5.3 g	2nd Fe^{III} precipitate	13.7 g
MgO	22.2 g	Residual solution	± 1.28 kg
Ferrite seed crystals	0.75 g		

Table 9.3 Overview of the input materials and products for the treatment of 1 liter RSC-solution.

Element	Magnetic ferrite [%]	2nd Fe^{III} precipitate [%]	Residual solution [%]	Amount present in system of 1 liter of RSC-solution
Fe	91.7	8.3	0.0	10.9 [g]
Mg	0.0	6.0	94.0	78.1 [g]
S	0.1	0.3	99.6	99 [g]
Ni	93.3	5.8	0.9	503 [mg]
Mn	3.0	94.0	3.0	127 [mg]
Co	92.6	7.4	0.0	71 [mg]
Si	22.7	10.5	66.7	170 [mg]

Table 9.4 Distribution [in %] of elements, present in the system of 1 liter of RSC solution, over the reaction products.

Experiments with an excess of nitrate

Experiments with excess amounts of nitrate were carried out to oxidize 67, 80 and 100 % of the Fe^{II} in RSC-solution (code Ox67, Ox80 and Ox 100, respectively). These experiments yielded 14.9, 16.7 and 17.4 g of a magnetic iron precipitate, respectively. The color of the three precipitates was black with a slight brownish tint, that increased with increasing amount of nitrate. Table 9.5 re presents the chemical analyses of the precipitates.

Nitrate added to oxidize % Fe^{II}	Fe [mg/g]	Mg [mg/g]	Ni [mg/g]	Mn [mg/g]	Co [mg/g]	Zn [mg/g]
67 % (Ox67)	688	18.0	39.2	0.7	2.7	0.6
80 % (Ox80)	674	19.7	35.7	2.5	2.7	0.5
100 % (Ox100)	597	31.3	33.5	1.2	2.3	0.5

Table 9.5 Chemical composition of ferrites produced from experiments with an excess of nitrate.

The table shows that the iron content of the ferrites drops and the magnesium content rises with increasing amounts of nitrate used. The decreasing contents of Ni, Co, and Zn in the ferrites can be considered to be a "dilution effect", caused by the higher yield of ferrite precipitate with increasing amounts of nitrate.

The magnesium content in the ferrite from experiment Ox100 is much lower than the theoretical concentration of 122 mg/g of a stoichiometric magnesioferrite ($MgFe^{III}_2O_4$). This fact, combined with the iron contents of the precipitates and the total yields of precipitate, suggests that by adding excess amounts of nitrate mixtures of metal-bearing ferrites ($MFe^{III}_2O_4$) and maghemite (γ-Fe_2O_3) are formed.

Conclusions

- The optimum synthesis conditions of magnetic ferrites in concentrated magnesium sulphate solutions, using MgO and $Mg(NO_3)_2$, depend on the composition of the sample. The synthesis is favored by a higher iron content of the initial solution. Increasing the temperature and the addition of magnetite seed crystals positively influence the synthesis. For the synthesis of magnetic iron precipitates in the residual solution (of the neutralization of clean sulphuric acid with olivine), for instance, a reaction time of 10 hours and the addition of magnetite seeds is required at 80 °C. However, at 90 °C, a reaction time of 7 hours is sufficient, and magnetite seeds are not necessary.
- In general, the magnetic precipitates consist of mixtures of magnetic ferrites and maghemite. Goethite is present in some, less magnetic, precipitates.
- The concentrations of magnesium and sulphur in the precipitates increase with decreasing iron concentration of the initial solutions. Microanalytical line-scans over some ferrite crystals revealed the presence of sulphur; magnesium was not significantly present.
- The grain size of the ferrites ranges from 50 to 750 nm, as demonstrated by TEM and studies on the magnetic properties. The ferrites synthesized from the residual solution of waste sulphuric acid, have a more homogeneous grain size distribution with an average size of 300 nm.
- In order to assess the metal separation efficiency, mass balances were calculated of the synthesis of magnetic precipitates, in the residual solution from clean sulphuric acid. The mass balance revealed that more than 90 % of the iron, nickel and cobalt is removed by the precipitation. However the main part of manganese remains in solution. The metals remaining in solution cannot be entirely removed, using MgO in combination with H_2O_2 to oxidize the residual iron. For complete removal, the use of a stronger base, such as sodium hydroxide, is necessary.
- When excess amounts of nitrate are used, magnetic precipitates are formed, even if sufficient nitrate is added for the oxidation of all iron in solution. Chemical analyses show that maghemite is formed, rather than magnesioferrite.

Appendix 9.1 Experimental conditions, and chemical composition of iron-precipitates

Solution	Reaction time [hours]	Reaction Temperature [°C]	Seed crystals	Experiment Code	Analyses T_c=Curie temperature MP=Magnetic properties
Pure Chemicals	6	80		6PC80	
	7	"		7PC80	
	8	"		8PC80	XRD, TEM, T_c, MP
	8	"	y	8PC80S	
	9	"		9PC80	MP
	9	"	y	9PC80S	T_c, MP
	6	90		6PC90	XRD, TEM, T_c, MP
	6	"	y	6PC90S	XRD, TEM, T_c, MP
	7	"		7PC90	
	8	"		8PC90	XRD, TEM, MP
Residual solution technical grade sulphuric acid	9	80		9RSC80	
	10	"		10RSC80	XRD
	10	"	y	10RSC80S	XRD, MP
	7	90		7RSC90	XRD, T_c, MP
	7	"	y	7RSC90S	T_c,
	8	"		8RSC90	MP
	9	"		9RSC90	
	2	150		2RSC150	T_c,
Residual solution waste sulphuric acid	10	80		10RSW80	
	10	"	y	10RSW80S	MP
	6	90		6RSW90	XRD, TEM, T_c, MP
	6	"	y	6RSW90S	T_c, MP
	2	150		2RSW150	XRD, T_c, MP

Table 9.6 Reaction conditions for all experiments, including analysis techniques used for characterization of the precipitates.

Solution	Experiment Code	Color	Magnetism - no + weak ++ strong	Fe [mg/g]	Mg [mg/g]	S [mg/g]
PC Pure Chemicals	6PC80	brown	-	364	22.9	57
	7PC80	greyish-black	+	491	2.2	11
	8PC80	"	+	546	< 0.2	14
	8PC80S	black	++	655	"	11
	9PC80	greyish-black	+	504	"	15
	9PC80S	black	++	697	"	17
	6PC90	black	++	675	"	12
	6PC90S	"	++	658	"	9.3
	7PC90	"	++	743	"	13
	8PC90	"	++	608	"	9.4
RSC Residual solution technical grade sulphuric acid	9RSC80	brown	-	185	97	89
	10RSC80	"	-	122	90	88
	10RSC80S	black	++	345	85	53
	7RSC90	greyish-black	++	347	78	29
	7RSC90S	black	++	478	107	60
	8RSC90	greyish-black	++	520	102	34
	9RSC90	black	++	486	56	22
	2RSC150	dark brown	+	336	?	37
RSW Residual solution waste sulphuric acid	10RSW80	greyish-brown	-	126	88	81
	10RSW80S	black	++	266	67	45
	6RSW90	"	++	649	< 0.2	13
	6RSW90S	"	++	485	91	39
	2RSW150	"	++	770	< 0.2	14

Table 9.7 Color and qualitative magnetism, determined by tests with a bar-magnet, of iron precipitates

Solution	Experiment Code	Ni [mg/g]	Co [mg/g]	Mn [mg/g]
RSC Residual solution technical grade sulphuric acid	9RSC80	10	0.4	< 0.1
	10RSC80	7	< 0.2	< 0.1
	10RSC80S	19	1.6	1.4
	7RSC90	19	1.6	1.0
	7RSC90S	25	2.3	2.2
	8RSC90	26	2.5	3.2
	9RSC90	25	2.3	0.5
RSW Residual solution waste sulphuric acid	10RSW80	8	< 0.2	< 0.1
	10RSW80S	15	1.0	0.5
	6RSW90	15	3.3	< 0.1
	6RSW90S	25	2.3	0.6

Table 9.8 Concentrations of Ni, Co and Mn in ferrites from RSC and RSW solution

Appendix 9.2 Magnetic properties of ferrite-precipitates

Experiment code	Curie temperature [°C]	Remanence coercivity $(B_0)_{cr}$ [mT]	Coercivity $(B_0)_c$ [mT]
8PC80	600	16.4	6.3
9PC80	-	17.2	6.2
9PC80S	590	17.0	7.1
6PC90	590	16.3	6.4
6PC90S	570	17.8	6.8
8PC90		17.1	7.0
10RSC80S	610	23.1	7.9
7RSC90	550	28.0	9.8
7RSC90S	550	21.4	7.8
8RSC90	-	26.0	10
2RSC150	520		
10RSW80S	-	22.3	7.9
6RSW90	610	27.3	7.5
6RSW90S	550	21.7	8
2RSW150	600	25.1	8.7

Table 9.9 Curie temperature and coercivities

Experiment code	Susceptibility [10^{-4} $m^3 \cdot kg^{-1}$]	Saturation remanence [$Am^2 \cdot kg^{-1}$] at 2.8 T	Saturation remanence [$Am^2 \cdot kg^{-1}$] at 200 mT	Saturation magnetization [$Am^2 \cdot kg^{-1}$]
8PC80	7.11	4.72	4.28	86
9PC80	6.69	4.14	3.84	77
9PC80S	7.97	7.18	5.01	100
6PC90	8.13	5.83	4.25	85
6PC90S	7.96	6.68	5.58	112
8PC90	7.62	6.00	4.84	97
10RSC80S	4.67	2.60	2.35	47
7RSC90	4.48	5.17	2.63	53
7RSC90S	5.30	3.32	2.83	57
8RSC90	4.59	4.98	2.74	55
10RSW80S	4.70	2.66	2.36	47
6RSW90	6.32	4.02	4.27	85
6RSW90S	5.13	3.35	2.88	58
2RSW150	7.26	5.84	4.15	83

Table 9.10 Mass specific magnetic properties

Appendix 9.3 SEM and TEM Images of Magnetic Ferrites

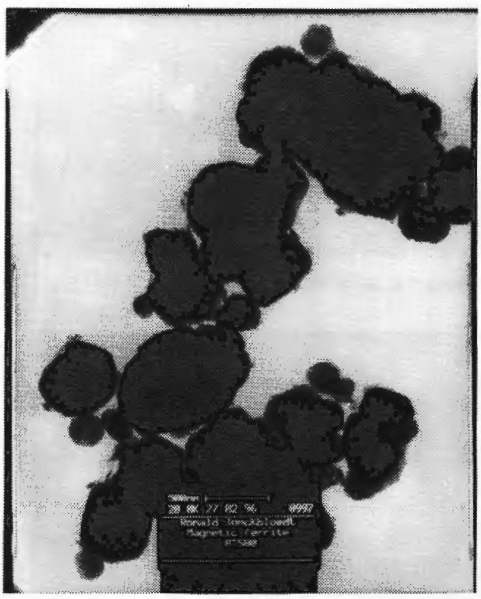

Picture 9.1 TEM Image of 8PC80

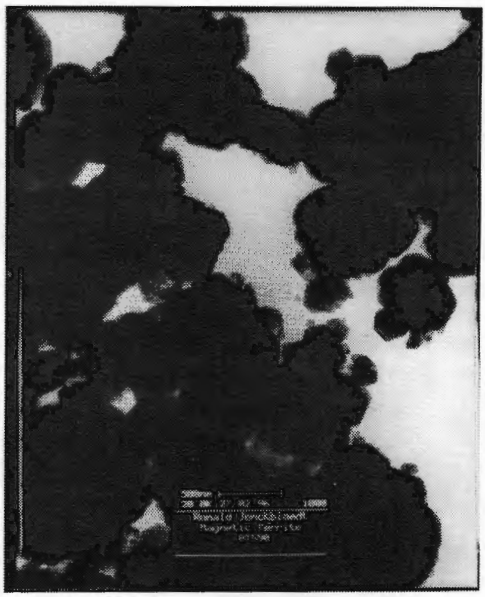

Picture 9.2 TEM Image of 8PC90

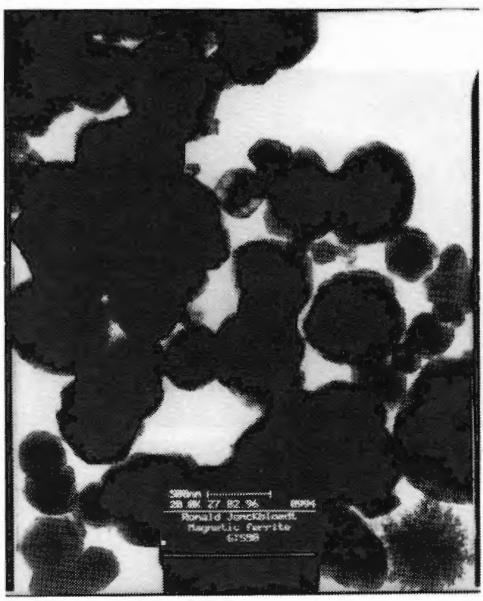

Picture 9.3 TEM Image of 6PC90

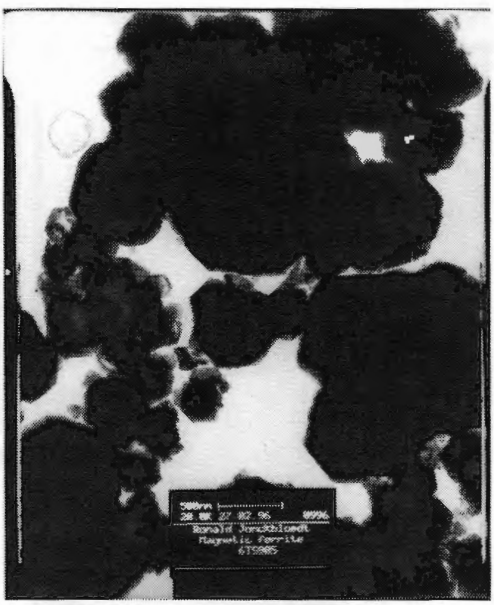

Picture 9.4 TEM Image of 6PC90S

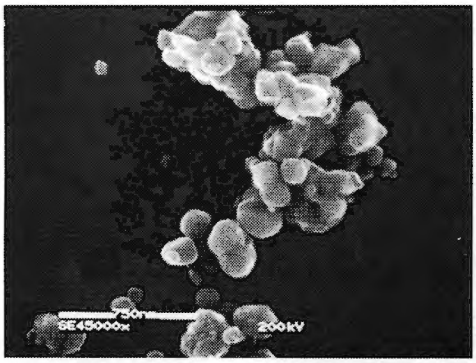

Picture 9.5 SEM Image of 8PC80

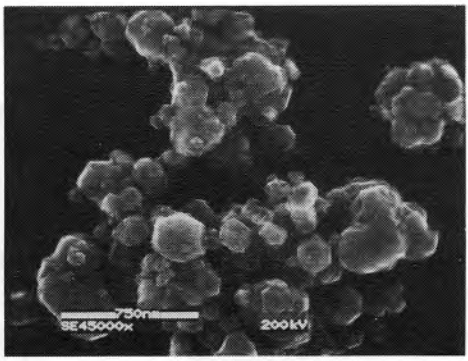

Picture 9.6 SEM Image of 8PC90

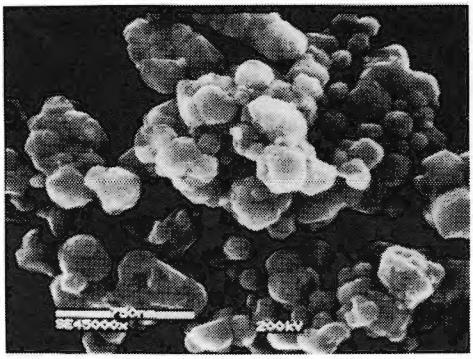

Picture 9.7 SEM Image of 6PC90

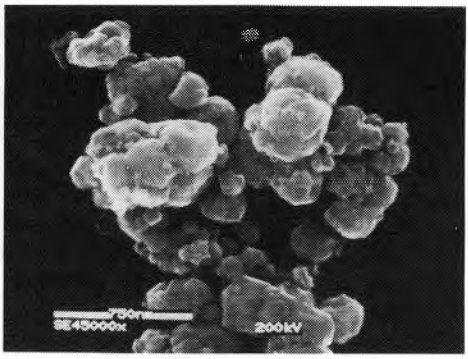

Picture 9.8 TEM Image of 6PC90S

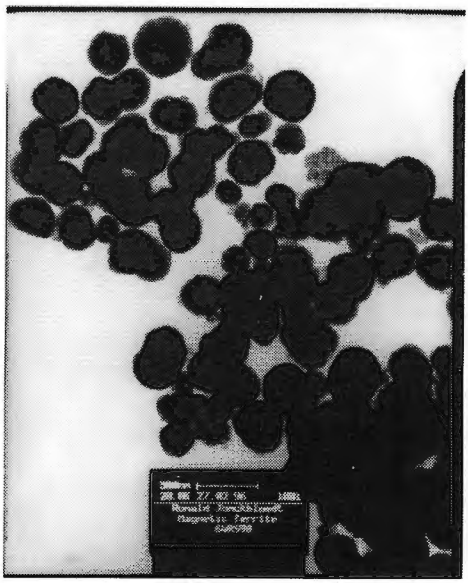

Picture 9.9 SEM Image of 6RSW90

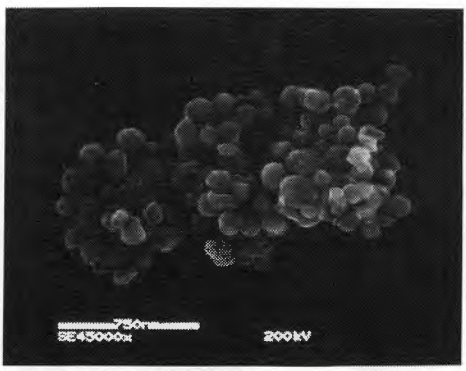

Picture 9.10 TEM Image of 6RSW90

Concluding Remarks

Introduction

This thesis addresses a wide range of subjects concerning the use of olivine for the neutralization of acids. A division into three parts is made. In the first part, "Olivine dissolution", the mechanism and the rate of the dissolution of olivine in sulphuric acid are studied, the dissolution behavior of several types of olivine are compared, and the heat of reaction of the dissolution of olivine in sulphuric acid is measured. In the second part, "Neutralization of waste acids", the use of the Olivine Process for the neutralization of several waste acids is investigated. In the third part "Synthesis of magnetic ferrites", a procedure is developed for the removal of metals from the neutralized solution, by the synthesis of magnetic ferrites.

The most important conclusions of the broad range of subjects are recapitulated.

1) Olivine dissolution

The design of an industrial plant for the neutralization of waste acids with olivine requires knowledge of the factors that determine the rate of dissolution of olivine in acids. Unfortunately, literature data are only available for the dissolution of olivine under natural weathering conditions. The reaction mechanisms are therefore identified by combining literature data with experimental studies on the dissolution of olivine in concentrated acid. It is shown that in concentrated acid, thick continuous layers of silica precipitate on the dissolving olivine grains, when the olivine is not agitated. The layers of precipitated silica inhibit further dissolution and lead, eventually, to complete solidification of the olivine bed. To prevent the precipitation of silica on the olivine grains the mixture of olivine and acid has to be stirred continuously. When the mixture is stirred vigorously, the dissolution rate of olivine is controlled by surface reactions.

Subsequently a kinetic model for the dissolution of one type of Norwegian olivine (FO_{93}) of grain sizes ranging from 63 to 300 μm, in 3 M sulphuric acid at temperatures from 60 to 90 °C is designed. Unfortunately, conventional procedures for the study of reaction kinetics are not applicable to investigate the rate of dissolution of olivine in sulphuric acid at high temperatures. The reaction rate is therefore studied by performing a range of complete neutralization experiments. The hydrogen ion activity, required for the interpretation of the experimental data, is calculated with the Pitzer model, using the computer program PHRQPITZ. The Pitzer model enables one to calculate chemical equilibria in solutions of a high ionic strength. Due to the high acidity and elevated temperatures it is not feasible to accurately determine the hydrogen ion activity by pH measurements. The study shows that the progress of the neutralization reaction can be satisfactorily modeled using the geometrical surface area of the dissolving olivine. The geometrical surface area can be calculated as a function of the volume of olivine, starting with the initial grain size distribution and assuming a spherical grain geometry.

The results of the study are summarized by the following rate equation:

$$\frac{d\,[H^+]}{dt} = - \; e^{-\frac{E_{act}}{R \cdot T}} \cdot 10^8 \cdot (1.92 \pm 0.12) \cdot S_{geom} \cdot A_{H^+}^{0.33} \qquad [mol \cdot minute^{-1}]$$

with E_{act} the activation energy of 66.5±2 kJ·mole^{-1}, S_{geom} the geometrical surface area of the

olivine grains, and A_{H^+} the hydrogen ion activity calculated with the Pitzer model. The equation enables one to calculate the progress of neutralization.
For the study of the dissolution rate the upper grain size limit of 300 μm is chosen, since it is the size of the largest olivine crystals of the Norwegian olivine used without internal fractures. An investigation on the dissolution behavior of olivine of grain size fractions ranging from 300 to 630 μm shows that the dissolution proceeds preferentially along the fractures and leads to fragmentation of the olivine grains. The disintegration results in a higher available olivine surface area, and consequently in a higher dissolution rate.
The properties of the natural raw material olivine are variable, and depend on the source of the olivine. The suitability of a type of olivine for the neutralization of waste acids is determined by the following factors, i) mineralogical composition of the olivine source rock, ii) deformation/alteration of the source rock, and iii) chemical composition of the olivine. The dissolution behavior of olivine types from two possible sources in Greece is studied. The performance of the Greek olivines is compared with the Norwegian olivine used in the study on the kinetics of olivine dissolution. The chemical composition of the Greek olivine samples ranges from FO_{90} to FO_{92}. The study shows that as compared to the Norwegian olivine, the Greek olivines initially react faster.
It is important to note that the effects of varying olivine properties on the neutralization rate are small as compared to, e.g., the effect of temperature on the reaction rate.
The low energy consumption of the olivine process is due to the fact that the dissolution of olivine in acid is an exothermic reaction. Accurate measurements on the heat of reaction of the dissolution of olivine in acid were not available. Therefore, the heats of reaction are measured for the dissolution of three olivine types (two Norwegian samples, both FO_{93}, and one Greek sample, FO_{92}) in 3 M sulphuric acid. Within the limits of precision of the measurement procedure the heats of reaction of the three olivine types are the same. An average heat of reaction of (223±2.9) $kJ \cdot mol^{-1}$ is determined for the dissolution of olivine in 3 M sulphuric acid.

2) Neutralization of waste acids

Each waste acid has a characteristic composition. For successful treatment of a waste acid by the olivine process it is important to assess whether specific adaptations must be made to optimize the reaction progress and the properties of the by-products. The application of the olivine process for the treatment of three different waste acids is investigated. The following waste acids are tested, i) sulphuric acid (2.9 M) with inorganic contaminants from the production of titanium dioxide, ii) sulphuric acid (12.8 M) with organic contaminants, and iii) hydrochloric acid (9.7 M) with organic contaminants.
The neutralization behavior of the waste acids is compared with that of technical grade sulphuric acid. The residual solution of the neutralization of the waste acid from the titanium dioxide production is further processed to investigate the possibility to produce a pure magnesium sulphate solution.
The concentrated sulphuric acid with organic contaminants was diluted to a concentration of 3 M to prevent the precipitation of magnesium sulphate during the neutralization. The dilution causes precipitation of more than 80 wt% of the organic matter, that is subsequently removed by filtration.
The neutralization rate of the waste acid from the titanium dioxide production is slightly lower as compared to the neutralization of technical grade sulphuric acid. The lower rate is

most likely due to the higher ionic strength of the waste acid. The presence of organic compounds in both the sulphuric and hydrochloric waste acid increases the neutralization rate.
The silica produced by neutralization of the three waste acids is white. Typically, the silica from the titanium dioxide waste acid contains about 2 wt% TiO_2. The specific surface areas of the silicas from both waste sulphuric acids are comparable to silica produced from technical grade sulphuric acid. The silica from the waste hydrochloric acid has a significantly lower specific surface area.
Most of the contaminating metals in the residual solution from the titanium dioxide waste acid can be separated by precipitation in two stages. In the first stage the pH is raised to a value of 4 to 5, which causes the precipitation of metals like Ti, Al, V, Cr, and Fe^{III}. The precipitate can subsequently be removed by filtration. In the second stage a magnetic ferrite is precipitated by increasing the pH to a value of 7 and simultaneously oxidizing the Fe^{II} in solution. A slurry of magnesium oxide can be used to raise the pH. This has the advantage that no new cations are introduced in the magnesium sulphate solution.

3) Synthesis of magnetic ferrites
In literature several procedures for the synthesis of magnetic ferrites from Fe^{II} solutions have been described. Magnetic ferrites can be formed by slow oxidation, e.g., with air or nitrate of Fe^{II} solutions at pH $\geq$ 8 and at temperatures higher than 50 °C. Unfortunately, the procedures described in literature cannot be applied directly to the residual solution of the olivine process. For instance, the required reaction time for the synthesis of magnetic ferrites using air as an oxidant is for the residual solution five times longer than the maximum oxidation time reported in literature.
The use of nitrate as an oxidant has two important advantages, i) it can be added in stoichiometrical amounts, and ii) it does not cause abundant evaporation, as compared to air.
A procedure to synthesize magnetic ferrites in concentrated sulphate solutions using a mixture of magnesium oxide and magnesium nitrate is developed. Three types of sulphate solution are used, i) a Mg/Fe sulphate solution prepared from pure chemicals, ii) a residual solution from the neutralization of technical grade sulphuric acid, and iii) a residual solution from waste acid from the production of titanium dioxide. The resulting precipitates are examined by ICP, XRD and TEM. Furthermore, a number of magnetic properties are measured. Experiments are carried out at several temperatures, ranging from 80 to 150 °C, for periods of time, ranging from 2 to 10 hours. The effects of the addition of magnetite seed crystals, and the amount of nitrate are investigated.
The experiments show that increasing temperature, longer reaction time, higher initial Fe^{II} concentration and addition of seed crystals favor the synthesis of magnetic ferrites. Remarkably, these parameters mainly influence the crystallinity of the precipitate, the grain size range of the ferrites (50-750 nm) remains approximately constant.
The calculation of a mass balance of the elements of interest shows that after synthesis and separation of the magnetic ferrite typically about 1 wt% of the total amount of Ni and 3 wt% of the total amount of Mn remains in solution.

General Conclusion

As compared to the conventional procedures for the treatment of waste acids, such as neutralization with limestone or regeneration processes, the olivine process provides a cheaper solution and does not produce new waste streams. The production of useful by-products, such as precipitated silica, the low energy consumption, and the wide availability and relative low price of olivine makes the process an interesting alternative for current disposal procedures.

References

Anbeek C. (1992) The Dependance of Dissolution Rates on Grain Size for some Fresh and Weathered Feldspars. Geochim. Cosmochim. Acta 56, 3957-3970.

Atkins P.W. (1990) Physical Chemistry. Oxford University Press. ISBN 0-19-855284-x.

Blum A., Lasaga A. (1988) Role of Surface Speciation in the Low-temperature dissolution of Minerals. Nature 331, 431-433.

Brady P.V., Walther J.V. (1989) Controls on Silicate Dissolution Rates in Neutral and Basic pH Solutions at 25 °. Geochim. Cosmochim. Acta 53, 2823-2830.

Brantley S.L., Chen Y. (1995) Chemical Weathering Rates of Pyroxenes and Amphiboles. Reviews in Mineralogy 31, 119-168.

Brower R.D., Visocky A.P., Guthrie M. (1989) Evaluation of Underground Injection of Industrial Waste in Illinois. Final Report ENR contracts AD-94, UI 8501. Department of Energy and Natural Resources.

Coulson J.M., Richardson J.F., Backhurst J.R., Harker J.H. (1991) Chemical Engineering, Volume 2 Particle Technology and Separation Processes. Pergamon Press. ISBN 0-08-037957-5.

Cussler E.L. (1984) Diffusion. Mass Transfer in Fluid Systems. Cambridge University Press. ISBN 0 521 23171

Davis, J.C. (1986) Statistics and Data Analysis in Geology 2nd edn. John Wiley & Sons, New York.

Day R., Fuller M., Schmidt V.A. (1977) Hysteresis Properties of Titanomagnetites: Grain-Size and Compositional Dependance. Physics of the Earth and Planetory Interiors 13, 260-267.

Deer W.A., Howie, R.A., Zussman (1975) An Introduction to the Rock Forming Minerals. Longman Group Limited. London. ISBN 0-582-44210-9.

Dekkers M.J., Pietersen H.S. (1992) Magnetic Properties of Low-Ca Fly Ash: A Rapid Tool for Fe-Assesment And a Survey For Potentially Hazardous Elements. In: Advanced Cementitious Systems: Mechanisms and Properties. Materials Reserach Society Symposium Proceedings 245, 37-47.

Drever, J.I. (1988) The Geochemistry of Natural Waters. 2nd edn. Englewood Cliffs, New Jersey: Prentice Hall.

Eggleston C.M., Hochella M.F, Parks G.A. (1989) Sample Preparation and Aging Effects on the Dissolution Rate and Surface Composition of Diopside. Geochim. Cosmochim. Acta 53, 797-804.

Ehlers E.G., Blatt H. (1982) Petrology, Igneous, Sedimentary and Metamorphic. W.H. Freeman and Company, San Francisco. ISBN 0-7167-1279-2.

Enk R.v. (1994) Acid Waste Production in the European Community. Brite Euram II Research Action Programme, E.C. Agreement Number BRE2-CT92-0.344. Olivine/Dunite for Industrial Applications (GR-OLIV). Technical Project No. 2.

Feiknecht W.v. (1959) Über die Oxydation von festen Hydroxyverbindungen des Eisens in wäßrigen Lösungen. Zeitschrift für Elektrochemie 63, 34-43.

Fogler H.S. (1986) Elements of Chemical Reaction Engineering. Prentice-Hall international series in the physical and chemical engineering sciences. Prentice-Hall Inc.

EC Report (1995) Brite Euram II Research Action Programme, E.C. Agreement Number BRE2-CT92-0.344. Olivine/Dunite for Industrial Applications (GR-OLIV). Final Technical Report.

Goldich S.S. (1938) A Study in Rock-Weathering. Journal of Geology 46, 17-58.

Gaans P.F.M. van, Schuiling R.D. (1997) The Waste Sulfuric Acid Lake of the TiO_2-Plant at Armyansk, Crimea, Ukraine. Part II. Modelling the Chemical Evolution with PHRQPITZ. Applied Geochemistry 12, 187-201.

Graaff J.W.M. de (1997) Acidic Waste Disposal by Underground Injection. (In prep.)

Grandstaff D.E. (1978) Changes in Surface Area and Morphology and the Mechanism of Forsterite Dissolution. Geochim. Cosmochim. Acta 42, 1899-1901.

Guise L., Castro F. (1996) Iron, Aluminium and Chromium Co-Elimination by Hydrolytic Precipitation from Nickel and Cobalt Containing Sulphuric Acid Solution. In: Iron Control and Disposal. Eds. Dutrizac J.E., Harris G.B. Canadian Institute of Mining, Metallurgy and Petroleum. ISBN 0-919086-71-3.

Hahn F., Hendriks J.H. (1994) Neutralisation of Waste Acids with Olivine. With the Production of Silica. Internal Report Onderzoek School Proces Technologie, University of Twente.

Herk J.v., Pietersen H.S. (1987) Neutralisatie van Afvalzuur met behulp van Olivijn. Rapportage 1e Onderzoeksfase. Ministerie VROM Contract 2.6.2/11.10.30.01.

Herk J.v., Pietersen H.S., Schuiling R.D. (1989) Neutralization of Industrial Waste Acids with Olivine. The Dissolution of Forsteritic Olivine at 40-70 °C. Chemical Geology 76, 341-352.

Holdren G.R., Berner R.A. (1979) Mechanism of Feldspar Weathering - I. Experimental Studies. Geochim. Cosmochim. Acta 43, 1161-1186.

Huang W.H., Keller W.D. (1970) Dissolution of Rock FormingSilicate Minerals in Organic Acids: Simulated First- Stage Weathering of Fresh Mineral Surfaces. The American Mineralogist 55, 2076-2094.

Iler R.K. (1979) The Chemistry of Silica. John Wiley & Sons.

Jonckbloedt R.C.L. (1995) Report on Neutralization Experiments of Tioxide Calais Waste Acid with Olivine. Report Geochem B.V. May 1995.

Jonckbloedt R.C.L. (1995) Brite Euram II Research Action Programme, E.C. Agreement Number BRE2-CT92-0.344. Olivine/Dunite for Industrial Applications (GR-OLIV). Final Technical Report.

Jonckbloedt R.C.L. (1996) The Neutralization of Waste Acids with Olivine. A Case Study in Geochemical Engineering. 3e Nederlands Aardwetenschappelijk Congres 2-3 Mei Veldhoven. KnGMG, ARA & GOA.

Jonckbloedt R.C.L. (1997) Olivine Dissolution in Strong Acids at Elevated Temperatures: Implications for the Olivine Process. Proceedings of the Fifth International Symposium on Hydrothermal Reactions. Eds. Palmer D.A. Wesolowski D.J. ORNL Oak Ridge, Tennessee, U.S.A.

Kaneko K., Katsura T. (1979) The Formation of Mg-bearing Ferrite by the Air Oxidation of Aqueous Suspensions. Bull. Chem. Soc. Jpn. 52, 747-752.

Keller W.D., Balgord W.D., Reesman A.L. (1963) Dissolved Products of Artificially Pulverized Silicate Minerals and Rocks: Part 1. Journal of Sedimentary Petrology 33, 191-204.

Kiyama M. (1978) The Formation of Manganese and Cobalt Ferrites by the Air Oxidation of Aqueous Suspensions and Their Properties. Bull. Chem. Soc. Jpn. 51, 134-138.

Koch Jr G.S., Link R.F. (1971) Statistical Analysis of Geological Data. Dover Publications Inc. New York.

Lasaga A.C. (1984) Chemical Kinetics of Water-Rock Interactions. Journal of Geophysical Research 89, 4009-4025.

Lax B., Button K.J. (1962) Microwave Ferrites and Ferrimagnetics. New York.

Lieftink D.J. (1997) The preparation and Characterization of Silica from Acid Treatment of Olivine. PhD thesis, University of Utrecht ISBN 90-393-1852-2.

Loughnan F.C. (1969) Chemical Weathering Rates of the Silica Minerals. American Elsevier Publishing Company.

Luce R.W., Bartlett R.W., Parks G.A. (1972) Dissolution Kinetics of Magnesium Silicates. Geochim. Cosmochim. Acta 36, 35-50.

Mullender T.A.T., van Velzen, A.J., Dekkers, M.J. (1993) Continuous Drift Correction and Separate Identification of Ferrimagnetic and Paramagnetic Contributions in Thermomagnetic Runs. Geophys. J. Int. 114, 663-672.

Murphy W.M., Helgeson H.C. (1987) Thermodynamic and Kinetic Constraints on Reaction Rates among Minerals and Aqueous Solutions. III. Activated Complexes and the pH-dependance of the Rates of Feldspar, Pyroxene, Wollastonite and Olivine Hydrolysis. Geochim. Cosmochim. Acta 51, 3137-3153.

Nockolds S.R., Knox R.W.O'B., Chinner G.A. (1979) Petrology for Students. Cambridge University Press. ISBN 0-521-21553-6.

O'Reilly W. (1984) Rock and Mineral Magnetism. Blackie Publishers, Bishopbrigs. ISBN 0-412-00401-1

Okkerse C. (1961) Submicroporous and Macroporous Silica. PhD thesis, Technical University Delft. Drukkerijen Hoogland en Waltman N.V. Delft.

Plummer L.N., Parkhurst D.L., Fleming G.W., Dunkle S.A. (1988) A Computer Program Incorporating Pitzer's Equations for Calculation of Geochemical Reactions in Brines. U.S. Geological Survey, Water-Resources Investigations Report 88-4153.

Robbins H. (1980) The Preparation of Mn-Zn Ferrites by Co-Precipitation. Ferrites: Proceedings of the International Conference Japan.

Roorda H.J., Queneau P.E. (1973) Recovery of Nickel and Cobalt from Limonites by Aqueous Chlorination in Seawater. Trans Inst. Mining Metallurgy C79-87.

Rothe U. (1988) Recycling of Spent Acid in Titanium Dioxide Production; Sulphur 88, British Sulphur's 13th Int. Conference, Vienna.

Schott J., Berner R.A. (1983) X-ray Photoelectron Studies of the Mechanism of Iron Silicate Dissolution during Weathering. Geochim. Cosmochim. Acta 47, 22300-2240.

Schuiling R.D., Herk J.v., Pietersen H.S. (1986) A Potential Process for the Neutralisation of Industrial Waste Acids by Reaction with Olivine. Geologie en Mijnbouw 65, 243-246.

Schuiling R.D. (1990) Geochemical Engineering: Some Thoughts on a New Research Field. Applied Geochemistry 5, 251-262.

Schuiling R.D. (1991) Engineering Aspects of Environmental Geochemistry. Journal of Geochemical Exploration 41, 59-64.

Schwertmann U., Cornell R.M. (1991) Iron Oxides in the Laboratory. VCH Verlagsgesellschaft, Weinheim. ISBN 3-527-26991-6.

Siegel D.I., Pfannkuch H.O. (1984) Silicate Mineral Dissolution at pH 4 and near Standard Temperatue and Pressure. Geochim. Cosmochim. Acta 48, 197-201.

Smit J., Wijn H.P.J. (1959) Ferrites: Physical Properties of Ferrimagnetic Oxides in Relation to Their Technical Applications. Philips Technical Library.

Sugimoto T., Matijević E. (1979) Formation of Uniform Spherical Magnetite Particles by Crystallization from Ferrous Hydroxide Gels. Journal of Colloid and Interface Science 74, 227-240

Sung W., Morgan J.J. (1980) Kinetics and Product of Iron Oxygenation in Aqueous Systems. Environm. Sci. & Techn. 14, 561-568.

Takada T., Kiyama M. (1970) Preparation of Ferrites by Wet Method. In: Ferrites: Proceedings of the International Conference, 1970, Japan.

Tamaura Y., Kanzaki T., Katsura T. (1980) Formation of Mg-, Cd-, Zn-, Pb-, Cr-, Ti- or V-bearing Ferrite by Air (or NO3-) Oxidation of Aqueous Suspension. Ferrites: Proceedings of the International Conference Japan.

Tamaura Y., Yoshida T., Katsura T. (1984) The Synthesis of Green Rust II (Fe^{III}_1-Fe^{II}_2) and its Spontaneous Transformation into Fe_3O_4. Bull. Chem. Soc. Jpn. 57, 2411-2416.

Tamaura Y. (1985) Ferrite Formation from the Intermediate, Green Rust II, in the Transformation Reaction of γ-FeOOH in Aqueous Suspension. Inorg. Chem. 24, 4363-4366.

Tamaura Y. (1986) Ni(II)-bearing Green Rust II and its Spontaneous Transformation into Ni(II)-bearing Ferrites. Bull. Chem. Soc. Jpn. 59, 1829-1832.

Thompson R., Oldfield F. (1986) Environmental Magnetism. Allen and Unwin, London.

Ullmanns Encyklopädie der Technischen Chemie (1982) Verlag Chemie GmbH, Weinheim.

Vogel A.I. (1953) Quantitative Inorganic Analysis. Longmans, Green and Co. London.

White A.F. (1995) Chemical Weathering Rates of Silicate Minerals in Soils. Reviews in Mineralogy 31, 407-458.

Wogelius R.A., Walther J.V. (1991) Olivine Dissolution at 25 °C: Effects of pH, CO_2, and Organic Acids. Geochim. Cosmochim. Acta 55, 943-954.

Wogelius R.A., Walther J.V. (1992) Olivine Dissolution Kinetics at Near-surface Conditions. Chemical Geology 97, 101-112.

Wogelius R.A., Fraser D.G. (1996) Surface Oxidation and Hydroxilation of Olivine Produced by Reaction with Aqueous Solutions: an Ex-situ XAS (REFLEXAFS) and ERDA Study.
Journal of Conference Abstracts 1, 684.

Wollast R., Garrels R.M. (1971) Diffusion Coefficient of Silica in Sea Water. Nature Physical Science 229, 94.

Acknowledgements

Gaarne wil ik iedereen bedanken die heeft geholpen bij het tot stand komen van dit proefschrift.

Allereerst bedank ik mijn promotores Prof. Ir J.W. Geus en Prof. Dr R.D.Schuiling voor de vrijheid die ze gegeven hebben bij het uitvoeren van het onderzoek en het schrijven van dit proefschrift. Ik dank Prof. Schuiling voor de gelegenheid die hij mij bood om deel te nemen aan een "Geochemical Engineering" onderzoek. Het heeft mij altijd zeer aangesproken dat met kennis van geochemische processen en natuurlijke materialen nieuwe en duurzame milieutechnologieën ontwikkeld kunnen worden. Het olivijn proces is hiervan een prima voorbeeld.

Vervolgens wil ik Geochem Research B.V. bedanken voor de financiering van het onderzoek, via een EG Brite Euram project (BRE2-CT92-0.344). V.M.L. (Ginette) Heidweiller bedank ik voor de coördinatie en de prettige samenwerking tijdens het verzorgen van de halfjaarlijkse rapportage. Tevens wil ik Rein van Enk bedanken voor de vruchtvolle discussies in de beginfases van het project. Huig Bergsma wordt bedankt voor de stimulerende samenwerking, o.a. bij de bereiding van talloze kilo's silica.
Ook de andere deelnemers aan het EG project, VerTech Treatment Systems en Kalkzandsteenfabriek Harderwijk, wil ik bedanken. De gesprekken met Piet Tessel van VerTech vond ik zeer leerzaam. Het was een uitdaging om aan zijn grote vraag naar "simpele" data, nodig voor een industrieel ontwerp voor het olivijn proces, te voldoen.

Furthermore, I would like to thank the Greek participants of the EG project, Mirtec S.A., IGME, BMTE S.A., Grecian Magnesite, and Magnomin.
Gaarne bedank ik Ivo Tijburg en Wim Dokter van AKZO voor de prettige samenwerking.

Aan diverse onderdelen van het onderzoek werd meegeholpen door studenten van de Universiteit Utrecht en het IHE (International Institute for Infrastructural, Hydraulic and Environmental Engineering) in Delft. Ik wil graag Gerard Cornelissen en Alex van Kan, van de Universiteit Utrecht bedanken.
It was a pleasure to work with the international students of the IHE. The differences in cultural background provided an additional challenging experience. I want to thank Xiao Zepeng from China, who worked on the neutralization of several waste acids. Many thanks also to Foday M. Jaward from Sierra Leone, who contributed substantially in the development of a procedure for synthesizing magnetic ferrites in the residual solution of the olivine process. Furthermore, I want to thank Stella Arachie from Nigeria, who studied the separation of Ni from the residual solution. Finally, I thank Rehab A. K. Al-Azazi from Yemen, who studied several procedures for the precipitation of iron oxides.
Ook wil ik graag Peter Kelderman van het IHE bedanken voor de prettige samenwerking tijdens de begeleiding van deze studenten.

Verder wil ik een aantal mensen bedanken die mij hebben geholpen bij analyses, technische problemen, of op andere wijze hebben geassisteerd.
Dhr. van Miltenburg bedank ik voor de faciliteiten en hulp bij het meten van de reactie warmte. Cor de Boer, Mark Dekkers en Tom Mullender van het paleomagnetisme lab in Fort Hoofddijk wil ik hartelijk bedanken voor de hulp bij het meten van diverse magnetische eigenschappen van magnetische ferrieten. Piet Elberse bedankt voor de metingen van het specifiek oppervlak van talloze silicas. Paul Anten en Marjan Reith van het sedimentologie lab bedank ik voor de talloze korrelgrootte analyses. Dank ook voor Helen de Waard, Arnold van Dijk, Gijs Nobbe en Mark van Alphen voor diverse analyses, met o.a. ICP, CNS-analyzer

etc. Wim Nieuwenhuis wordt bedankt voor de snelle fabricage, of reparatie van allerhande glaswerk. Pieter Kleingeld wil ik graag bedanken voor zijn inventieve hulp bij de meest uiteenlopende technische en elektronische problemen. Dank ook voor Toni van de Gon en Hans Bliek van de werkplaats.
Ruud Rikers van de TU Delft wordt hartelijk bedankt voor zijn informatie over magnetische scheidings methoden en het beschikbaar stellen van een onmisbaar gebleken elektromagneet.

Graag wil ik Paulien van Gaans bedanken voor de discussie over het gebruik van het computer programma PHRQPITZ bij het uitvoeren van chemische evenwicht berekeningen in sterk zure oplossingen. Alexis van Erp wordt bedankt voor zijn hulp bij het oplossen van problemen bij de mathematische beschrijving van het oplosgedrag van olivijn.

Ik bedank alle promovendi van de vakgroep Anorganische Chemie, en van de vakgroep Geochemie voor de nodige gezelligheid. In het bijzonder noem ik de "Geochemical Engineers", Jeroen de Graaff, Hans Hage, Arian Steenbruggen, Patrick Speck, Ineke Joosten, Guido Hollman, Hans Zijlstra, Ding Mei, Arthur Schmidt, Fred Hahn, Thijs Noordewier, Sieger van der Laan en Gerben Mol. Verder bedank ik Hélène van den Bos, Jan Geert Koops, Dick Lieftink, Berend Wilkens, Peter Pruysers, Foeke Postma, Giuseppe Frapporti, Heddy de Wijs en Patrick van Santvoort.

Tenslotte dank ik Simon Vriend voor alle hulp. Het is verbazingwekkend hoe hij allerlei zaken vanuit verassende invalshoeken weet te benaderen en zo met creatieve ideeën op de proppen komt. Ik ben er van overtuigd dat zonder de vele discussies dit proefschrift niet in de huidige vorm tot stand was gekomen. De jaarlijkse statistiek cursus en het tweede jaars veldwerk in het Massif Central waren gedurende mijn promotie onderzoek welkome afwisselingen. Ook de gezamenlijke organisatie van een Nederlandse afvaardiging bij de wereldkampioenschappen goudpannen in Frankrijk in '95 was onvergetelijk.

Curriculum Vitae

Ronald Cristian Leonard Jonckbloedt werd geboren op 28 juli 1969 te Woudsend, gemeente Wymbritseradeel. In 1987 behaalde hij het VWO diploma aan het Murmellius Gymnasium te Alkmaar, waarna hij in september van dat jaar begon aan de studie Geologie aan de Universiteit Utrecht. Het doctoraal examen met judicium cum laude werd behaald in april 1993. Zijn afstudeer-onderzoek richtte zich op het bestuderen van goud verertsingen, bij Tebedo, West Flores, Indonesië en de Goldlund mineralisatie, Noord west Ontario, Canada. Van juni 1993 to juni 1997 was hij werkzaam als assistent in opleiding bij de vakgroep Anorganische Chemie van de Universiteit Utrecht. Gedurende deze periode werd het onderzoek verricht dat in dit proefschrift wordt gepresenteerd.